iScience

CellPress

Article

A Bacterial Pathogen Senses Host Mannose to Coordinate Virulence

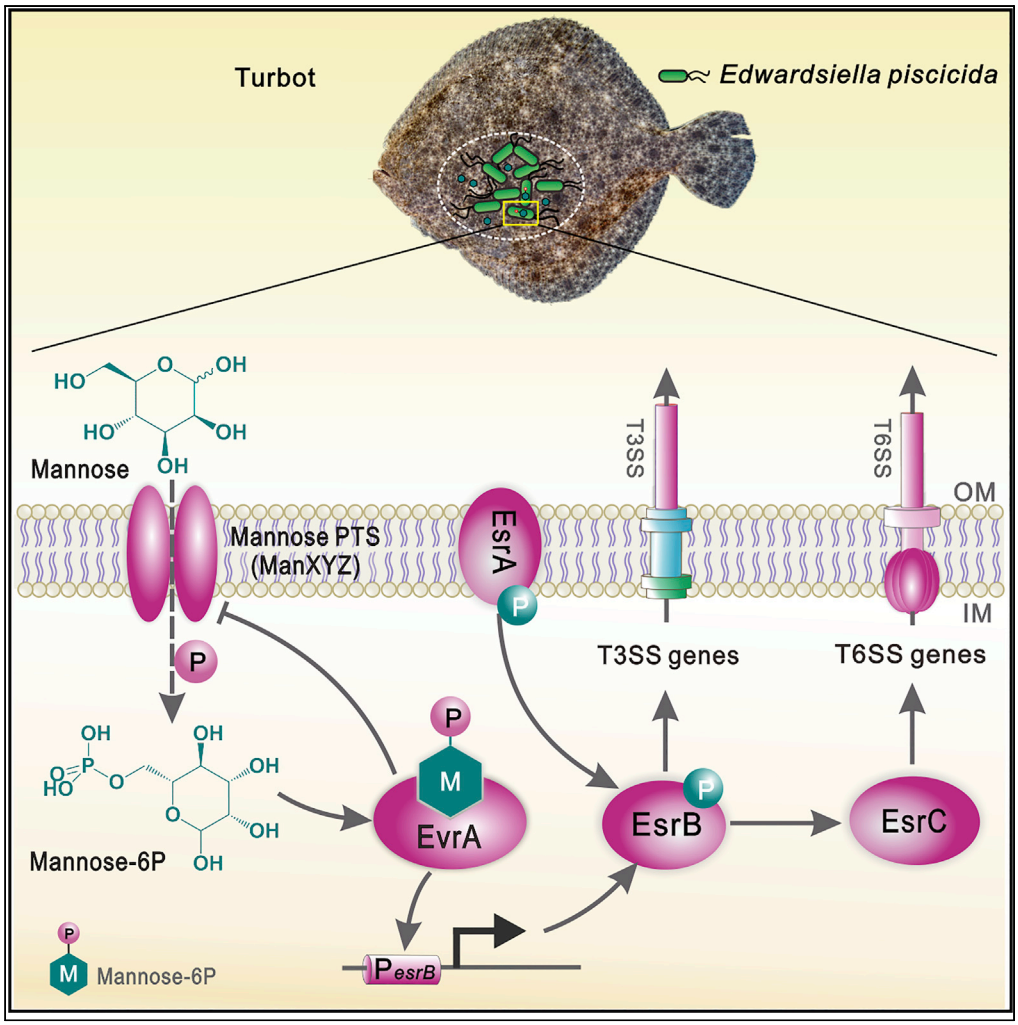

Lifan Wei, Haoxian Qiao, Brandon Sit, ..., Yuanxing Zhang, Matthew K. Waldor, Qiyao Wang

oaiwqiyao@ecust.edu.cn

HIGHLIGHTS

An *E. piscicida* defined mutant library is generated and analyzed *in vitro* and *in vivo*

EvrA is a key transcriptional activator of the known virulence regulator *esrB*

EvrA is directly bound and activated by mannose-6-phosphate from imported mannose

Extracellular mannose augments *E. piscicida* virulence in an *evrA*-dependent manner

Wei et al., iScience *20*, 310–323
October 25, 2019
https://doi.org/10.1016/j.isci.2019.09.028

iScience

CellPress

Article

A Bacterial Pathogen Senses Host Mannose to Coordinate Virulence

Lifan Wei,[1] Haoxian Qiao,[1] Brandon Sit,[4] Kaiyu Yin,[1] Guanhua Yang,[1] Ruiqing Ma,[1] Jiabao Ma,[1] Chun Yang,[6] Jun Yao,[7] Yue Ma,[1,3] Jingfan Xiao,[1] Xiaohong Liu,[1,3] Yuanxing Zhang,[1,3] Matthew K. Waldor,[1,4,5] and Qiyao Wang[1,2,3,8,*]

SUMMARY

Bacterial pathogens are thought to activate expression of virulence genes upon detection of host-associated cues, but identification of the nature of such signals has proved difficult. We generated a genome-scale defined transposon mutant library in *Edwardsiella piscicida*, an important fish pathogen, to quantify the fitness of insertion mutants for intracellular growth in macrophages and in turbot (*Scophthalmus maximus*). These screens identified EvrA, a transcription activator that induces expression of *esrB*, a key virulence regulator. EvrA is directly bound and activated by mannose-6-phosphate (man-6P) derived from actively imported mannose. Mutants lacking EvrA or expressing an EvrA unable to bind man-6P were similarly attenuated in turbot. Exogenously added mannose promoted *E. piscicida* virulence, and high levels of mannose were detected in fish tissue. Together, these observations reveal that binding of a host-derived sugar to a transcription factor can facilitate pathogen sensing of the host environment and trigger virulence programs.

INTRODUCTION

Edwardsiella piscicida (formerly included in *Edwardsiella tarda*) is a Gram-negative facultative intracellular bacterial pathogen that causes edwardsiellosis, a serious systemic infectious disease that afflicts more than 20 species of freshwater and marine fish (Abayneh et al., 2013; Shao et al., 2015; Wang et al., 2009; Yang et al., 2012). This organism is also an opportunistic pathogen of humans, where it can cause gastroenteritis or wound infections and occasionally septicemia (Leung et al., 2012). All close relatives of *E. piscicida*, including *E. tarda*, *E. hoshinae*, *E. ictaluri*, and *E. anguillarum*, also infect farmed fish (Shao et al., 2015). As a result, edwardsiellosis causes severe economic losses in the aquaculture industry worldwide (Park et al., 2012). Moreover, these pathogens are increasingly becoming resistant to multiple antibiotics (Wang et al., 2009), limiting treatment options for the aquaculture industry and highlighting the need for the development of new prevention strategies, including vaccines (Park et al., 2012).

E. piscicida is thought to initiate infection by attaching to the epithelia of its principal host entry sites, the gastrointestinal tract or gills. Subsequently, the organism can survive and proliferate within host cells, particularly phagocytes (Leung et al., 2012), evading innate immune defenses, before causing hemorrhagic septicemia. Like phylogenetically related Enterobacteriaceae bacteria *Salmonella* spp., *E. piscicida* pathogenicity depends on both its type III secretion system (T3SS) and type VI secretion system (T6SS) as well as their distinct sets of effectors in animal models of infection (Chen et al., 2017; Liu et al., 2017; Srinivasa Rao et al., 2004; Zheng and Leung, 2007). Expression of these virulence-associated secretion systems requires a two-component system, EsrA-EsrB, and an AraC family transcriptional regulator EsrC in *Edwardsiella* bacteria (Rogge and Thune, 2011; Zheng et al., 2005). However, there is little knowledge of the environmental factors that trigger activation of these virulence-associated secretion systems or of non-T3/T6SS *E. piscicida* gene products required for fitness during infection or in aquatic environments.

Transposon-insertion site sequencing (TIS) is a potent high-throughput approach for determining the genetic requirements for bacterial fitness in distinct conditions (Chao et al., 2016; Price et al., 2018). Usually, highly saturated transposon mutant libraries are created so that TIS-based screens can provide high-resolution maps of the fitness contributions of individual loci and domains (Chao et al., 2016). However, less complex libraries, e.g., arrayed libraries containing mutants with a single insertion in a known genomic location, can also be useful, particularly when experimental bottlenecks are limiting (Abel et al., 2015; Fu et al., 2013), such as in some animal models of infection. Defined (or arrayed) mutant libraries, which usually

[1]State Key Laboratory of Bioreactor Engineering, East China University of Science and Technology, Shanghai 200237, China

[2]Laboratory for Marine Fisheries Science and Food Production Processes, Qingdao National Laboratory for Marine Science and Technology, Qingdao 266071, China

[3]Shanghai Engineering Research Center of Maricultured Animal Vaccines, Shanghai 200237, China

[4]Division of Infectious Diseases, Brigham and Women's Hospital and Harvard Medical School, Boston, MA 02115, USA

[5]Howard Hughes Medical Institute, Boston, MA 02115, USA

[6]State Key Laboratory of Genetic Engineering, Department of Physiology and Biophysics, School of Life Sciences, Fudan University, Shanghai, 200433, China

[7]Institutes of Biomedical Sciences, Fudan University, Shanghai, 200433, China

[8]Lead Contact

*Correspondence: oaiwqiyao@ecust.edu.cn

https://doi.org/10.1016/j.isci.2019.09.028

contain one or two insertions per gene, have been created for several pathogens and model organisms, e.g., *Pseudomonas aeruginosa* and *Vibrio cholerae* (Cameron et al., 2008; Jacobs et al., 2003; Liberati et al., 2006), and have proved to be of value for screens where bottlenecks constrain the number of mutants that can screened (Fu et al., 2013). Moreover, such defined libraries serve as valuable resources because they often consist of collections of insertion mutants in almost all non-essential loci for an organism of interest.

Here, we created a comprehensive defined transposon mutant library in *E. piscicida* EIB202, a highly pathogenic isolate derived from a moribund turbot (*Scophthalmus maximus*) (Wang et al., 2009). We used pooled subsets of this library to analyze the fitness consequences of >7,000 insertion mutants during growth in media, in phagocytes and *in vivo*. An additional screen of the insertion mutants that had reduced fitness in turbot led to the identification of EvrA (ETAE_ 2071, Edwardsiella virulence regulator A), a transcription factor that directly activates expression of *esrB*, thereby leading to increased T3/T6SS expression (Liu et al., 2017; Zheng et al., 2005). Mannose imported into *E. piscicida* as mannose-6-phosphate (man-6P) binds to EvrA, promoting its activation of *esrB* expression. Moreover, mannose is present in host tissue and elevates *E. piscicida* virulence in fish. Thus, mannose appears to serve as a host-derived cue that activates a genetic circuit facilitating pathogenicity.

RESULTS

Identification of Genes Important for Pathogen Growth in Fish Using a Defined Transposon Insertion Mutant Library

To facilitate genome-scale studies of the fish pathogen *E. piscicida* (formerly included in *E. tarda*) (Wang et al., 2009; Abayneh et al., 2013; Shao et al., 2015), we created a library of transposon mutants, where the site of each insertion was determined. MKGR, a derivative of the mariner transposon *Himar1* (Rubin et al., 1999), was engineered for these studies (Figure 1A). Mutants generated by MKGR insertion should be resistant to gentamicin (Gm) and exhibit mCherry fluorescence, and a subset of mutants, with insertions downstream of active promoters, will be resistant to Km and exhibit GFP fluorescence; this expectation was confirmed experimentally (Figures S1A and 1B).

The MKGR transposon was delivered by conjugation into *E. piscicida* EIB202 (ΔP), an otherwise wild-type (WT) and fully virulent strain cured of the endogenous R plasmid pEIB202 encoding genes resisting to various antibiotics, including chloramphenicol (Cm) (Figures 1A and S2A) (Wang et al., 2009). Individual insertion mutants were manually picked into 96-well plates. The insertion sites of mutants were sequenced and mapped to the EIB202 genome (Figures 1A and S2B–S2E, Tables S1 and S2). A total of 2,806 of the 3,599 predicted coding genes were disrupted with an average of approximately five insertions per gene (Table S1). The 78.0% ORF coverage (2,806/3,599) in the *E. piscicida* defined mutant library is similar to that reported for defined libraries created in other pathogens (Cameron et al., 2008; Gallagher et al., 2007, 2013).

To overcome experimental limitations present with very-high-density transposon libraries, e.g., infection bottlenecks (Chao et al., 2016; Fu et al., 2013), a subset library composed of 7,299 randomly selected mutants, including one or two distinct insertions for each disrupted protein coding gene and intergenic region, was assembled from the set of 20,346 unique insertion mutants (Tables S1, S2, S3, S4, S5, S6, and S7). We compared the fitness consequences of the insertion mutations present in this library after growth in Dulbecco's Modified Eagle's medium (DMEM), murine macrophage-like J774A.1 cells, where *E. piscicida* grows intracellularly (Chen et al., 2017; Liu et al., 2017; Okuda et al., 2009), and in turbot, a natural *E. piscicida* host (Figures 1B–1D) (Wang et al., 2009). The library was grown in LB medium, the source of the "input" for TIS analyses, before inoculation into each condition. Mutant bacteria recovered from DMEM, J774A.1 cells, or turbot livers (the most robustly colonized tissue [Yang et al., 2017]), were used as "outputs" for TIS analyses. In each condition, correlation coefficients of three biological replicates were high (Figure S3), suggesting that these experiments were not severely compromised by infection bottlenecks or other factors that might stochastically limit library complexity.

There was no overlap in the genes categorized as conditionally depleted (fold change [FC] cutoff = 4, $p < 0.05$) after growth in DMEM and J774A.1 cells (Figure 1E) (Tables S8 and S9). Genes encoding the T3SS (e.g., *eseB* and *esaM*) (Liu et al., 2017; Zheng et al., 2005) and T6SS (e.g., *evpC* and *evpI*) (Zheng and Leung, 2007) were not found to be required for growth in DMEM (Figure 1B), even though this medium is known to

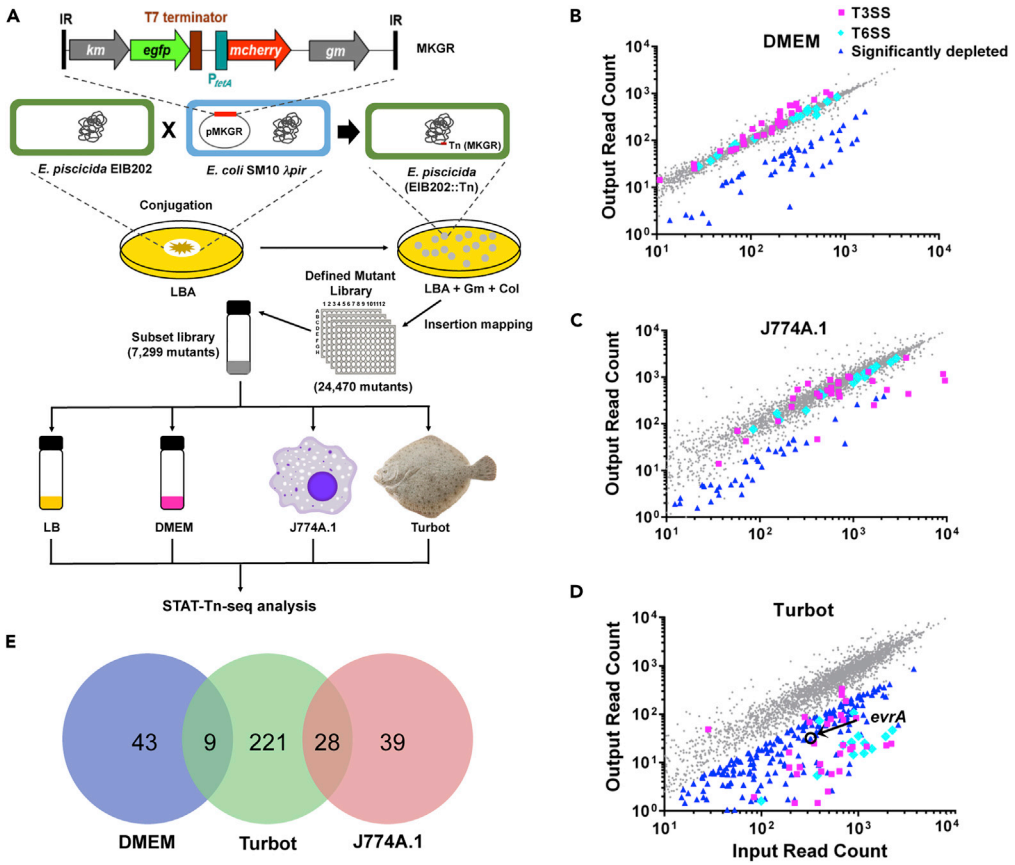

Figure 1. Utilization of a Defined *E. piscicida* Transposon Insertion Mutant Library to Characterize Requirements for Pathogen Growth in Different Environments

(A) Schematic of the MKGR transposon and workflow overview for defined mutant library generation and subsequent TIS analysis.

(B–D) Scatterplots of input (LB grown) and output abundance of transposon insertion mutants after growth in DMEM (B), J774A.1 macrophages (C), and turbot fish (D). Genes with under-representation in the outputs ("significantly depleted"), based on a cutoff of Log_2(Output/Input) (fold change, FC) ≤ -2.0 and $p < 0.05$, are highlighted in blue triangles; the FC of T3SS (pink squares) and T6SS (cyan diamonds) genes are also shown.

(E) Venn diagram depicting conditionally depleted genes from the three conditions tested. There were no depleted genes in common across all conditions.

promote the transcription of T3SS genes (Liu et al., 2017), illustrating the difference between the genetic requirements for growth and the transcriptional reprogramming that may occur in different environments. In fact, insertions in several key activators of T3SS gene expression including *esrC*, *esrA,* and *esrB*, displayed slightly enhanced fitness (FC > 1) in DMEM (Figure 1B), presumably due to reduced metabolic costs associated with production of the T3SS in these mutants (Figure S4A). In contrast to growth in DMEM, *E. piscicida* growth in J774A.1 cells was dependent on several T3SS genes (Figures 1C and 1E, Table S9), revealing the importance of the pathogen's T3SS for macrophage infection. However, T6SS genes did not contribute to the pathogen's fitness within J774.A1 cells (Figure 1C). This observation was confirmed using turbot-derived macrophages and *E. piscicida* strains containing single deletions of *evpP*, *evpC*, or *evpI*, critical T6SS structural genes (Zheng and Leung, 2007); these deletion mutants grew as robustly inside turbot macrophages as the WT strain (Figures S5A and S5B). Thus, the T6SS, which is important for *E. piscicida* growth in turbot (Yang et al., 2017), may primarily promote extracellular growth of the pathogen *in vivo*.

More genes (258) (Table S10) were categorized as conditionally depleted after growth in turbot than in DMEM or macrophages (Figure 1E), consistent with the idea that the pathogen must rely on a broader array of genes to confront the diverse and changing challenges present in fish tissues. Nearly all of *E. piscicida*'s

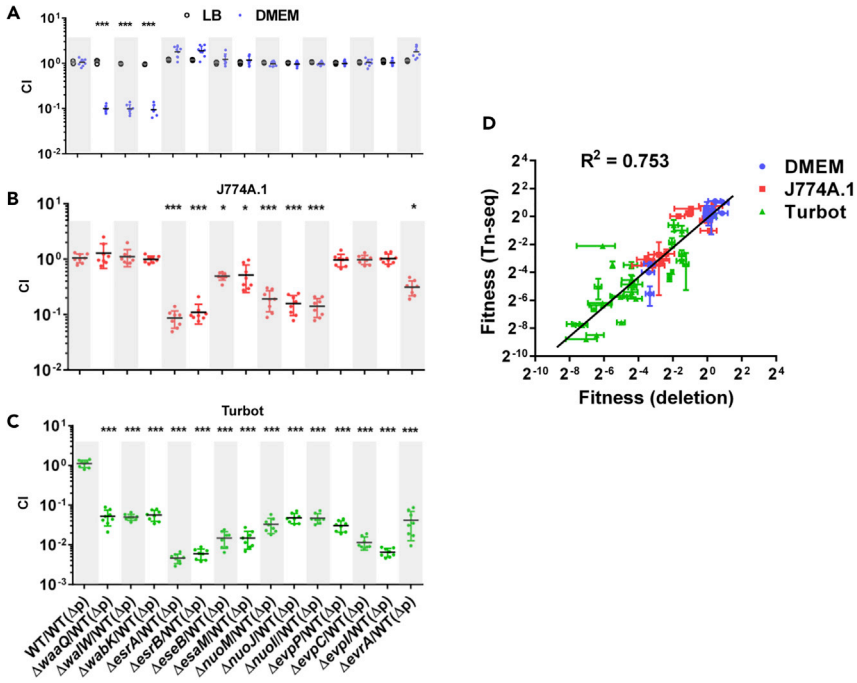

Figure 2. Validation of TIS Studies with Competitive Assays in DMEM, Macrophages, and Turbot

(A–C) Selected in-frame deletion mutants were competed 1:1 versus WT(Δp) in LB and DMEM (A), J774A.1 (B), and turbot fish (C). Competitive indices are shown, and the data presented are mean ± SD from three to nine replicates. *$p < 0.05$, ***$p < 0.001$ based on ANOVA followed by Bonferroni's multiple-comparison post-test to compare the data with the values from the WT/WTΔp competitions.

(D) Correlation of FC values derived from competition experiments with deletion mutants and from the TIS screen (panels A–C). Each point represents the FC value and standard error (SE) for one gene in both screens. In total, 28 deletion mutants were tested in DMEM, J774A.1, and turbot. A linear regression analysis was used to determine the correlation.

genes associated with T3SS (29 of 34) and T6SS (16 of 16) (Figure 1D) were conditionally depleted in turbot, confirming the importance of these pathogenesis-linked secretion systems (Srinivasa Rao et al., 2004; Yang et al., 2017; Zheng and Leung, 2007). A genome-scale comparison highlighted the importance of four gene clusters, encoding LPS (region 1, including *waaG*, *waaQ*, *waaL*, *waaF*, *waaC*, *walW*, *walR*, *wabH*, *wabK* [ETAE_0073–0082]), and NADH dehydrogenase (region 3, including *nuoM*, *nuoJ*, *nuoI*, *nuoF*, *nuoD*, and *nuoA*), in addition to the T3SS (region 2) and the T6SS (region 4), as particularly important for *E. piscicida* growth in turbot (Figure S4B) (Table S11). Region 3 genes were also important for growth in J774A.1 cells, suggesting that the pathogen relies on oxidative phosphorylation for growth inside macrophages as well as in fish. Notably, the largest number (56) of conditionally depleted genes in turbot were of unknown function (Figure S4A); future studies defining the functions of these genes will reveal new aspects of pathogen physiology enabling growth *in vivo*.

Validation of Conditional Depleted Genes

Specific genes from the above-mentioned four regions of interests were chosen (Figure S4B) (*waaQ*, *walW*, *wabK*, *esrA*, *esrB*, *eseB*, *esaM*, *nuoM*, *nuoA*, *nuoI*, *evpP*, *evpC*, and *evpI*) for validation using in-frame deletion mutants. In these experiments, *E. piscicida* ΔP (WT(ΔP)) was mixed 1:1 with each of these mutants and inoculated into LB, DMEM, J774A.1 cells, or turbot in competition assays. In LB, none of the mutants exhibited growth defects, whereas in DMEM, the mutants with insertions in LPS synthesis genes (*waaQ*, *walW*, and *wabK*) were significantly outcompeted by the WT (Figure 2A), mirroring the findings from the screen. Similarly, in the competition experiments in J774A.1 cells and turbot, all insertion mutants that were classified as conditionally depleted in the screens exhibited significant defects in the competition assays (Figures 2B and 2C). Furthermore, the competitive indices found with the *waaQ*, *esrB*, *eseB*, *nuoM*, *evpP*, and *evpI* deletion mutants were similar in J774A.1 cells and turbot primary macrophages (Figure S5B). Thus, the observations from the competition assays strongly correlate with TIS screens. Moreover, there was also an excellent correlation in the fitness measures calculated from the competition and TIS assays

(R^2 = 0.753, Figure 2D). This correlation was calculated using data presented in Figures 2A–2C along with similar data obtained with 16 additional mutants containing in-frame deletions in genes that covered a range of FC values calculated in the TIS screens. The strong correlation over a large range of FC values derived from the TIS and competition experiments with deletion mutants suggests that the genome-scale datasets presented in Figure 1 and Tables S8–S10 constitute a robust resource for *E. piscicida* studies.

Identification and Characterization of *evrA*, an *In Vivo* Virulence Regulator

To identify mutants with defective activation of *E. piscicida*'s T3SS, we individually screened the 258 insertion mutants found to have growth defects in turbot (Table S10) along with 34 mutants displaying auto-aggregation defects when grown in DMEM (Table S12) for their capacities to enter into and proliferate within J774A.1 cells. Although fewer insertion mutants (34 versus 67) showed deficiencies in intracellular growth from this screen as compared with the initial TIS analysis in J774A.1 cells (Tables S9 and S12), most of the mutants that answered this secondary screen (24/34) contained insertions in T3SS-related genes (Table S12). Several of the other mutants had insertions in genes implicated in metabolic processes. One of these genes, ETAE_3493, encodes a homologue of *glnA* (glutamine synthetase), which is known to modulate production of the *E. piscicida* T3SS and to be required for *E. piscicida* pathogenicity (Guan et al., 2018; Yang et al., 2017). We focused our work on another mutant, which contained an insertion in ETAE_ 2071 (hereafter referred to as EvrA for *E*dwardsiella *v*irulence *r*egulator *A*) because this gene had not previously been linked to the pathogen's expression of its T3SS or virulence. Since EvrA bears similarity to the DeoR family of transcriptional regulators, which modulate sugar and nucleotide metabolism in diverse bacteria (Figure S6) (Gaigalat et al., 2007; Ishikawa et al., 2002), we speculated that it could provide insight into the metabolic control of expression of *E. piscicida*'s T3SS. In the initial TIS turbot screen, the *evrA* insertion mutant had an ~8-fold reduced abundance (FC = 0.13, $p < 0.001$) (Figure 1D) and the *evrA* deletion mutant exhibited a competitive defect versus WT(ΔP) in turbot and in J774A.1 cells and turbot macrophages (Figures 2 and S5B), but not in LB or DMEM (Figure 2A). Similarly, assayed on its own, the *evrA* deletion mutant exhibited reduced invasion of and/or proliferation within J774A.1 cells and caused less cytotoxicity as well, and both these defects were complementable (Figures S5C and S5D). Moreover, *evrA* transcript abundance was elevated in turbot relative to DMEM (Figure 3A). Together, these observations suggested that *evrA* may be an *in vivo*-induced regulator of *E. piscicida* virulence.

We next investigated if EvrA promotes expression of the pathogen's T3SS and T6SS. *E. piscicida* aggregates due to the production of EseB, a T3SS apparatus protein, whose expression is directly activated by EsrB, a critical activator of the pathogen's T3SS and T6SS (Gao et al., 2015; Liu et al., 2017; Yin et al., 2018). The *evrA* deletion mutant did not auto-aggregate (Figure 3B) and produced reduced amounts of T3SS and T6SS proteins in cell lysates (Figure S5E) and in cell supernatants (Figures 3B and S5E) as determined by western blot analysis. Reintroduction of *evrA* into Δ*evrA* fully complemented the auto-aggregation and T3/T6SS production defects (Figures 3B and S5E), demonstrating that EvrA augments expression of *E. piscicida*'s T3/T6SS.

In vivo bioluminescence imaging was used to investigate T3SS expression during *E. piscicida* infection of turbot (Yin et al., 2018). A luciferase reporter of P_{eseB} expression was introduced into a neutral position on the chromosome of WT, Δ*evrA* and Δ*evrA* complemented strains, and these strains were inoculated intraperitoneally into turbot. By 8 days post infection (d.p.i.), when luciferase activity was detected in the WT and complemented strains, P_{eseB}-*luc* activity was not detectable in the Δ*evrA* background (Figure 3C). Moreover, there was ~10–16x fewer Δ*evrA* than WT or the complemented strain CFU recovered from infected fish at this time point (Figure 3C). Together, these observations suggest that EvrA contributes to *E. picicida* growth in the host by activation of T3SS and T6SS genes.

EvrA Binds Directly to the *esrB* Promoter to Activate Virulence Gene Expression

To further elucidate how EvrA modulates *E. piscicida* growth *in vivo*, we used RNA sequencing (RNA-seq) to define the EvrA regulon by comparing the transcriptomes of the WT and Δ*evrA* strains. Transcripts of 166 genes were significantly decreased ($\log_2FC < -1$ and $p < 0.05$) and 78 were increased ($\log_2FC > 1$ and $p < 0.05$) in Δ*evrA* compared with the WT (Figure 3D and Table S13). Many genes in the T3/T6SS gene clusters had lower transcript levels in the *evrA* mutant, consistent with the idea that their expression is activated by EvrA (Figure 3D and Table S13). qRT-PCR assays corroborated that transcript levels of established T3SS regulatory genes (*esrA*, *esrB*, and *esrC*), T3SS structural genes (*eseB* and *esaM*), and T6SS gene *evpP* were all reduced in the absence of *evrA* but restored in the complemented strain, Δ*evrA* + pUTt-*evrA*

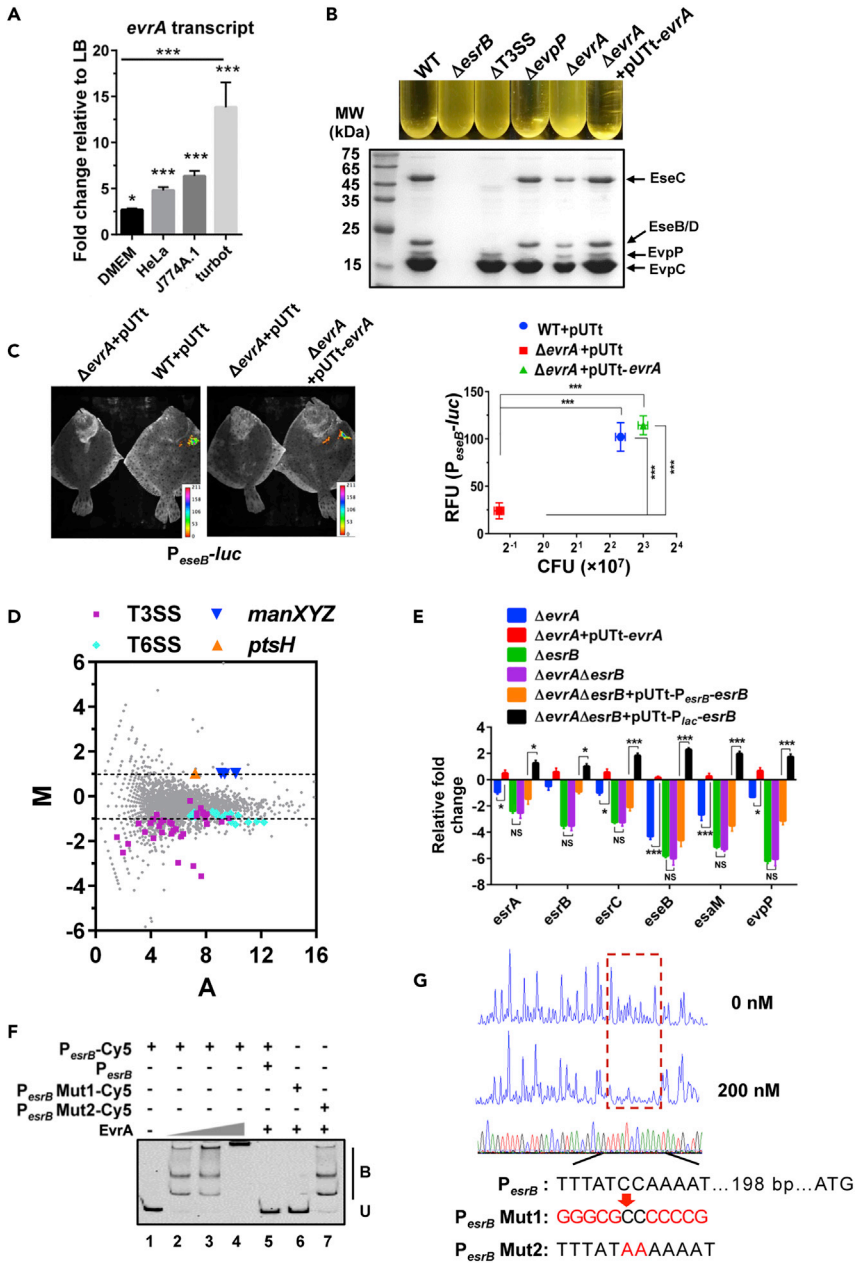

Figure 3. EvrA Regulates *E. piscicida* Virulence

(A) *evrA* transcript levels in WT *E. piscicida* grown in DMEM (12 h), HeLa cells (8 h.p.i.), J774A.1 cells (6 h.p.i.), and turbot liver (8 d.p.i.), relative to that in the bacteria grown in LB for 12 h. *gyrB* was used as an internal housekeeping control. $n = 3$, *, $p < 0.05$; ***, $p < 0.001$ as compared with LB (arbitrarily set as 1) and DMEM based on Student's t test.

(B) Auto-aggregation and extracellular protein (ECP) profiles in the indicated strains.

(C) Expression of *eseB* in turbot and associated CFU burdens; the indicated strains harboring P_{eseB}-*luc* reporter plasmids were inoculated into turbot and luminescence and bacterial burden was measured at 8 d.p.i. ***, $p < 0.001$ based on ANOVA analysis of the relative fluorescence units (RFU) and the bacterial burden ($n = 3$).

(D) Comparison of transcriptomes of WT and Δ*evrA*. The $\log_2$ of the ratio of the abundances of each transcript in Δ*evrA* versus WT (M) was plotted against the average $\log_2$ of the abundance of that transcript in both strains. T3SS, T6SS, and PTS-related genes are highlighted.

(E) qRT-PCR analysis of the transcript levels of indicated T3/T6SS genes in Δ*evrA* and Δ*esrB* strains bearing *evrA* or *esrB* expressing plasmids driven by their native promoters or a constitutive P_{lac} promoter for *esrB*, relative to that in WT. *gyrB* was used as a control. $n = 3$, *$p < 0.05$, ***$p < 0.001$ based on Student's t test.

Figure 3. *Continued*

(F) EMSA of EvrA binding to P_{esrB}. Purified EvrA was added to 20 ng of P_{esrB} or mutant (P_{esrB} Mut1 and P_{esrB} Mut2) Cy5-labeled probes. B, bound DNA; U, unbound DNA.

(G) DNase I footprinting analysis of EvrA binding to a site in the *esrB* promoter (shown in the dashed box). Electropherograms show a DNase I digestion of the P_{esrB} probe after incubation with 0 or 200 nM of EvrA. The corresponding nucleotide sequence (198 bp 5′ of the translational start codon) protected by EvrA is indicated below. The mutant P_{esrB} motifs used for the EMSA in (C) are shown.

(Figure 3E). Levels of these six transcripts were even lower in the Δ*esrB* mutant, but their levels were not reduced further in an Δ*evrA*Δ*esrB* mutant, suggesting that *evrA* acts upstream of and in the same pathway as *esrB*. Introduction of *esrB* driven by its native promoter into the double mutant only partially restored transcript levels, whereas introduction of *esrB* driven by the unrelated *lac* promoter fully restored transcript amounts to WT or greater levels (Figure 3E). Collectively, these findings support the idea that EvrA promotes *esrB* expression.

Electrophoretic mobility shifts assays (EMSAs) using purified EvrA were carried out to begin to test whether EvrA directly regulates *esrB* expression. EvrA bound to a DNA probe that included the upstream region of the *esrB* gene (Figure 3F). The binding site of EvrA in the *esrB* promoter region was defined with a DNase I footprint assay performed on a DNA fragment that encompassed the entire intergenic region between *esrB* and ETAE_0887, the adjacent upstream gene. EvrA protected a region (5′-TTTATCCAAAAT-3′) bearing an AT-rich palindrome structure found 198 bp upstream of the *esrB* start codon (Figure 3G); this AT-rich sequence is similar to the known binding sites for other DeoR family proteins (Gaigalat et al., 2007). Substitution of the AT nucleotides with GC (P_{esrB} Mut1) but not the replacement of CC with AA (P_{esrB} Mut2) abolished the capacity of EvrA to bind to this fragment (Figure 3F), demonstrating that EvrA binds to a distinct site in the *esrB* promoter. These observations are consistent with the idea that EvrA modulates *E. piscicida* virulence gene expression by directly activating EsrB transcription.

Mannose Stimulates *evrA*-Dependent Virulence Gene Activation

DeoR family proteins often modulate sugar utilization (Figure S6) (Anantharaman and Aravind, 2006; Gaigalat et al., 2007; Ishikawa et al., 2002), and the RNA-seq experiment revealed changes in transcript levels of several sugar transport/utilization genes (e.g., *ptsH* and *manXYZ*) in the *evrA* mutant (Figure 3D). After testing various sugars, we found that supplementation of DMEM with mannose, a C-2 epimer of glucose, selectively induced P_{esrB}-*luxAB* reporter expression, even though bacterial growth was similar in all of the fermentable carbohydrates screened (Figures 4A and S7A). Activation of *esrB* promoter activity during growth in mannose required *evrA* (Figures 4A and S7B), suggesting that mannose promotes *evrA*-dependent induction of *esrB* transcription. Consistent with this idea, we found that growth in mannose augmented *evrA*-dependent production of T3/T6SS proteins (Figure 4B).

Chromatin immunoprecipitation (ChIP)-qPCR analyses revealed that EvrA binding to P_{esrB} was greater in cells grown in mannose than in glucose (Figures 4C and S7C), suggesting that mannose can regulate EvrA DNA-binding activity. However, EMSA analysis showed that addition of mannose to EvrA did not modify its binding to the *esrB* promoter region (Figure S7D). We hypothesized that EvrA may be directly responsive to a mannose-derived metabolite instead of the native sugar, as bacterial import systems such as the phosphotransferase system (PTS) couple sugar import to modifications such as phosphorylation. Accordingly, we found that mannose-6-phosphate (man-6P), but not mannose-1-phosphate (man-1P) or GDP-mannose, enhanced EvrA binding to the *esrB* promoter (Figures 4D and S8A–S8D). Electrospray ionization mass spectrometry revealed that purified EvrA forms a folding-dependent complex with man-6P, strongly suggesting that EvrA can directly bind man-6P (Figures 5A and S9).

EvrA shares secondary structure with *Pyrococcus horikoshii* d-ribose-5-phosphate-isomerase (RpiA) (Figure S6F). We performed homology modeling using the known crystal structure of RpiA bound to its ligand (PDB 1LK7) (Ishikawa et al., 2002), to predict how EvrA binds man-6P (Figure 5B). The modeling suggests that EvrA binding to man-6P is dominated by ionic interactions between the phosphate group of the sugar and the sidechain of R221, which protrudes into the binding pocket. The main chain nitrogen atoms of S96 and T97 also likely participate in ligand coordination through hydrogen bonds. Besides R221, two additional arginines were targeted for mutagenesis: R178 from the DeoRC domain, which is predicted to be dispensable for ligand binding, and R7 from the unmodeled HTH domain, which is likely critical for EvrA promoter recognition (Figures 5B, S6D, and S6E).

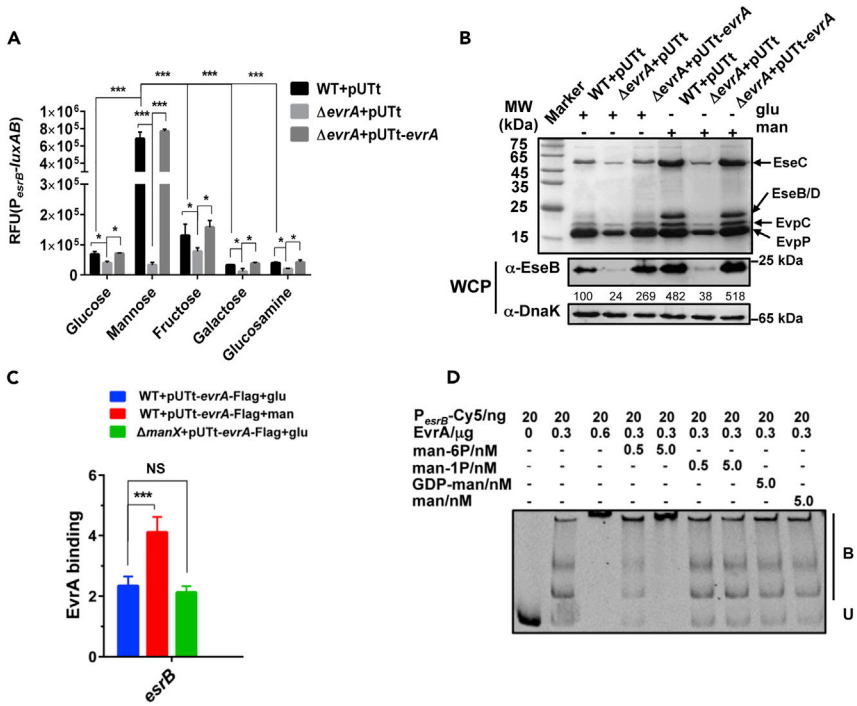

Figure 4. Mannose Promotes EvrA-Dependent Virulence Gene Expression

(A) Chromosomal P_{esrB}-*luxAB* reporter activity in the indicated strains grown for 12 h in DMEM medium supplemented with the 5 mg/mL of indicated sugars. Data shown are the mean ± SEM of results for triplicate assays. *p < 0.05; ***, p < 0.001 based on Student's t test.

(B) ECP profiles (upper panel) and western blot (lower panel) analysis of T3SS protein EseB expression in cell lysates (WCP) of the indicated strains in the presence of 5 mg/mL glucose (glu) or mannose (man). DnaK was used as the loading control. The numbers correspond to densitometry measurements.

(C) ChIP-qPCR analysis of the relative enrichment in P_{esrB} DNA molecules bound to EvrA from cells grown in glucose (glu) or mannose (man). The results are normalized to the control gene *gyrB* as well as to ChIPs from Δ*evrA* + pUTt-Flag cells. ***p < 0.001, t test. NS, not significant.

(D) EMSA of the binding of EvrA to P_{esrB} in the presence of various mannose derivatives. Purified EvrA was mixed with mannose-6-phosphate (man-6P), mannose-1-phosphate (man-1P), GDP-man, or man and then added to 20 ng of Cy5-labeled P_{esrB} probe. B, bound DNA; U, unbound DNA.

Biophysical characterization of man-6P-EvrA binding by isothermal titration calorimetry indicated that the complex forms at a micromolar K_d (22.5 μM) with a 1:1 stoichiometry, comparable with other known DeoR-ligand interactions (Figure S8A) (Ishikawa et al., 2002). Alanine substitutions at R221, but not the predicted DNA-contacting R7 or the neutral R178, substantially eliminated man-6P binding to EvrA (Figures S8E–S8G), supporting the role of the R221 in coordinating ligand binding (Figure 5B). The binding studies were corroborated with EMSA-based binding analyses. Man-6P stimulated binding of WT and R178A EvrA to P_{esrB} (Figure 5C) but did not modify binding of the R7A or R221A forms of the protein, presumably because of the loss of their DNA or ligand recognition capacities, respectively (Figures 5C and S8H). The reasons why $EvrA^{R221A}$ bound the P_{esrB} probe with lower apparent affinity than the WT protein (Figure S8H) are not known, but it is possible that the WT protein may co-purify with bound man-6P. Next, we expressed the mutant EvrA proteins in *E. piscicida* (Figure S10A) to test their function in cells. Only *E. piscicida* strains expressing EvrA or $EvrA^{R178A}$ led to auto-aggregation (Figure S10B) and exhibited mannose augmentation of *esrB* expression and EseB production (Figures 5D, 5E, and S10C). Thus, EvrA's capacity to bind man-6P and DNA appear to be critical for the protein to promote virulence gene expression.

We speculated that EvrA might also play a role in mannose uptake because the transcriptomic data suggested that EvrA modestly represses *manX* (FC ~ 2) (Figure 3D and Table S13), a component of the mannose-specific PTS, which imports mannose into the cell (Erni et al., 1987). Growth of WT *E. piscicida* in mannose augmented *evrA* expression but decreased *manX* expression, suggestive of negative feedback

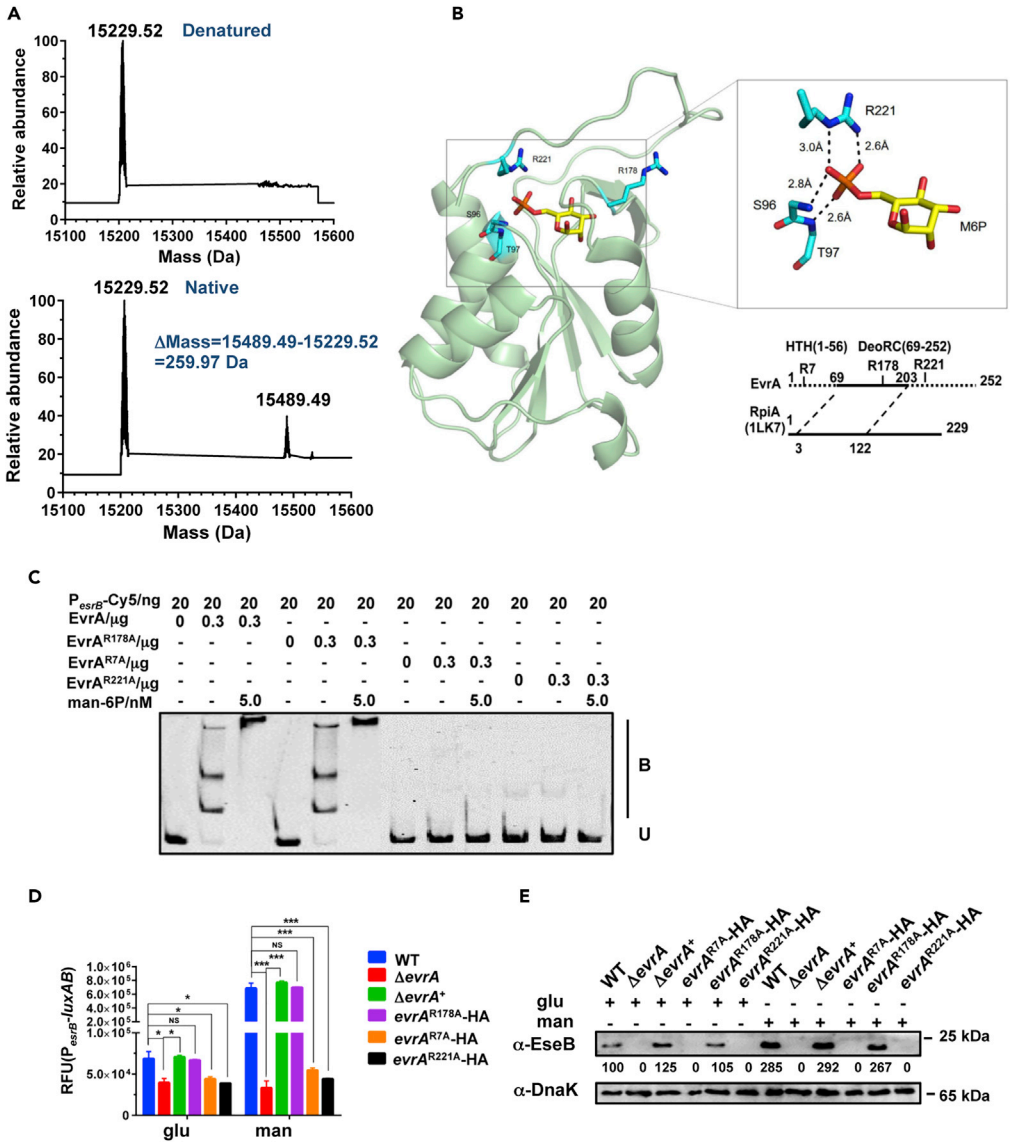

Figure 5. Mannose-6-Phosphate (man-6P) Binding to EvrA Enhances *esrB* Expression

(A) Electrospray ionization mass spectrometry of native and denatured EvrA C-domain complex with man-6P.

(B) Structural model of EvrA interacting with an *in silico*-docked man-6P based on homology alignment to the D-ribose-5-phosphate isomerase RpiA (PDB_ID: 1LK7) (Ishikawa et al., 2002). The ligand M6P and residues involved in the interaction, as well as R178 were highlighted as sticks with C atoms colored in yellow and cyan (P, orange; N, blue; O, red), respectively.

(C) EMSA of binding of WT or mutant EvrA to P_{esrB} in the presence of man-6P. Purified EvrA or its variants mixed with man-6P and 20 ng of Cy5-labeled P_{esrB} probe were added to the EMSA reactions. B, bound DNA; U, unbound DNA.

(D) Chromosomal P_{esrB}-*luxAB* reporter activity in the indicated strains grown for 12 h in DMEM medium supplemented with glucose or mannose. Data shown are the mean ± SEM of results for triplicate assays. *p < 0.05; ***, p < 0.001 based on Student's t test. NS, not significant.

(E) Western blot analysis of T3SS protein EseB expression in cell lysates of the indicated strains in the presence of glucose or mannose. DnaK was used as the loading control.

(Figure S7E). Consistent with the RNA-seq data, the Δ*evrA* mutant had higher levels of *manX* transcripts than the WT grown in mannose as well as in glucose, suggesting that EvrA represses *manX* expression (Figure S7E). Since EvrA binds to the *manX* promoter region via an AT-rich palindrome (Figure S7F), these findings suggest that EvrA directly represses the *manXYZ* operon. Collectively, these observations are

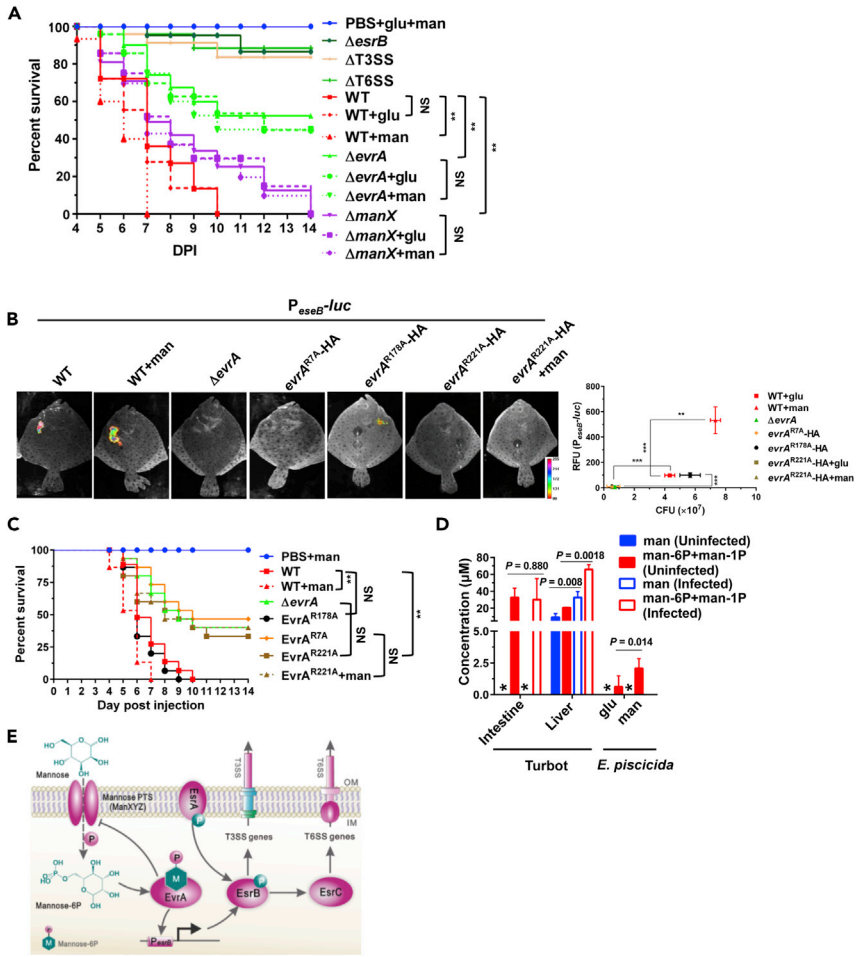

Figure 6. Mannose Promotes *E. piscicida* pathogenicity in an EvrA-Dependent Manner

(A) Survival curves of turbot challenged with the indicated strains. Phosphate-buffered saline (PBS, pH 7.4) supplemented with 5 mg/mL glucose and mannose was used as a control. The bacterial strains were suspended in PBS with or without 5 mg/mL glucose or mannose and injected into each turbot at a dose of 2.0×10^4 CFU/fish ($n = 30$ fish/group). Kaplan-Meier survival analysis with a log rank test is shown. **, $p < 0.001$; NS, not significant, $p > 0.05$.

(B) *In vivo* P_{eseB}-*luc* plasmid reporter activity and associated liver CFU burden at 8 d.p.i. from fish inoculated with the indicated strains. ***, $p < 0.001$ based on ANOVA analysis of the relative fluorescence units (RFU) and the bacterial burden ($n = 3$).

(C) Survival curves of turbot challenged with the indicated strains. PBS supplemented with 5 mg/mL mannose was used as a control; otherwise these data were acquired and analyzed identically to that in (A).

(D) Mannose (blue) and man-6P/man-1P (red) levels in extracts from turbot intestines or livers before (filled) or after (open) infection with WT *E. piscicida* (left) and in WT *E. piscicida* grown in DMEM supplemented with glucose or mannose (right). Mean ± SE from five fish or three bacterial samples are shown; there was no detectable mannose in the intestine of turbot or in *E. piscicida*, which is indicated by *, below detection limit. p Values are calculated based on unpaired two-tailed Student's t test.

(E) Schematic of *E. piscicida* mannose responsive virulence gene regulatory circuit.

consistent with the idea that EvrA directly represses *manX* expression, potentially creating a negative feed-back loop dampening mannose-induced, *evrA*-dependent induction of *esrB* expression (Figure S4C).

Mannose Augments *E. piscicida* Virulence in an *evrA*-Dependent Manner

Finally, we investigated the roles of *evrA*, *manX*, and mannose in *E. piscicida* virulence in turbot. As shown previously, the Δ*esrB*, ΔT3SS, and ΔT6SS mutant strains were highly attenuated and ~90% of fish remained alive at 14 d.p.i (Figure 6A) (Yin et al., 2018). The Δ*evrA* and Δ*manX* mutants were also attenuated with a median survival time of over 14 and 7 days, respectively (Figure 6A). More than 50% of fish survived infection

with the Δ*evrA* mutant, and although no animals survived infection with the Δ*manX* mutant, these animals survived longer than animals infected with the WT strain ($p = 0.0038$, Figure 6A). These observations are congruent with the diminished *in vivo* fitness of both the *evrA* (FC = 0.13) and *manX* (FC = 0.24) transposon mutants observed in the TIS screen (Table S10) and demonstrate that *evrA* and *manX* contribute to *E. piscicida* virulence.

Co-inoculation of the WT strain with mannose (5 mg/mL), but not glucose (5 mg/mL), accelerated the mortality of the fish ($p = 0.0045$, Figure 6A), consistent with the prior observation in carp that elevated tissue mannose, and man-6P levels are correlated with lethal *E. tarda* infection Guo et al., 2014. In contrast, co-inoculation of the Δ*evrA* or Δ*manX* strains in mannose or glucose did not alter the kinetics of fish survival ($p > 0.05$, Figure 6A). Mannose supplementation also led to increased expression of *eseB in vivo* and greater *E. piscicida* proliferation (Figure 6B). In this assay, strains expressing the *evrA* mutants that were incapable of mannose-stimulated *esrB* expression in culture ($EvrA^{R221A}$ and $EvrA^{R7A}$) phenocopied the *evrA* deletion mutant (Figure 6B). Similarly, strains expressing these non-functional EvrA mutants were as attenuated *in vivo* as the strain lacking *evrA* (Figure 6C); in contrast, the strain expressing the mannose-response *evrA* mutant ($EvrA^{R178A}$) killed fish with similar kinetics as the WT.

The observation that $EvrA^{R221A}$ phenocopied the Δ*evrA* strain, even in the absence of mannose supplementation, suggests that during infection, the EvrA ligand is present and detected by EvrA. Mannose and mannose phosphates (man-6P and man-1P) were found at micromolar levels in the intestines and livers of uninfected turbot (Figure 6D). Consistent with their micromolar presence *in vivo*, man-6P/man-1P accumulated to micromolar levels in *E. piscicida* grown in mannose-supplemented cultures, suggesting that the ligand of EvrA (but not its precursor) can naturally accumulate in the intracellular bacterial space (Figure 6D). Furthermore, levels of mannose and man-6P/man-1P were greater in livers from infected fish than those in naive fish, suggesting that *E. piscicida* growth *in vivo* may stimulate host production of this sugar. Moreover, *esrB* expression could be efficiently activated by mannose concentrations detected *in vivo* (20–200 μM, Figure S11). These findings are consistent with the idea that mannose stimulation of EvrA-dependent induction of virulence gene expression can promote *E. piscicida* pathogenicity during infection and that exposure to host mannose can prime *E. piscicida*'s virulence.

DISCUSSION

E. piscicida and closely related *Edwardsiella* species are important fish pathogens that inflict great damage on the aquaculture industry globally. These facultative intracellular organisms are particularly compelling for pathogenesis studies because their virulence depends on both T3SS and T6SS (Srinivasa Rao et al., 2004; Yang et al., 2017; Zheng and Leung, 2007). The defined *E. piscicida* transposon mutant library (Tables S1 and S2) and the resulting genome-scale datasets representing the genetic requirements for the pathogen's growth in DMEM, J774A.1 cells, and fish (Tables S8–S10, Figure S4C) presented here should provide a valuable resource for future analyses of this pathogen's virulence and functional genomics. There was a remarkable congruence in the observations derived from the three TIS screens and in studies using 28 deletions mutants (Figure 2), including in the magnitudes of the calculated fitness defects for both insertion and deletion mutants, suggesting that the findings from the screens are robust. Besides confirming the importance of the *E. piscicida* T3/T6SS for turbot growth, our findings delineated many metabolic pathways that the organism depends on to proliferate during infection (Figure S4C) and revealed a new positive regulator of virulence, EvrA.

The genes found to facilitate *E. piscicida* fitness in the DMEM, J774A.1, and turbot screens were largely distinct, reflecting the manifold differences in these conditions. The genes enabling robust growth in J774A.1 cells and in DMEM did not overlap, and only 28/67 genes facilitating growth in these murine macrophage-like cells were scored as important for fitness in turbot (Figures 1E and S4C). Furthermore, there were nearly 4x as many genes required for fitness in turbot than in J774A.1 cells, illustrating the more diverse demands imposed by an intact host versus the intracellular milieu. The 230 genes facilitating growth in turbot but not J774A.1 cells enable both extracellular and intracellular growth *in vivo*; furthermore, the pathogen may proliferate within more than one cell type *in vivo* (Hu et al., 2019). Entry into and growth within J774A.1 cells and turbot macrophages required *E. piscicida's* T3SS but not its T6SS, even though both secretion systems are required *in vivo*. Thus, the organism may rely on its T6SS primarily for extracellular growth in fish where it may facilitate competition with tissue-resident microbiota to support pathogen colonization (Anderson et al., 2017; Fu et al., 2018; Zhao et al., 2018).

The utility of the defined mutant library is underscored by the secondary screen that led to the rapid identification of EvrA, a new regulator of *E. piscicida* virulence. EvrA acts upstream of the master virulence regulator EsrB to influence the expression of both the T3SS and T6SS, while also likely coordinating a negative feedback loop with its ligand, man-6P, to fine-tune its activity (Figure 6E). We found that EvrA is specifically activated by man-6P, the cytosolic form of mannose imported by the PTS, and that mannose is found in the tissues of *E. piscicida*'s host. Our discovery of the EvrA-man-6P regulatory axis suggests that specific carbohydrates may be co-opted as signaling intermediaries between host and microbe in addition to their known roles as substrates for metabolism (Bäumler and Sperandio, 2016; Olive and Sassetti, 2016). For example, availability of fucose in the mammalian intestine acts as a spatial cue for virulence regulation in enterohemorrhagic *Escherichia coli* (Pacheco et al., 2012). Additionally, the conservation of EvrA in other virulent microbes, including the close relative *Salmonella enterica* (Figure S6), suggests that directly coupling detection of host sugars to virulence regulation may be a common theme in bacterial pathogenesis.

We posit that mannose detection by *E. piscicida* can be used both to regulate its virulence and to support its metabolism, although the exact contribution of host mannose to bacterial growth *in vivo* remains to be determined. In the proposed model, EvrA serves as a "metabolic switch" that links availability of a specific nutrient to activation of the virulence program (Figure 6E). Although it is not clear whether mannose is present outside the host, upregulation of host-specific colonization factors such as the T3SS would suggest it may serve as a host niche-specific signal. Future analysis of additional transposon libraries in *E. piscicida* strains lacking EvrA will enable additional understanding of the pathogen's metabolic priorities and whether other sugars may play complementary roles to mannose in virulence regulation. This work deepens our understanding of how bacterial pathogens can unite sugar availability and virulence regulation and establishes a framework for future studies that employ high-throughput genetics to dissect the metabolic cross talk between pathogen and host.

Limitations of the Study

The principal limitation of the study is that we were unable to obtain structural data that confirmed direct binding of man-6P to EvrA. Crystallization of the EvrA-man-6P complex proved extremely difficult because purified EvrA is prone to precipitation. Co-expression of protein tags, chaperones, or protein truncations may circumvent these issues and facilitate the future structural and biochemical analysis of EvrA and EvrA-man-6P complex.

METHODS

All methods can be found in the accompanying Transparent Methods supplemental file.

SUPPLEMENTAL INFORMATION

Supplemental Information can be found online at https://doi.org/10.1016/j.isci.2019.09.028.

ACKNOWLEDGMENTS

This work was supported by grants from the National Key Research and Development Program of China (2018YFD0900504 to Q.W.), National Natural Science Foundation of China (31430090 to Y.Z., 31602200 to X.L.), Ministry of Agriculture of China (CARS-47), and the Science and Technology Commission of Shandong and Shanghai Municipality (2017CXGC0103 and 17391902000). B.S. is supported by the Natural Sciences and Engineering Council of Canada (PGSD3-487259-2016). M.K.W. is supported by the Howard Hughes Medical Institute (HHMI) (CC30430) and the National Institutes of Health (RO1-AI-042347).

AUTHOR CONTRIBUTIONS

Conceptualization, L.W. and Q.W.; Investigation, L.W., H.Q., K.Y., G.Y., R.M., J.M., C.Y., J.Y., Y.M., J.X., and X.L.; Writing – Original Draft, L.W. and B.S.; Writing – Review & Editing, Y.Z., Q.W., and M.K.W.; Funding Acquisition, Q.W., B.S., and M.K.W. All authors edited and agreed on the final version.

DECLARATION OF INTERESTS

The authors declare no competing interests.

Received: May 13, 2019
Revised: August 19, 2019
Accepted: September 20, 2019
Published: October 25, 2019

REFERENCES

Abayneh, T., Colquhoun, D.J., and Sørum, H. (2013). *Edwardsiella piscicida sp. nov.*, a novel species pathogenic to fish. J. Appl. Microbiol. *114*, 644–654.

Abel, S., Abel zur Wiesch, P., Chang, H.H., Davis, B.M., Lipsitch, M., and Waldor, M.K. (2015). Sequence tag-based analysis of microbial population dynamics. Nat. Methods *12*, 223–226.

Anantharaman, V., and Aravind, L. (2006). Diversification of catalytic activities and ligand interactions in the protein fold shared by the sugar isomerases, eIF2B, DeoR transcription factors Acyl-CoA transferases and methenyltetrahydrofolate synthetase. J. Mol. Biol. *356*, 823–842.

Anderson, M.C., Vonaesch, P., Saffarian, A., Marteyn, B.S., and Sansonetti, P.J. (2017). *Shigella sonnei* encodes a functional T6SS used for interbacterial competition and niche occupancy. Cell Host Microbe *21*, 769–776.

Bäumler, A.J., and Sperandio, V. (2016). Interactions between the microbiota and pathogenic bacteria in the gut. Nature *535*, 85–93.

Cameron, D.E., Urbach, J.M., and Mekalanos, J.J. (2008). A defined transposon mutant library and its use in identifying motility genes in *Vibrio cholerae*. Proc. Natl. Acad. Sci. U S A *105*, 8736–8741.

Chao, M.C., Abel, S., Davis, B.M., and Waldor, M.K. (2016). The design and analysis of transposon insertion sequencing experiments. Nat. Rev. Microbiol. *14*, 119–128.

Chen, H., Yang, D.H., Han, F.J., Tan, J.C., Zhang, L.Z., Xiao, J.F., Zhang, Y.X., and Liu, Q. (2017). The bacterial T6SS effector EvpP prevents NLRP3 inflammasome activation by inhibiting the Ca^{2+}-dependent MAPK-Jnk pathway. Cell Host Microbe *21*, 47–58.

Erni, B., Zanolari, B., and Kocher, H.P. (1987). The mannose permease of *Escherichia coli* consists of three different proteins. J. Biol. Chem. *262*, 5238–5247.

Fu, Y., Waldor, M.K., and Mekalanos, J.J. (2013). Tn-Seq analysis of *Vibrio cholerae* intestinal colonization reveals a role for T6SS-mediated antibacterial activity in the host. Cell Host Microbe *14*, 652–663.

Fu, Y., Ho, B.T., and Mekalanos, J.J. (2018). Tracking *Vibrio cholerae* cell-cell interactions during infection reveals bacterial population dynamics within intestinal microenvironments. Cell Host Microbe *23*, 274–281.

Gaigalat, L., Schlüter, J.P., Hartmann, M., Mormann, S., Tauch, A., Pühler, A., and Kalinowski, J. (2007). The DeoR-type transcriptional regulator SugR acts as a repressor for genes encoding the phosphoenolpyruvate:sugar phosphotransferase system (PTS) in *Corynebacterium glutamicum*. BMC Mol. Biol. *8*, 104.

Gallagher, L.A., Ramage, E., Jacobs, M.A., Kaul, R., Brittnacher, M., and Manoil, C. (2007). A comprehensive transposon mutant library of *Francisella novicida*, a bioweapon surrogate. Proc. Natl. Acad. Sci. U S A *104*, 1009–1014.

Gallagher, L.A., Ramage, E., Patrapuvich, R., Weiss, E., Brittnacher, M., and Manoil, C. (2013). Sequence-defined transposon mutant library of *Burkholderia thailandensis*. MBio *4*, e604–e613.

Gao, Z.P., Nie, P., Lu, J.F., Liu, L.Y., Xiao, T.Y., Liu, W., Liu, J.S., and Xie, H.X. (2015). Type III secretion system translocon component EseB forms filaments on and mediates autoaggregation of and biofilm formation by *Edwardsiella tarda*. Appl. Environ. Microbiol. *81*, 6078–6087.

Guan, Y., Yin, K.Y., Zhou, M., Yang, M., Zhang, Y.X., Liu, X.H., and Wang, Q.Y. (2018). EsrB negatively regulates expression of the glutamine synthetase GlnA in the fish pathogen *Edwardsiella piscicida*. FEMS Microbiol. Lett. *365*, fny007.

Guo, C., Huang, X.Y., Yang, M.J., Wang, S., Ren, S.T., Li, H., and Peng, X.X. (2014). GC/MS-basedmetabolomics approach to identify biomarkers differentiating survivals from death in cruciancarps infected by Edwardsiella tarda. Fish Shellfish Immunol. *39*, 215–222.

Hu, T., Zhang, L., Wang, W., Yang, D., Xiao, J., Zhang, Y., Liu, X., and Liu, Q. (2019). *Edwardsiella piscicida* enters nonphagocytic cells via a macropinocytosis-involved hybrid mechanism. J. Bacteriol. *201*, e00548–18.

Ishikawa, K., Matsui, I., Payan, F., Cambillau, C., Ishida, H., Kawarabayasi, Y., Kikuchi, H., and Roussel, A. (2002). A hyperthermostable D-ribose-5-phosphate isomerase from *Pyrococcus horikoshii* characterization and three-dimensional structure. Structure *10*, 877–886.

Jacobs, M.A., Alwood, A., Thaipisuttikul, I., Spencer, D., Haugen, E., Ernst, S., Will, O., Kaul, R., Raymond, C., Levy, R., et al. (2003). Comprehensive transposon mutant library of *Pseudomonas aeruginosa*. Proc. Natl. Acad. Sci. U S A *100*, 14339–14344.

Leung, K.Y., Siame, B.A., Tenkink, B.J., Noort, R.J., and Mok, Y. (2012). *Edwardsiella tarda* – virulence mechanisms of an emerging gastroenteritis pathogen. Microbes Infect. *14*, 26–34.

Liberati, N.T., Urbach, J.M., Miyata, S., Lee, D.G., Drenkard, E., Wu, G., Villanueva, J., Wei, T., and Ausubel, F.M. (2006). An ordered, nonredundant library of *Pseudomonas aeruginosa* strain PA14 transposon insertion mutants. Proc. Natl. Acad. Sci. U S A *103*, 2833–2838.

Liu, Y., Zhao, L.Y., Yang, M.J., Yin, K.Y., Zhou, X.H., Leung, K.Y., Liu, Q., Zhang, Y.X., and Wang, Q.Y. (2017). Transcriptomic dissection of the horizontally acquired response regulator EsrB reveals its global regulatory roles in the physiological adaptation and activation of T3SS and the cognate effector repertoire in *Edwardsiella piscicida* during infection toward turbot. Virulence *8*, 1355–1377.

Okuda, J., Kiriyama, M., Suzaki, E., Kataoka, K., Nishibuchi, M., and Nakai, T. (2009). Characterization of proteins secreted from a type III secretion system of *Edwardsiella tarda* and their roles in macrophage infection. Dis. Aquat. Organ. *84*, 115–121.

Olive, A.J., and Sassetti, C.M. (2016). Metabolic crosstalk between host and pathogen: sensing, adapting and competing. Nat. Rev. Microbiol. *14*, 221–234.

Pacheco, A.R., Curtis, M.M., Ritchie, J.M., Munera, D., Waldor, M.K., Moreira, C.G., and Sperandio, V. (2012). Fucose sensing regulates bacterial intestinal colonization. Nature *492*, 113–117.

Park, S.B., Aoki, T., and Jung, T.S. (2012). Pathogenesis of and strategies for preventing *Edwardsiella tarda* infection in fish. Vet. Res. *43*, 67.

Price, M.N., Wetmore, K.M., Waters, R.J., Callaghan, M., Ray, J., Liu, H., Kuehl, J.V., Melnyk, R.A., Lamson, J.S., Suh, Y., et al. (2018). Mutant phenotypes for thousands of bacterial genes of unknown function. Nature *557*, 503–509.

Rogge, M.L., and Thune, R.L. (2011). Regulation of the *Edwardsiella ictaluri* type III secretion system by pH and phosphate concentration through EsrA, EsrB, and EsrC. Appl. Environ. Microbiol. *77*, 4293–4302.

Rubin, E.J., Akerley, B.J., Novik, V.N., Lampe, D.J., Husson, R.N., and Mekalanos, J.J. (1999). *In vivo* transposition of mariner-based elements in enteric bacteria and mycobacteria. Proc. Natl. Acad. Sci. U S A *96*, 1645–1650.

Shao, S., Lai, Q.L., Liu, Q., Wu, H.Z., Xiao, J.F., Shao, Z.Z., Wang, Q.Y., and Zhang, Y.X. (2015). Phylogenomics characterization of a highly virulent *Edwardsiella* strain ET080813^T encoding two distinct T3SS and three T6SS gene clusters: propose a novel species as *Edwardsiella anguillarum* sp. nov. Syst. Appl. Microbiol. *38*, 36–47.

Srinivasa Rao, P.S., Yamada, Y., Tan, Y.P., and Leung, K.Y. (2004). Use of proteomics to identify

novel virulence determinants that are required for *Edwardsiella tarda* pathogenesis. Mol. Microbiol. *53*, 573–586.

Wang, Q.Y., Yang, M.J., Xiao, J.F., Wu, H.Z., Wang, X., Lv, Y.Z., Xu, L.L., Zheng, H.J., Wang, S.Y., Zhao, G.P., et al. (2009). Genome sequence of the versatile fish pathogen *Edwardsiella tarda* provides insights into its adaptation to broad host ranges and intracellular niches. PLoS One *4*, e7646.

Yang, M.J., Lv, Y.Z., Xiao, J.F., Wu, H.Z., Zheng, H.J., Liu, Q., Zhang, Y.X., and Wang, Q.Y. (2012). *Edwardsiella* comparative phylogenomics reveal the new intra/inter-species taxonomic relationships, virulence evolution and niche adaptation mechanisms. PLoS One *7*, e36987.

Yang, G.H., Billings, G., Hubbard, T.P., Park, J.S., Leung, K.Y., Liu, Q., Davis, B.M., Zhang, Y.X., Wang, Q.Y., and Waldor, M.K. (2017). Time-resolved transposon insertion sequencing reveals genome-wide fitness dynamics during infection. MBio *8*, e1517–e1581.

Yin, K.Y., Guan, Y.P., Ma, R.Q., Wei, L.F., Liu, B., Liu, X.H., Zhou, X.S., Ma, Y., Zhang, Y.X., Waldor, M.K., and Wang, Q.Y. (2018). Critical role for a promoter discriminator in RpoS control of virulence in *Edwardsiella piscicida*. PLoS Pathog. *14*, e1007272.

Zhao, W., Caro, F., Robins, W., and Mekalanos, J.J. (2018). Antagonism toward the intestinal microbiota and its effect on *Vibrio cholerae* virulence. Science *359*, 210–213.

Zheng, J., and Leung, K.Y. (2007). Dissection of a type VI secretion system in *Edwardsiella tarda*. Mol. Microbiol. *66*, 1192–1206.

Zheng, J., Tung, S.L., and Leung, K.Y. (2005). Regulation of a type III and a putative secretion system in *Edwardsiella tarda* by EsrC is under the control of a two-component system, EsrA-EsrB. Infect. Immun. *73*, 4127–4137.

ISCI, Volume *20*

Supplemental Information

A Bacterial Pathogen Senses Host Mannose to Coordinate Virulence

Lifan Wei, Haoxian Qiao, Brandon Sit, Kaiyu Yin, Guanhua Yang, Ruiqing Ma, Jiabao Ma, Chun Yang, Jun Yao, Yue Ma, Jingfan Xiao, Xiaohong Liu, Yuanxing Zhang, Matthew K. Waldor, and Qiyao Wang

Supplemental Materials

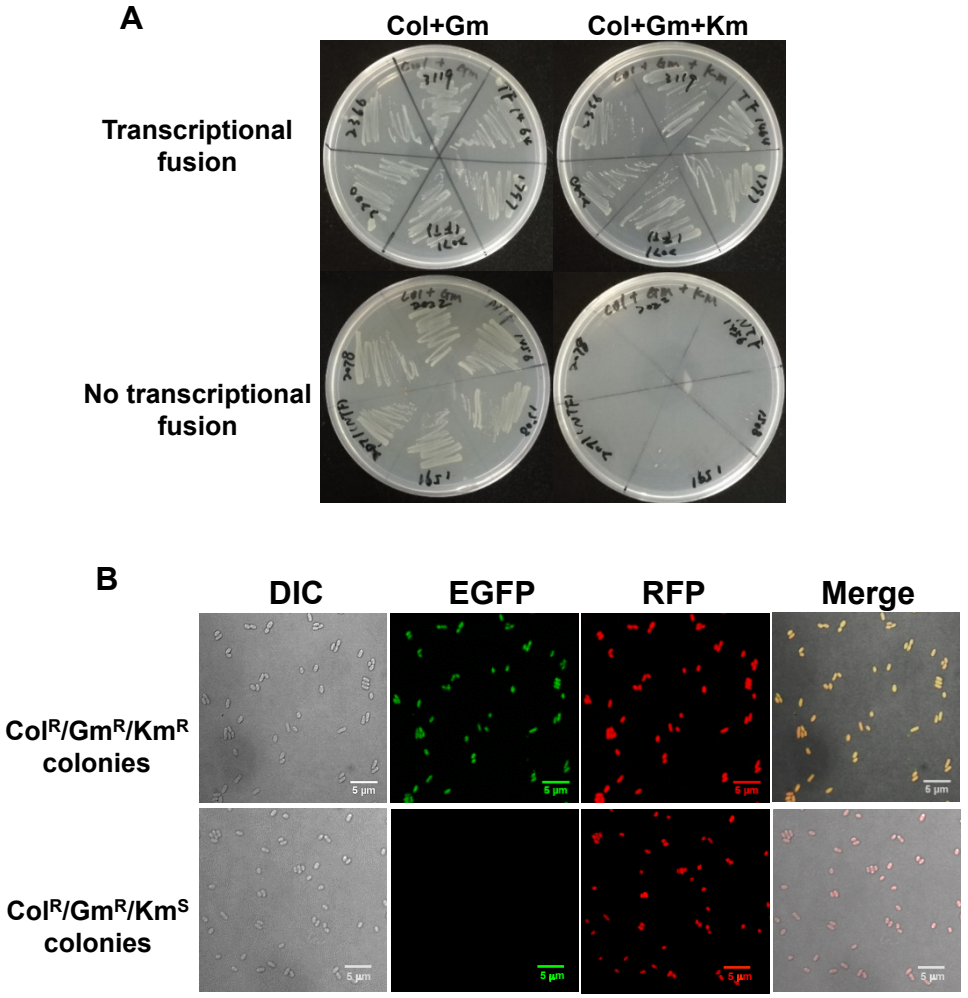

Supplemental Figure S1. Validation of the properties of the MKGR transposon insertion mutants. Related to Figure 1. **(A)** Antibiotic resistance of 6 insertion mutants (ETAE_1464, ETAE_1797 (*hemR*), ETAE_2071 (*evrA*), ETAE_2200, ETAE_2366 (*hybA*), and EATE_3119) that are predicted to generate active transcriptional fusions and 6 insertion mutants (ETAE_1456 (*yoaA*), ETAE_1508 (*adhE*), ETAE_1591 (*gloA*), ETAE_2071 (*evrA*), ETAE_2078, and ETAE_2022) that do not create transcriptional fusions. The 6 insertions creating transcriptional fusions are resistant to Km as well as Col and Gm, whereas the latter 6 are not resistant to Km. **(B)** Detection of GFP and RFP fluorescence in Km^R and Km^S Tn insertion mutants. Scale bar represents 5 µM.

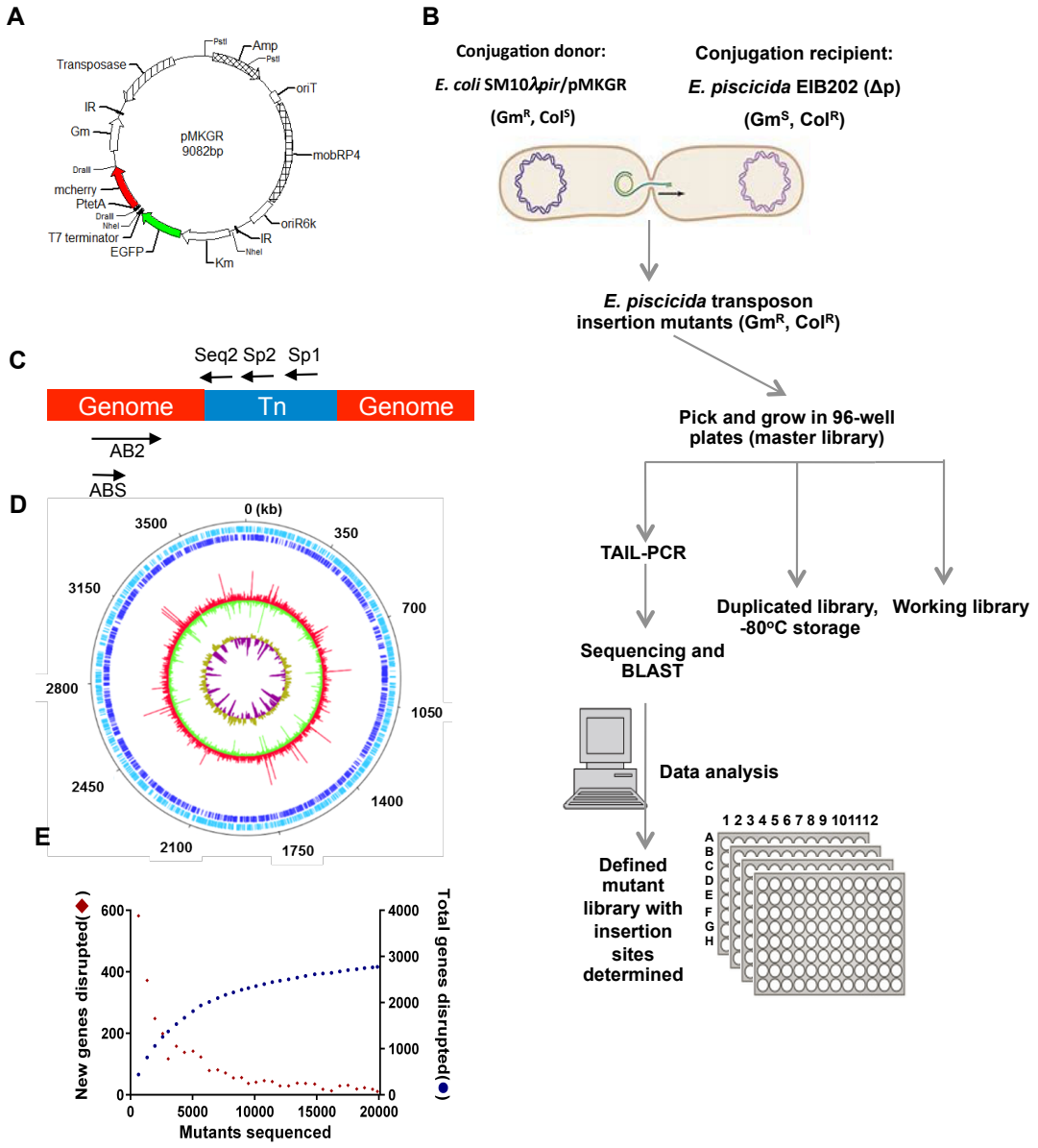

Supplemental Figure S2. Work flow for construction of the defined mutant library.

Related to Figure 1. **(A)** Vector map of pMKGR. **(B)** *E. coli* SM10 λ*pir* and *E. piscicida* EIB202 (ΔP) were used as the conjugation donor and recipient strains, respectively. To determine the transposon insertion sites, TAIL-PCRs were performed to amplify the junctions of the genome and transposon and the PCR products were sequenced and analyzed. The mutants were re-arrayed into different subset libraries for various screens. The master libraries and the subset libraries were duplicated for -80°C storage or as working libraries. **(C)** Schematic of TAIL-PCR amplification used for determination of the transposon insertion sites. The primer pair Sp1/AB2 was used for the first round of PCR and the primer pair Sp2/ABS was used for second round of PCR. The Seq2 primer was used for sequencing of the amplification products. **(D)** Distribution of mapped transposon insertions on the *E. piscicida* chromosome. The most

outward circle represents the genes encoded in the two strands of DNA. The second circle displays the distribution of the transposon insertions, with the red and green bars representing the forward and reverse orientation of insertions within genes, respectively. The inner purple and olive circles corresponded to TA and GC contents on genome, respectively. **(E)** Sequencing saturation plot of the defined mutant library. The number of new ORFs disrupted (brown diamonds) and the total number of ORFs disrupted in the library (blue circles) are shown.

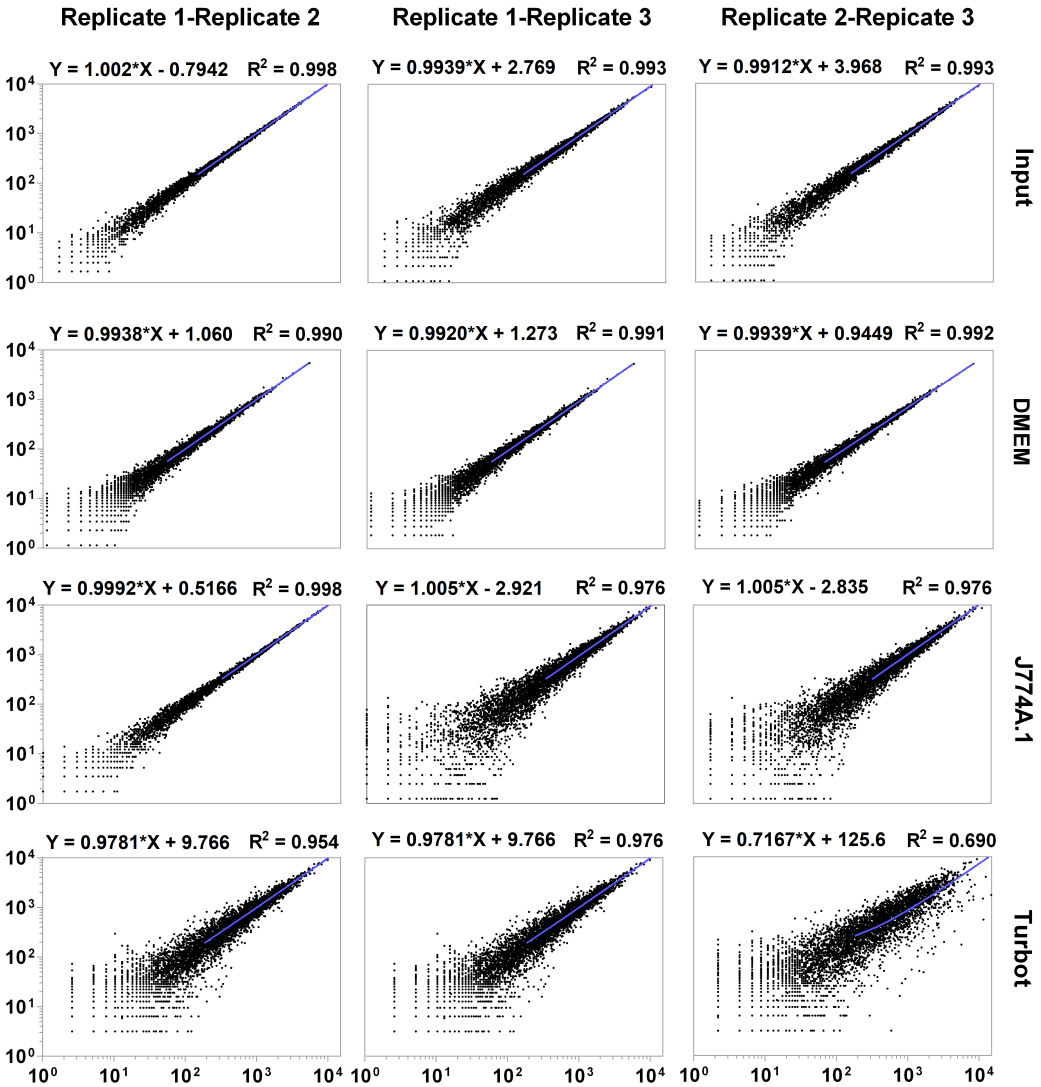

Supplemental Figure S3. Correlation of experimental replicates from TIS experiments. Related to Figure 1. The sequencing data from experimental replicates of input libraries (*n* = 3) and output libraries (*n* = 3) recovered after growth in DMEM (*n* = 3), J774A.1 (*n* = 3), and turbot (*n* = 3) are shown.

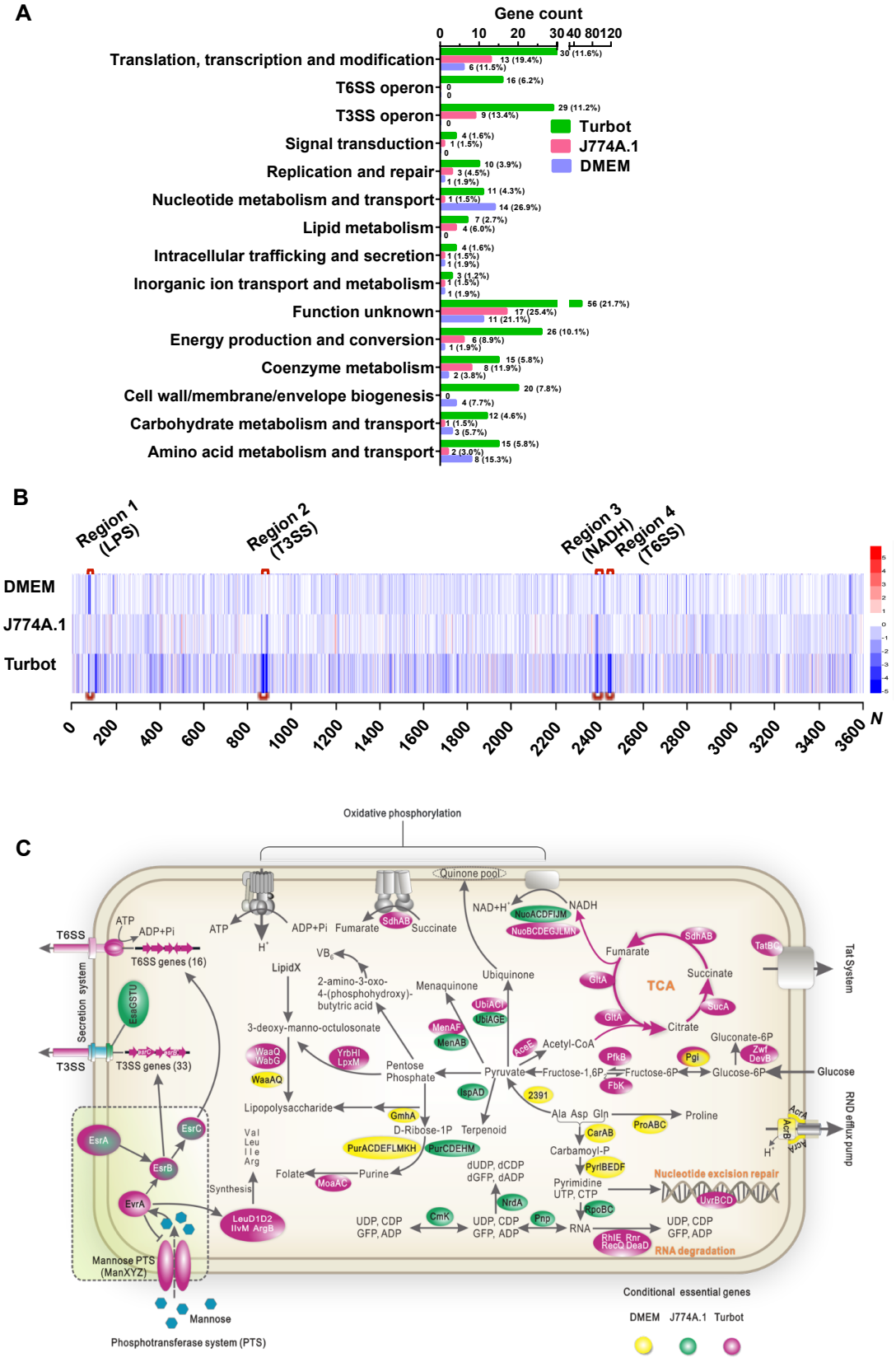

Supplemental Figure S4. Fitness of *E. piscicida* transposon mutants in DMEM, macrophages and turbot. Related to Figure 1. **(A)** COG categories of depleted genes in the three conditions. The number of depleted genes in each category is shown; the percentages

shown are the fraction of the total number of depleted genes represented by the number of depleted genes/category. **(B)** Heatmap of relative abundances of mutants in indicated conditions. Colored lines represent FC values of the genes across the genome (N). Four gene clusters, associated with LPS synthesis, T3SS, NADH, and T6SS, exhibiting reduced abundance in the turbot outputs, are highlighted. **(C)** Schematic model of genes and pathways essential for *in vivo* and *in vitro* growth in *E. piscicida*. Yellow, green, and pink colors respectively represented the growth conditions of DMEM, J774A.1 cells, and in turbot. The genes required for growth in specific conditions were highlighted in the colored ovals. The upstream regulatory network of T3/T6SS as well as the putative mannose metabolic pathways were highlighted in a dashed box.

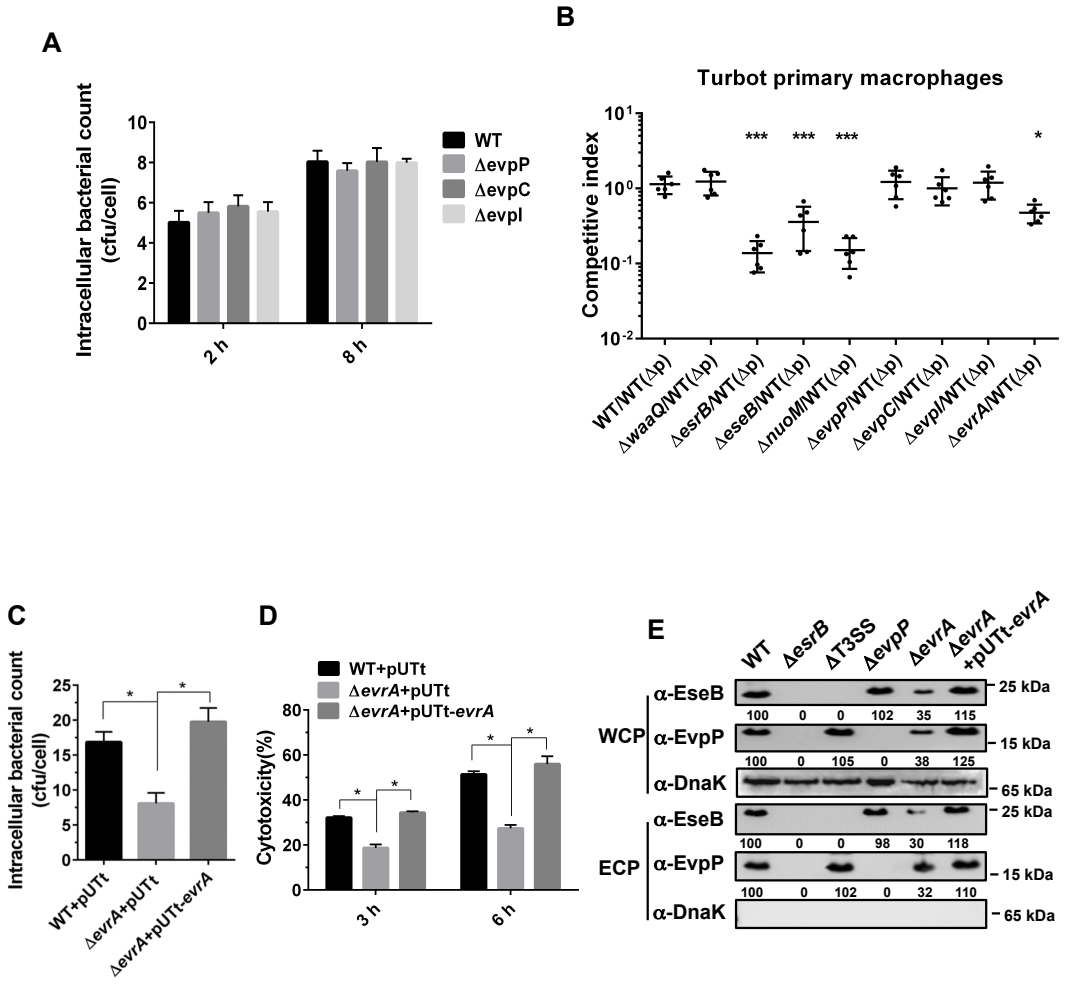

Supplemental Figure S5. Intracellular growth of various *E. piscicida* mutants in J774A.1 and turbot primary macrophages. Related to Figure 1. **(A)** Intracellular bacterial counts of WT or individual T6SS deletion mutants grown in primary turbot macrophages; the means and SD from 3 replicates are shown. **(B)** Competition assays between the indicated deletion mutant vs. WT(ΔP) in primary turbot macrophages. Data presented are the mean ± SD from 6

replicates. *$P < 0.05$, *** $P < 0.001$ based on ANOVA followed by Bonferroni's multiple-comparison post-test comparing the data to the values from the WT/ WTΔp competitions. **(C-D)** Intracellular *E. piscicida* CFU recovered (C), and cytotoxicity (D) of WT, Δ*evrA* and the complemented strain towards J774A.1 cells. After incubation in DMEM for 12 h, WT, Δ*evrA* and the complemented strain were used to infect J774A.1 cells at an MOI of 10. Cytotoxicity was detected at 3 and 6 hours post infection using an LDH assay. Data were shown as the mean ± SEM of results for triplicate cultures or assays. *, $P < 0.05$ based on student's *t*-test. **(E)** Western blot analysis of EseB and EvpP expression and secretion in the indicated strains. The cell lysates (WCP) and extracellular proteins (ECPs) were analyzed by western blotting with the indicated antibodies. DnaK levels were used as the loading control.

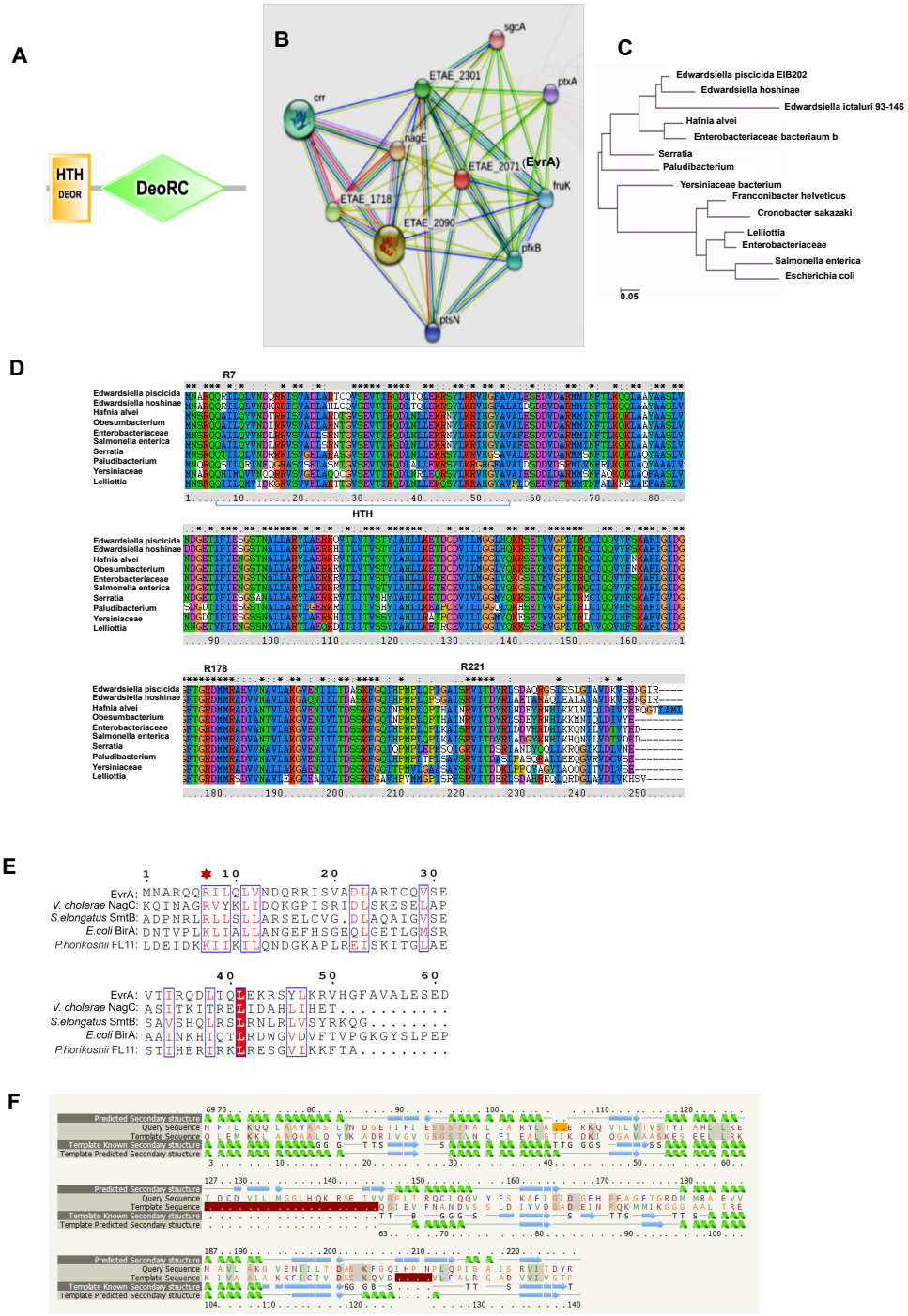

Supplemental Figure S6. EvrA is a DeoR family protein. Related to Figure 3. **(A)** Domain structure of EvrA. **(B)** The protein network of EvrA as predicted by STRING includes PTS-related proteins, e.g. *crr*, *nagE*, *fruK*, *pfkB*, *ptxA*, *ptsN*, *sgcA*, 2301 (Fructose-specific PTS system IIBC component), 2090 (glucose-specific IIBC subunit), and 1718 (Beta-glucoside-specific PTS system components IIABC). **(C)** Phylogenetic tree of EvrA multiple sequence alignments. The phylogenetic tree was inferred with a Neighbor-Joining algorithm built in MEGA (v6.0.6). **(D)** Conservation of EvrA in other bacterial species. The conserved residues are highlighted with various colors. The residues R7, R178 and R221 as

well as the N-terminal HTH were as indicated. **(E)** The sequence alignment of the N-terminal HTH domain of EvrA. The conserved R7 residue was indicated by an asterisk. **(F)** Sequence alignment and predicted secondary structures between the indicated regions of EvrA (query) with the model RpiA (1LK7) (template).

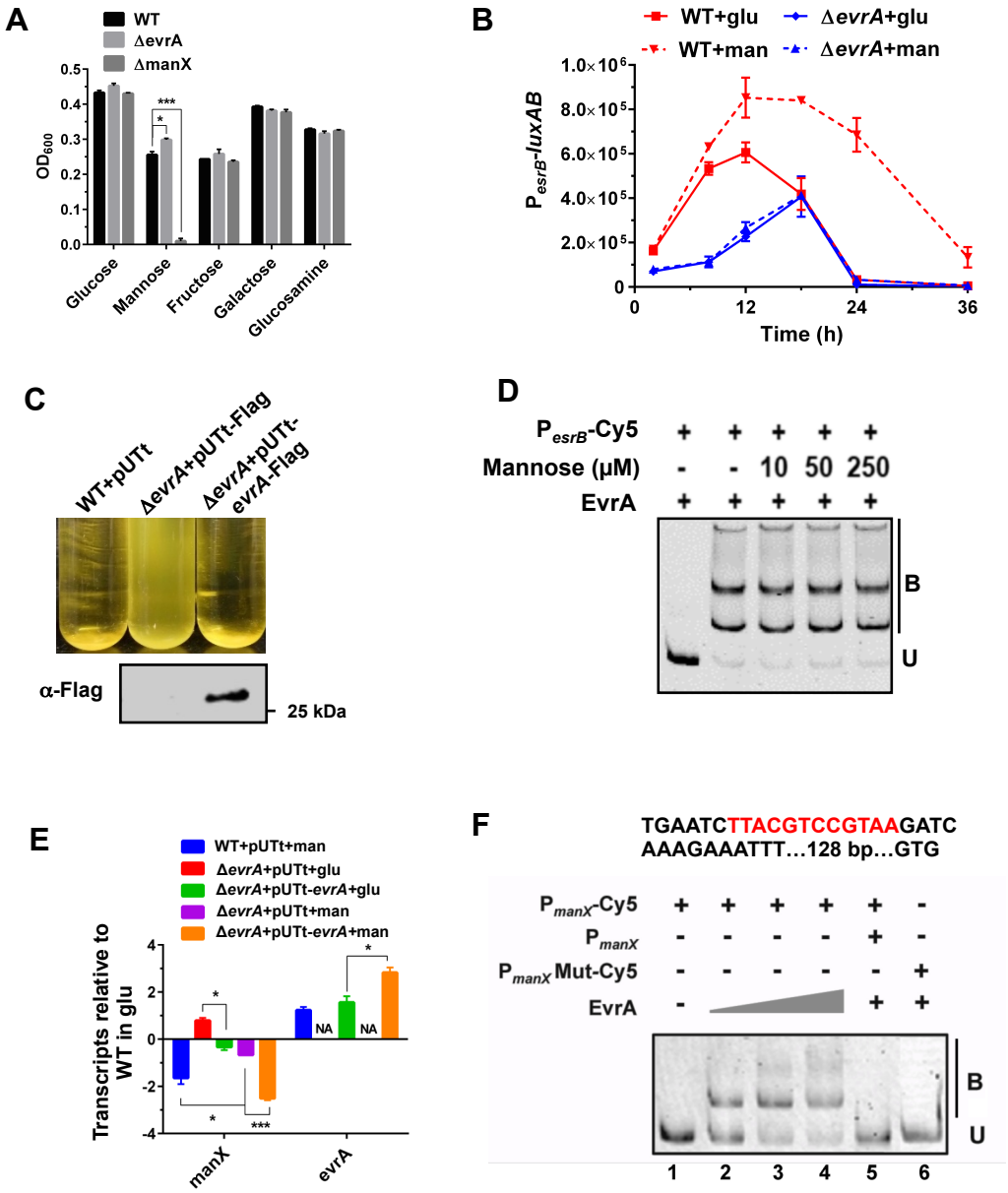

Supplemental Figure S7. Mannose stimulates *evrA*-dependent induction of *esrB* expression. Related to Figure 4. **(A)** Optical density at 600 nm (OD_{600}) of 24 h cultures of WT, Δ*evrA* and Δ*manX* in DMEM medium supplemented with 5 mg/mL of the indicated sugar. Results shown are mean ± SD from 3 replicates, * $P < 0.05$; ***, $P < 0.001$ based on the student's *t*-test. **(B)** P_{esrB}-*luxAB* activity in the indicated strains grown in DMEM supplemented with glucose (glu) or mannose (man). **(C)** Auto-aggregation and protein expression in *E. piscicida* strains bearing an empty FLAG vector or a vector with EvrA-FLAG. **(D)** EMSA of

EvrA binding to *esrB* promoter in the presence of increasing concentrations of mannose. **(E)** qRT-PCR analyses of *manX* and *evrA* transcript levels in cells grown in glucose or mannose compared to those in WT cells grown in glucose. *gyrB* was used as a control. $n = 3$, * $P < 0.05$ based on Student's *t*-test. NA, not applicable. **(F)** EMSA of EvrA binding to the predicted *manX* promoter (P_{manX}). 5-fold excess of un-labeled P_{manX} probe was added to lane to confirm the specificity of the mobility shift. The putative binding motif in P_{manX} was mutated (T to G and A to C) in P_{manX}Mut.

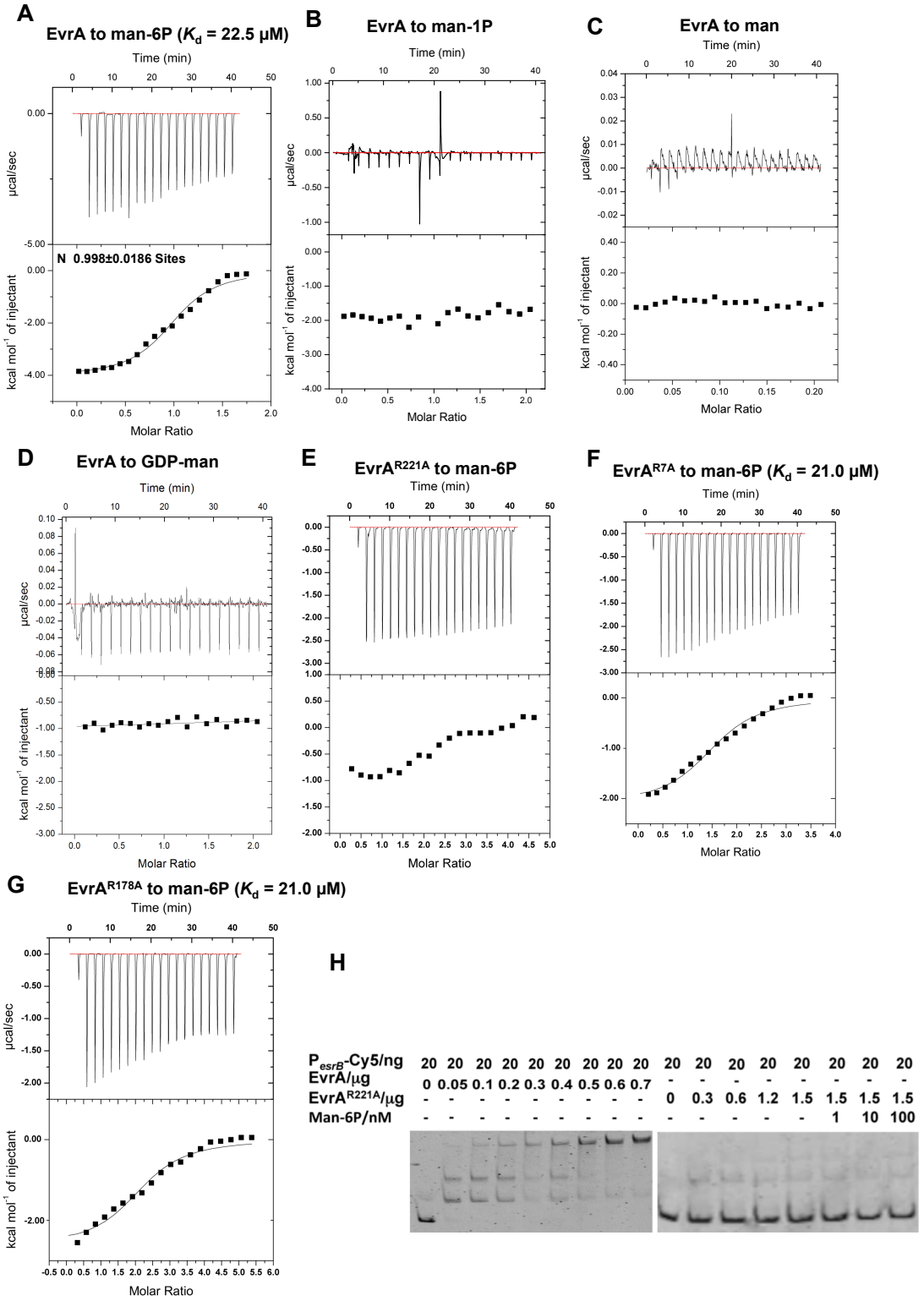

Supplemental Figure S8. Binding behaviors of EvrA or EvrA^{R141A} binding to *esrB* in the presence of various sugars. Related to Figure 5. **(A-G)** Isothermal titration calorimetry (ITC) analyses of interaction of EvrA protein with mannose-6P (man-6P) (A), mannose-1P (man-1P) (B), mannose (man) (C), and GDP-mannose (GDP-man) (D). EvrA^{R221A} (E), EvrA^{R7A} (F), and EvrA^{R178A} (G) were also tested for interactions with man-6P. The top panel shows the raw

calorimetric data for the interaction and bottom panel the integrated heat changes, corrected for heat of dilution, and fitted to a single-site binding model. K_d, dissociation constant. **(H)** EMSA of EvrA or EvrA^{R221A} binding to *esrB* promoter probe in the absence or presence of excess man-6P. In EMSA experiments, 20 ng of each Cy5-labeled probe was added to the EMSA reactions. B: bound DNA; U: unbound DNA.

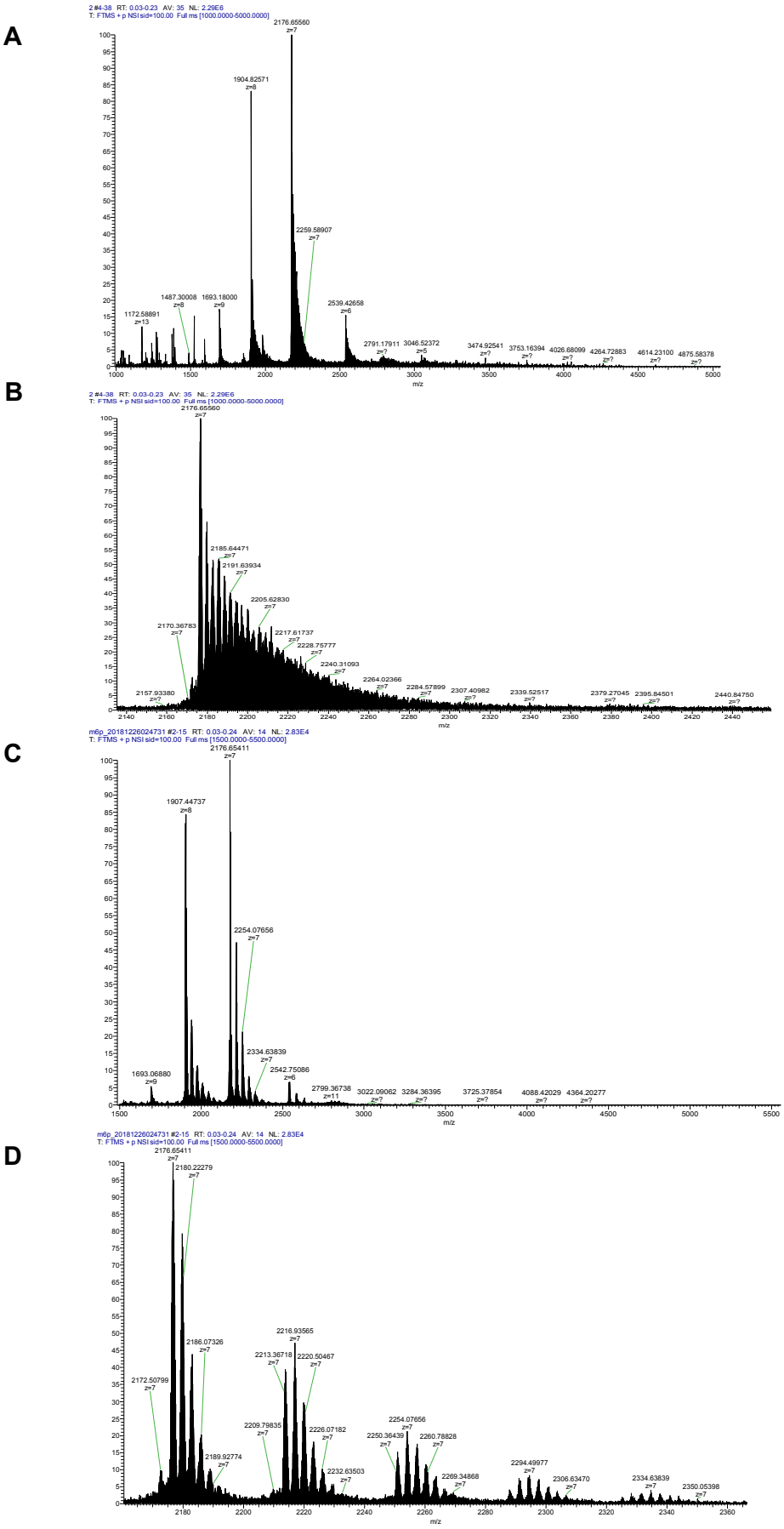

Supplemental Figure S9. Related to Figure 5. **Mass spectrometry of EvrA in complex**

with Man-6P after denatured with the addition of formic acids (A and B) or in the native condition (non-formic acid-treated) (C and D). Mass spectrometry B and D were zoomed in from the respective peak clusters with z = 7 (A and B).

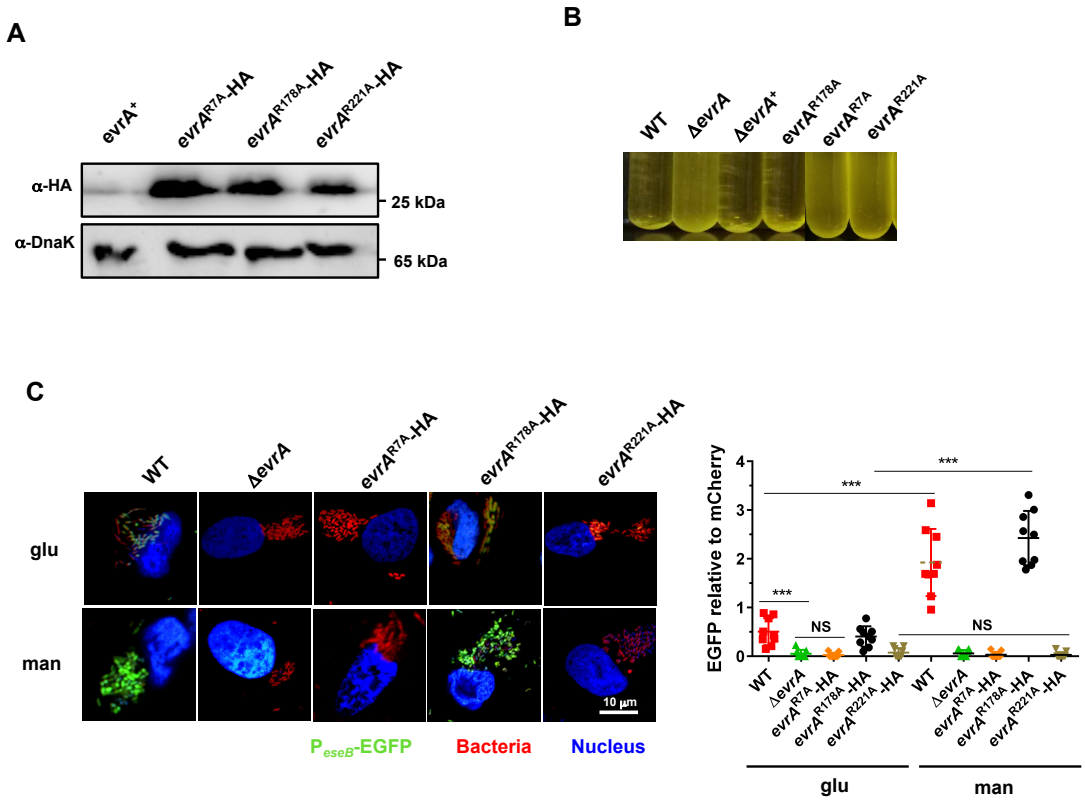

Supplemental Figure S10. Characterization of critical Arg residues in EvrA regulation of virulence gene expression. Related to Figure 5. **(A)** Western blot of expression levels of EvrA or EvrA-HA in various *E. piscicida* strains used in Figures 5 and 6. DnaK was used as a loading control. **(B)** Auto-aggregation phenotypes of WT, Δ*evrA*, Δ*evrA*$^{+}$, and various Δ*evrA* strains expressing R7A, R178A and R221A of EvrA variants. **(C)** Detection of *eseB* expression in HeLa cells infected by the indicated *E. piscicida* strains carrying a P_{eseB}-EGFP reporter plasmid. Bacteria were pre-incubated in glucose or mannose before infection at an MOI of 10 for 8 h. mCherry fluorescence (red) was used to identify intracellular bacterial cells. DAPI was used to label cell nuclei (blue). Scale bar represents 10 μM. Quantification results are shown for at least 9 cells. *** $P < 0.0001$ based on Student's *t*-test.

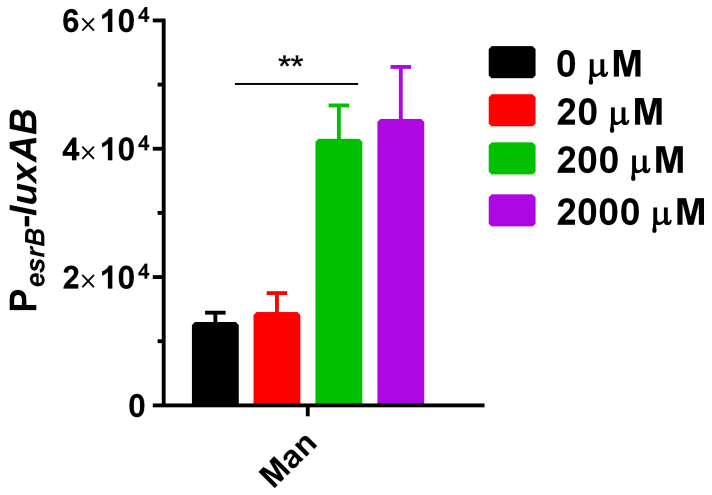

Supplemental Figure S11. Activation of *esrB* expression by Mannose of physical concentrations. Related to Figure 6. Chromosomal P_{esrB}-*luxAB* reporter activity in WT grown for 12 h in DMEM medium supplemented with mannose at indicated concentrations. Data shown are the mean ± SEM of results for triplicate assays. * $P < 0.05$; **, $P < 0.01$ based on the student's *t*- test.

Table S1 Characteristics of the *E. pisicicida* EIB202 derived defined transposon mutant library

Data set	*N*
Master library	
Transposon mutants isolated	34,560
Mutants with well-defined insertion locations	24,470
Mutants in unique genomic locations	20,346
Insertions inside ORFs	18,128
Insertions between ORFs	6,342
Insertions inside 5-85% ORFs	14,028
Insertions outside 5-85% ORFs	4,100
Transcriptional fusion	12,295
Transposon with – frame insertions [a]	12,383
Transposon with + frame insertions [b]	12,087
Annotated ORFs in *E. piscicida*	3,599
ORFs disrupted	2,806
ORFs without hits	793
Average hits per annotated ORF	5.04
Predicted essential genes	496
Conditional essential genes/ intergenic regions in DMEM medium	52/20
Conditional essential genes/ intergenic regions in J774A.1	67/62
Conditional essential genes/ intergenic regions in turbot	258/108
Subset libraries [c]	
1st NR subset (single mutant for each disrupted ORF) [d]	2,759
2nd NR subset (single mutant for each disrupted ORF) [e]	2,235
3rd NR subset (Tn transcriptionally fused to the disrupted gene) [f]	3,705
4th NR subset (mutants with intergenic insertions) [g]	2,305
5th NR subset (composite library of equally mixed 1st, 2nd, and 4th subsets)	7,299

[a, b] "+" and "-" indicates that the direction of transposon insertion is consistent with or reverse with the direction of gene, respectively;
[c] the number indicated the mutants included in the specific subset:
[d, e] No. 1 and 2 non-redundant (NR) libraries are parallel containing distinct insertion (20-80% region in the gene) mutants in the same allelic genes;
[f, g] No more than two transcriptional fusion mutants for each disrupted ORF were selected for the 3rd and 4th subset.

Table S7 List of 5th subset of defined transposon insertion mutant library

Name of Composite Collection	Annotation
1st subset composite collection	composite collection of 1st subset, Col^r and Gm^r, consist of 10 μl bacterium culture which contains 2 × 10^6 c.f.u of 2,759 defferent mutants.
2nd subset composite collection	composite collection of 2nd subset, Col^r and Gm^r, consist of 10 μl bacterium culture which contains 2 × 10^6 c.f.u of 2,235 defferent mutants.
4th subset composite collection	composite collection of 4th subset,Col^r and Gm^r,consist of 10 μl bacterium culture which contains 2 × 10^6 c.f.u of 2,305 defferent mutants.

Table S8 Conditional essential genes grown in DMEM medium

Gene_ID	Gene	Annotation-nr	No.TA	LB_01	LB_02	LB_03	DMEM_01	DMEM_02	DMEM_03	DMEM/LB	P value
ETAE_0075	waaQ	heptosyl III transferase	45	260	311	282	37.63220892	35.31304348	43.93933988	-2.856865972	8.37407E-05
ETAE_0076	walW	lipopolysaccahride biosynthesis	46	211	178	154	26.22850925	20.50434783	18.69759144	-3.033742991	0.000673513
ETAE_0078	walR	putative glycosyltransferase	52	254	259	309	45.61479869	64.93043478	33.65566459	-2.503221036	0.000337238
ETAE_0079	wabK	putative glycosyltransferase	78	161	172	160	24.2898803	16.5173913	15.61248885	-3.104561798	6.61277E-06
ETAE_0083	rfaD	ADP-L-glycero-D-manno-heptose-6-epimerase	45	3	2	4	0.540369967	0	0.934879572	-2.008433752	0.015635015
ETAE_0185	purD	phosphoribosylamine-glycine ligase	37	227	225	199	42.19368879	52.4	47.67885816	-2.186744767	5.48257E-05
ETAE_0186	purH	phoribosylaminoimidazolecarboxamide formyltransferase/IM	51	780	741	680	167.6343852	119.6086957	153.3202498	-2.318332308	5.38948E-05
ETAE_0204	pgi	glucose-6-phosphate isomerase	60	50	45	55	13.68443961	12.53043478	7.479036574	-2.118770112	0.000377832
ETAE_0246	0	hypothetical protein	9	222	272	288	3.421109902	4.556521739	3.739518287	-5.943288669	0.000204106
ETAE_0358	purA	adenylosuccinate synthase	48	52	46	64	13.68443961	12.53043478	12.15343443	-2.052408584	0.001674465
ETAE_0368	rplI	50S ribosomal protein L9	15	32	25	36	1.140369967	4.556521739	2.804638715	-3.296101516	0.001275789
ETAE_0459	folB	bifunctional dihydroneopterin aldolase/dihydroneopterin trip	10	40	31	37	2.280739935	1.139130435	1.869759144	-4.114148411	0.000221066
ETAE_0593	carA	carbamoylphosphate synthase small subunit	26	183	168	180	46.75516866	43.28695652	32.72078501	-2.105702307	2.44036E-05
ETAE_0594	carB	carbamoylphosphate synthase large subunit	89	1,304	1,340	1,268	366.0587595	389.5826087	203.8037467	-2.026405802	9.22999E-05
ETAE_0771	pspE	rhodanese-related sulfurtransferase	9	292	304	258	55.44069641	40.49565217	39.74843889	-2.653415605	0.000519648
ETAE_0774	purL	phosphoribosylformylglycinamidine synthase	74	1,631	1,646	1,640	458.4287269	439.7043478	330.0124888	-2.000454698	6.86623E-06
ETAE_0796	proB	gamma-glutamyl kinase	27	260	265	263	60.43960827	54.67826087	56.09277431	-2.19596383	1.01296E-07
ETAE_0797	proA	gamma-glutamyl phosphate reductase	24	436	470	423	84.38737758	67.20869565	75.72524532	-2.54196643	1.66033E-05
ETAE_0802	0	hypothetical protein	8	225	226	197	28.50924918	35.31304348	35.52542373	-2.693134931	4.85458E-05
ETAE_0808	0	hypothetical protein	3	38	61	43	10.52665941	12.66956522	11.89295272	-2.113968356	0.013236919
ETAE_0837	0	putative phospholipid biosynthesis acyltransferase	26	473	452	476	119.3014146	110.6173913	118.3621766	-2.211522028	5.18511E-05
ETAE_0891	0	hypothetical protein	6	12	14	6	1.140369967	1.417391304	2.804638715	-2.562229382	0.030152916
ETAE_1010	acrB	RND family, acridine/multidrug efflux pump/acriflavin resist	104	809	875	824	84.38737758	103.6608696	114.0553078	-3.049164806	4.70073E-06
ETAE_1011	acrA	efflux transporter, RND family, MFP subunit	42	458	423	424	109.4755169	63.79130435	99.09723461	-2.256245111	4.39294E-05
ETAE_1020	dnaX	DNA polymerase III, subunits gamma and tau	34	20	28	23	1.140369967	1.139130435	4.674397859	-3.166150504	0.001156244
ETAE_1053	purB	adenylosuccinate lyase	29	344	300	333	66.14145811	54.67826087	67.31132917	-2.369860097	4.67743E-05
ETAE_1086	purM	phosphoribosylformylglycinamidine cyclo-ligase	20	307	300	318	77.54515778	67.20869565	68.24620874	-2.111973611	2.70844E-06
ETAE_1098	purC	phosphoribosylaminoimidazole-succinocarboxamide synth	17	132	138	158	21.66702938	46.70434783	36.4603033	-2.016136161	0.000540506
ETAE_1248	pyrD	dihydroorotate dehydrogenase 2	47	187	231	209	39.91294886	58.09565217	43.0044603	-2.145275549	0.000316366
ETAE_1520	0	ferritin Dps family protein	22	877	892	871	106.054407	186.8173913	208.4781445	-2.394696475	2.33859E-05
ETAE_1563	0	hypothetical protein	7	166	190	173	40.43960827	39.23478261	34.50669045	-2.014143443	9.14137E-05
ETAE_1689	pdxH	pyridoxamine 5'-phosphate oxidase	20	27	21	13	1.140369967	1.139130435	5.609277431	-2.812698256	0.014153307
ETAE_1867	pspA	hock protein A (IM30), suppresses sigma54-dependent tran	10	715	705	688	21.66702938	38.73043478	44.87421945	-4.310206022	3.81692E-07
ETAE_1894	0	hypothetical protein	11	1,203	1,245	1,143	86.66811752	72.90434783	101.9018733	-3.774829304	3.48145E-06
ETAE_1951	wza	polysaccharide export-related protein	14	1,372	1,373	1,295	117.4581066	76.32173913	125.2738626	-3.658414808	2.03634E-06
ETAE_1961	0	hypothetical protein	11	75	84	75	9.122959739	9.113043478	5.609277431	-3.244205294	2.74928E-05
ETAE_2082	pyrF	OMP decarboxylase; OMPDCase; OMPdecase	16	87	76	74	23.94776931	19.36521739	14.95807315	-2.003738305	0.000250875
ETAE_2138	0	hypothetical protein	8	244	245	309	25.08813928	18.22608696	31.78590544	-3.392868407	0.00038499
ETAE_2159	mukE	condesin subunit E	22	2	3	1	0	0	0	-2.885963624	0.021610065
ETAE_2160	mukF	chromosome segregation and condensation protein	46	6	9	7	1.140369967	0	0.934879572	-2.883327261	0.001283873
ETAE_2256	0	hypothetical protein	22	3	4	4	0	0	0	-3.566250389	0.000585947
ETAE_2262	0	hypothetical protein	12	9	9	7	0	0	0	-4.683175648	0.000117254
ETAE_2274	0	hypothetical protein	2	8	6	5	1.280739935	1.27826087	1.869759144	-2.653415605	0.010712579
ETAE_2391	0	aminotransferase class I and II	31	539	597	548	139.125136	119.6086957	82.26940232	-2.300582757	5.34221E-05
ETAE_2409	purF	amidophosphoribosyltransferase	56	996	1,017	881	249.7410229	213.0173913	164.5388046	-2.20403196	0.000103139
ETAE_2519	0	hypothetical protein	14	582	477	690	21.66702938	29.6173913	35.52542373	-4.316392181	0.000853337
ETAE_2700	purE	phosphoribosylaminoimidazole carboxylase catalytic subur	8	57	54	54	13.68443961	17.08695652	8.413916146	-2.047184308	0.000102292
ETAE_2701	purK	phosphoribosylaminoimidazole carboxylase	22	285	245	254	65.00108814	95.68695652	34.59054416	-2.000616641	0.000776871
ETAE_2736	0	inorganic polyphosphate/ATP-NAD kinase	23	10	4	7	0	1.139130435	0.934879572	-2.866993196	0.01891615
ETAE_3124	pyrI	aspartate carbamoyltransferase regulatory subunit	9	241	257	273	60.43960827	58.09565217	63.57181088	-2.076427757	3.19392E-05
ETAE_3125	pyrB	aspartate carbamoyltransferase	24	369	364	387	78.68552775	58.09565217	44.87421945	-2.616665381	1.3228E-05
ETAE_3261	aroK	shikimate kinase I	12	15	10	17	0	2.27826087	3.739518287	-2.569333197	0.008092284

Table S9 Conditional essential genes grown in J774A.1 cells

Gene_ID	Gene	Annotation-nr	No.TA	Input_01	Input_02	Input_03	J774A.1_01	J774A.1_02	J774A.1_03	J774A.1/Input	P value
ETAE_0147	ubiE	ubiquinone/menaquinone biosynth	30	337	245.3632144	364.569027	52	49.01921317	17.51487414	-2.98699558	0.001843319
ETAE_0217	ubiA	4-hydroxybenzoate polyprenyltrar	26	10	11.10240789	4.873917473	1	0	1.251062439	-3.07361928	0.016011176
ETAE_0228	citA	sensor histidine kinase	51	15,575	15291.34639	14869.34743	2179	2095.571363	2468.346192	-2.761697089	6.29927E-07
ETAE_0314	groEL	chaperonin GroEL (HSP60 family	49	112	145.4415434	113.0748854	8	12.25480329	66.30630925	-2.086046428	0.012039748
ETAE_0340	poxA	lysyl-tRNA synthetase, class II	27	6	4.440963156	2.924350484	0	1.750686185	0	-2.40826283	0.024368157
ETAE_0345		hypothetical protein	8	8	6.661444735	6.823484463	1	0	0	-3.510960361	0.000370855
ETAE_0348		putative ATPase	19	15	9.992167102	7.798267957	0	0	1.251062439	-3.888652536	0.006983543
ETAE_0381	fbp	fructose-1,6-bisphosphatase	38	1,127	1101.358863	1073.236628	311	248.5974382	226.4423014	-2.068955919	9.30721E-06
ETAE_0405	infB	translation initiation factor 2	73	2	1.110240789	3.899133979	0	0	0	-3.015807311	0.044556486
ETAE_0409	pnp	polyribonucleotide nucleotidyltran	66	223	135.4493763	180.3349465	31	26.26029277	12.51062439	-2.93240182	0.003842202
ETAE_0494		conserved hypothetical protein	34	2,133	2167.19002	2076.288844	422	434.1701738	321.5230467	-2.435754806	2.58749E-06
ETAE_0578	nhaA	Na+/H+ antiporter	31	9	3.330722367	11.69740194	0	0	0	-4.665765179	0.031036263
ETAE_0600	ksgA	dimethyladenosine transferase (rI	19	45	68.83492892	49.71395823	3	7.002744739	8.757437071	-3.055157261	0.003097679
ETAE_0735	glnD	PII uridylyl-transferase	67	59	97.70118944	111.1253184	17	5.252058554	27.54037267	-2.428617931	0.029865787
ETAE_0743	cdsA	CDP-diglyceride synthetase	25	15	11.10240789	3.899133979	0	0	0	-4.933236128	0.034874421
ETAE_0859	esaH	putative type III secretion apparat	6	326	445.2065564	463.9969435	35	43.76715462	61.3020595	-3.131867732	0.001128871
ETAE_0860	esaG	putative type III secretion system	7	1,716	1646.48709	1628.86322	298	320.3755718	130.1104936	-2.735750711	2.74968E-05
ETAE_0861	esrC	putative transcriptional regulator	19	9,378	9548.070786	9813.145441	833	835.0773102	870.7394573	-3.500291293	2.68861E-07
ETAE_0881	esaS	type III secretion apparatus	6	1,971	2061.717145	2830.771268	475	540.9620311	582.9950964	-2.101048748	0.003078484
ETAE_0882	esaT	type III secretion system EscT ho	24	8,523	8790.886568	10104.60571	1309	1253.491308	942.0500163	-2.967488623	9.18513E-05
ETAE_0883	esaU	type III secretion system EscU ho	24	25,085	23348.36379	25658.25115	1773	1685.910796	2047.989212	-3.749764336	5.33059E-06
ETAE_0884		putative transglycosylase signal p	29	22,079	22106.00435	23736.95288	1780	1755.938243	2249.410265	-3.553164088	3.45632E-06
ETAE_0885	esrA	two-component sensor/regulator	69	28,010	26593.59762	27164.29165	2687	2718.815645	3121.400785	-3.261240893	6.01382E-07
ETAE_0886	esrB	two-component sensor/regulator	15	3,963	3894.724688	3782.159959	423	395.6550778	499.173913	-3.141890979	5.98632E-07
ETAE_0956	ahpC	alkyl hydroperoxide reductase, sn	23	82	81.0475776	115.9992359	1	3.50137237	48.79143511	-2.367407153	0.017561024
ETAE_0975	ribH	riboflavin synthase beta-chain	14	3	5.551203945	2.924350484	0	0	0	-3.654629928	0.010241266
ETAE_0981	xseB	exonuclease VII small subunit	6	193	203.1740644	212.5028018	40	26.26029277	48.79143511	-2.394045236	4.34837E-05
ETAE_0982	thiI	thiamine biosynthesis ATP pyroph	41	622	659.4830287	643.3571065	116	140.0548948	125.1062439	-2.332897594	2.46509E-06
ETAE_1011	acrA	efflux transporter, RND family, MF	42	1,836	1708.660574	1838.441671	397	409.6605672	455.4717228	-2.092453133	3.56829E-05
ETAE_1179		hypothetical protein	3	1	3.330722367	3.899133979	0	0	0	-3.212450606	0.034395192
ETAE_1207	neuB	sialic acid synthase	81	246	253.1348999	194.9566989	15	24.50960659	96.33180778	-2.345389683	0.004132014
ETAE_1258		hypothetical protein	6	27	38.85842762	23.39480387	6	3.50137237	7.012749264	-2.434590438	0.020812777
ETAE_1439	ruvA	holliday junction resolvasome, DN	10	25	26.64577894	12.67218543	1	0	3.753187316	-3.503834232	0.011998685
ETAE_1489		hypothetical protein	9	85	89.92950392	75.05832909	0	0	60.05099706	-2.040847657	0.036458424
ETAE_1518	cls	cardiolipin synthetase	50	214	235.3710473	269.0402445	19	17.50686185	50.04249755	-3.038873742	0.000391098
ETAE_1553	cysB	transcriptional regulator	35	22	8.881926313	10.72261844	1	0	0	-4.407065168	0.029325456
ETAE_1554	cspC	cold shock protein	6	67	44.40963156	97.47834947	4	8.753430924	33.77868585	-2.139344416	0.039699662
ETAE_1617		hypothetical protein	5	68	66.61444735	41.91569027	11	8.753430924	16.27231121	-2.289212007	0.012457067
ETAE_1654		hypothetical protein	5	34	23.31505657	32.16785532	4	0	2.502124877	-3.597042675	0.001458571
ETAE_1675		hypothetical protein	5	59	31.08674209	34.11742231	6	5.252058554	12.01699902	-2.419068426	0.037475334
ETAE_1725		chain length determinant protein	60	131	95.48070786	88.70529801	7	1.750686185	27.52337365	-3.084356147	0.003691597
ETAE_1787		hypothetical protein	17	98	61.0632434	52.63830871	12	5.252058554	31.27656097	-2.100472168	0.026801951
ETAE_1792	aroH	3-deoxy-7-phosphoheptulonate sy	25	208	112.1343197	185.208864	29	22.7589204	36.28081072	-2.507241479	0.008836873
ETAE_1831		hypothetical protein	5	11	33.30722367	20.47045339	0	0	0	-6.048996085	0.026652392
ETAE_1906		hypothetical protein	33	1,832	2100.575573	1334.478604	300	309.8714547	447.8803531	-2.315023038	0.003620538
ETAE_1967		HpcH/HpaI aldolase family protein	9	116	113.2445605	68.23484463	9	10.50411711	32.55312194	-2.516609241	0.03758009
ETAE_2030		hypothetical protein	10	21	18.87409341	7.798267957	0	1.750686185	0	-4.138930251	0.020389422
ETAE_2176	cmk	cytidylate kinase	19	9	2.220481578	7.798267957	0	0	0	-4.34859903	0.040666975
ETAE_2305		hypothetical protein	7	57	59.95300261	75.05832909	12	14.00548948	13.77018634	-2.272479392	0.002027673
ETAE_2374	nuoM	NADH:ubiquinone oxidoreductase	45	106	153.2132289	184.2340805	17	15.75617566	45.03824779	-2.495901617	0.007809592
ETAE_2376	nuoK	NADH:ubiquinone oxidoreductase	7	28	34.41746446	40.94090678	5	8.753430924	8.757437071	-2.199844664	0.002320357
ETAE_2377	nuoJ	NADH:ubiquinone oxidoreductase	12	43	72.16565129	76.03311258	0	0	15.01274926	-3.582410392	0.007401223
ETAE_2381	nuoF	NADH:ubiquinone oxidoreductase	29	81	74.38613287	94.55399898	5	5.252058554	8.757437071	-3.648998663	0.000220093
ETAE_2383	nuoD	NADH:ubiquinone oxidoreductase	49	220	229.8198433	233.9480387	2	3.50137237	135.1147434	-2.274364101	0.014988342
ETAE_2385	nuoA	NADH:ubiquinone oxidoreductase	15	22	27.75601973	39.96612328	5	8.753430924	1.251062439	-2.500223919	0.012525015
ETAE_2412	folC	bifunctional folylpolyglutamate syn	31	8	11.10240789	17.5461029	1	3.50137237	1.251062439	-2.491135459	0.021687059
ETAE_2549		hypothetical protein	6	19	28.86626052	36.0669893	2	0	0	-4.818341079	0.005853485
ETAE_2650	lipA	lipoate synthase	16	24	22.20481578	18.5208864	0	0	1.251062439	-4.865709546	0.000210904
ETAE_2745		phage/plasmid primase	3	45	59.95300261	51.66352522	13	10.50411711	12.51487414	-2.117579482	0.001483348
ETAE_2858	sdhC	succinate dehydrogenase cytochr	7	109	65.50420656	45.81482425	7	7.002744739	8.757437071	-3.220389352	0.024439934
ETAE_2859	alaS	alanyl-tRNA synthetase	72	12	15.54337105	10.72261844	1	0	1.251062439	-3.61155638	0.001134151
ETAE_2873	rpoS	RNA polymerase sigma factor	24	830	749.4125326	865.6077433	42	31.51235133	41.28506048	-4.401035826	2.32167E-05
ETAE_3055		truncated integrase	5	11	13.32288947	17.5461029	1	1.750686185	5.004249755	-2.306271159	0.00621337
ETAE_3147		hypothetical protein	7	113	87.70902234	86.75573102	26	15.75617566	6.255312194	-2.558665358	0.001539308
ETAE_3211	secY	preprotein translocase subunit Se	67	11	33.30722367	23.39480387	0	0	0	-6.111348871	0.022930809
ETAE_3474		transcriptional regulator, TetR fan	19	14,913	14799.50972	15576.06546	3132	3119.722781	2394.533508	-2.388865778	3.73911E-06
ETAE_3539	pstC	ABC-type phosphate transport sy	37	195	178.748767	160.8392766	58	43.02470265	15.01274926	-2.204925796	0.001870957

Table S10 Conditional essential genes grown in turbot

Gene_ID	Gene	Annotation-nr	*No.TA*	Input_01	Input_02	Input_03	Turbot_01	Turbot_02	Turbot_03	Turbot/Input	P value
ETAE_0023		conserved hypothetical protein	20	1058.3721	1049.0489	1100.714	28.6	70.41	15.9	-4.767325	1.452E-06
ETAE_0026	gltS	Na+/glutamate symporter	35	684.67741	628.76223	643.16231	205.43	132.02	101.76	-2.147757	0.000134
ETAE_0074	waaG	lipopolysaccharide core biosynthesis protein	40	181.2634	175.95336	85.25138	18.01	14.62	13.14	-3.191256	0.013268
ETAE_0075	waaQ	heptosyl III transferase	45	353.07706	332.72696	372.30033	64.09	102.28	89.35	-2.036103	7.522E-05
ETAE_0076	walW	lipopolysaccahride biosynthesis	46	133.15558	129.25484	112.22967	16.22	20.61	18.16	-2.703136	8.352E-05
ETAE_0101	rfe	UDP-N-acetylmuramyl pentapeptide phosphotransferase	50	2675.9977	2650.975	2437.7578	52.01	44.01	85.86	-5.392832	5.048E-06
ETAE_0103	wecB	UDP-N-acetylglucosamine 2-epimerase	35	627.11984	668.78953	675.53625	91.01	28.61	111.3	-3.077361	3.747E-05
ETAE_0104	wecC	UDP-N-acetyl-D-mannosaminuronate dehydrogenase	31	525.74978	607.08077	547.11962	104.01	138.63	130.38	-2.162111	8.002E-05
ETAE_0105	rfbB	dTDP-D-glucose 4,6-dehydratase	36	768.00703	806.38339	858.98859	62.41	66.01	60.42	-3.666763	9.255E-06
ETAE_0106	rfbA	glucose-1-phosphate thymidylyltransferase	30	391.73513	376.08987	403.59514	13	4.4	9.54	-5.293731	1.371E-06
ETAE_0107	wecD	TDP-D-fucosamine acetyltransferase	15	214.76707	219.31627	226.61759	5.2	0	0	-6.338766	5.846E-07
ETAE_0108	wecE	TDP-4-oxo-6-deoxy-D-glucose transaminase	38	814.39672	751.34585	875.17556	13	15.4	0	-6.282288	2.396E-05
ETAE_0109	wzxE	membrane protein involved in the export of O-antigen and teichoic acid	45	21.476707	39.193402	21.582628	2.6	0	0	-3.928247	0.0111494
ETAE_0110	wecF	4-alpha-L-fucosyltransferase	31	492.24612	497.00569	459.70997	15.6	0	3.18	-6.058856	2.96E-06
ETAE_0112	wecG	UDP-N-acetyl-D-mannosaminuronic acid transferase	25	1117.6478	1102.4187	1019.7792	241.83	195.84	171.72	-2.404738	1.821E-05
ETAE_0121		putative lipoprotein	6	66.148257	60.874858	69.064409	10.4	0	0	-3.893098	0.0001251
ETAE_0126	uvrD	DNA-dependent helicase II	62	1102.1846	1097.4152	1130.9297	161.22	44.01	254.4	-2.84912	0.0001013
ETAE_0131	recQ	ATP-dependent DNA helicase	54	1637.3841	1729.5131	1638.1215	411.99	452.54	273.44	-2.133979	3.214E-05
ETAE_0137	zntA	zinc/cadmium/mercury/lead-transporting ATPase	43	1553.1954	1618.6041	1587.4023	465.46	107.82	407.05	-2.275881	0.0003606
ETAE_0147	ubiE	ubiquinone/menaquinone biosynthesis methyltransferase	30	238.82098	226.82139	240.6463	5.2	8.8	3.18	-5.135375	9.939E-07
ETAE_0151	tatB	Sec-independent protein secretion pathway component	8	183.84061	205.97383	208.27236	52.01	33.01	54.06	-2.08087	0.0001185
ETAE_0152	tatC	twin arginine-targeting protein translocase	27	2030.8374	2067.2435	2218.6941	725.5	189.23	343.45	-2.325099	0.0005729
ETAE_0158	fre	FMN reductase	23	77.316144	72.549488	74.460066	5.2	0	12.72	-3.441806	6.336E-05
ETAE_0185	purD	phosphoribosylamine-glycine ligase	37	853.91386	869.75995	887.04601	137.82	211.24	149.46	-2.381725	9.029E-06
ETAE_0186	purH	bifunctional phosphoribosylaminoimidazolecarboxamide formyltransferase/i	51	1780.8485	1819.5745	1810.7825	161.22	402.67	181.26	-2.85535	3.779E-05
ETAE_0204	pgi	glucose-6-phosphate isomerase	60	47.248755	42.52901	57.193964	11.4	13	9.5	-2.022998	0.0010548
ETAE_0220	dgkA	diacylglycerol kinase	12	688.11368	659.61661	773.73721	101.41	178.23	76.32	-2.565206	0.0002151
ETAE_0340	poxA	lysyl-tRNA synthetase, class II	27	19.75857	17.511945	9.7121826	5.2	0	3.18	-2.134928	0.0193541
ETAE_0341		putative membrane transport protein	67	1832.3926	1883.785	1783.8042	440.87	363.07	499.27	-2.077357	2.351E-05
ETAE_0351	miaA	tRNA delta(2)-isopentenylpyrophosphate transferase	21	35.221799	35.857793	52.877438	7.8	0	12.72	-2.43238	0.0073778
ETAE_0360	rnr	exoribonuclease R	72	3864.9481	3793.4209	3534.1553	731.15	992.38	878.04	-2.103805	2.203E-05
ETAE_0379		conserved hypothetical protein	16	156.35042	141.76337	140.28708	52.01	28.61	15.9	-2.149031	0.000633
ETAE_0384	argR	arginine repressor	13	42.953413	50.868032	62.589621	2.6	13.2	12.72	-2.338412	0.003075
ETAE_0396	greA	transcription elongation factor	9	322.1506	316.04892	296.76113	83.21	88.82	54.06	-2.048008	0.0003635
ETAE_0397	yhbY	RNA-binding protein	6	67.007325	58.373151	33.453073	0	0	3.18	-4.71076	0.0068413
ETAE_0406	rbfA	ribosome-binding factor A	11	18.899502	22.515358	34.532205	0	6.6	4.72	-2.74612	0.0343798
ETAE_0409	pnp	polyribonucleotide nucleotidyltransferase	66	61.852915	60.040956	69.064409	2.6	0	3.18	-4.465382	2.978E-05
ETAE_0410	nlpI	lipoprotein NlpI, contains TPR repeats	47	572.13947	538.7008	544.96135	132.62	96.82	101.76	-2.311358	8.343E-06
ETAE_0411	deaD	ATP-dependent RNA helicase	53	538.6358	509.51422	502.87523	117.02	72.61	118.54	-2.320235	2.427E-05
ETAE_0412		hypothetical protein	7	32.644594	35.857793	22.661759	10.4	4.4	3.18	-2.166163	0.0058712
ETAE_0479	prfC	peptide chain release factor RF-3	50	113.39701	103.40387	123.02098	0	0	0	-6.836353	3.687E-05
ETAE_0488	deoB	phosphopentomutase	40	1005.1099	1015.6928	1095.3184	249.63	211.24	265.71	-2.100558	0.0001505
ETAE_0494		conserved hypothetical protein	34	301.53296	316.88282	334.53073	96.21	24.2	111.3	-2.026051	0.0010837
ETAE_0497	rpoN	RNA polymerase factor sigma-54	43	734.50337	761.35267	721.9389	52.01	55.01	143.1	-3.133183	3.37E-05
ETAE_0501	kdsC	3-deoxy-D-manno-octulosonate 8-phosphate phosphatase	14	133.15558	125.91923	111.15053	62.41	0	15.9	-2.198542	0.0079791
ETAE_0502	yrbH	D-arabinose 5-phosphate isomerase	24	161.50483	179.28896	213.66802	43.21	35.21	47.7	-2.110161	0.0008186
ETAE_0517	sspA	stringent starvation protein A	18	126.28304	136.75995	106.83401	2.6	2.2	25.44	-3.487708	0.0006291
ETAE_0530		hypothetical protein	10	188.99502	175.11945	160.79058	26	6.6	28.62	-3.039184	0.0001336
ETAE_0543	trpR	Trp operon repressor	8	123.70583	150.10239	132.73316	26	36.01	25.44	-2.216872	0.0034108
ETAE_0570	talB	transaldolase B	34	542.07208	527.86007	637.76665	111.82	33.01	50.88	-3.105849	0.0002753
ETAE_0600	ksgA	dimethyladenosine transferase (rRNA methylation)	19	23.194843	26.684869	16.186971	0	0	0	-4.524956	0.0020409
ETAE_0601	pdxA	4-hydroxythreonine-4-phosphate dehydrogenase	32	106.52447	121.74972	111.15053	0	0	0	-6.834681	1.494E-05
ETAE_0618	leuD	3-isopropylmalate dehydratase small subunit	17	376.2719	376.08987	367.98381	123.45	77.25	64.63	-2.065722	9.474E-05
ETAE_0627	fruR	DNA-binding transcriptional regulator	35	370.25842	356.91013	426.2569	49.41	129.82	47.7	-2.330406	0.0008546
ETAE_0629	mraW	S-adenosyl-methyltransferase	22	142.60533	128.42093	96.042694	0	0	12.72	-4.557121	0.0012091
ETAE_0644		conserved hypothetical protein	17	97.933783	108.40728	131.65403	39.01	13.2	6.36	-2.469452	0.0027042
ETAE_0661		hypothetical protein	6	15.463229	12.508532	15.10784	3.8	2.2	0	-2.84397	0.0116221
ETAE_0670	hpt	hypoxanthine-guanine phosphoribosyltransferase	24	88.484032	64.210466	97.121826	5.2	2.2	6.36	-3.914996	0.0013724
ETAE_0671	cynT	carbonic anhydrase	21	18.899502	24.183163	31.29481	7.8	6.6	0	-2.152826	0.0099271
ETAE_0697		hypothetical protein	11	18.899502	13.342435	20.503497	2.6	4.4	0	-2.478854	0.0037511
ETAE_0712	recD	exonuclease V subunit alpha	35	224.21682	230.157	192.08539	48.01	28.61	59.5	-2.24768	0.0016972
ETAE_0746	ompH	periplasmic chaperone	19	72.161735	80.88851	99.280088	7.8	2.2	6.36	-3.721214	0.0006499
ETAE_0751	rnhB	ribonuclease HII	14	139.16906	150.93629	139.20795	39.81	11	50.88	-2.077853	0.0027116
ETAE_0769		hypothetical protein	15	384.86258	401.10694	332.37247	52.01	114.42	76.32	-2.189963	0.0004505
ETAE_0774	purL	phosphoribosylformylglycinamidine synthase	74	3371.843	3461.5279	3226.6029	702.1	889.2	833.17	-2.052885	4.836E-05
ETAE_0783	apbE	membrane-associated lipoprotein involved in thiamine biosynthesis	29	240.53912	245.16724	237.40891	2.6	4.4	34.98	-4.012843	2.965E-05
ETAE_0854	esaL	putative type III secretion apparatus	30	660.6235	662.95222	673.37799	135.22	59.41	92.22	-2.786588	1.391E-05
ETAE_0856		conserved hypothetical protein	15	390.01699	428.62571	423.01951	0	19.8	0	-5.770577	7.7E-06
ETAE_0857	esaJ	putative type III secretion system apparatus lipoprotein	22	693.26809	662.95222	731.65109	13	24.2	31.8	-4.859964	5.249E-06
ETAE_0859	esaH	putative type III secretion apparatus	6	94.49751	80.88851	76.618329	2.6	0	3.18	-4.860157	0.0001157
ETAE_0860	esaG	putative type III secretion system needle protein	7	180.40434	191.7975	209.35149	0	11	12.72	-4.451343	3.715E-05
ETAE_0861	esrC	putative transcriptional regulator	19	842.74597	830.56655	805.03202	5.2	35.21	15.9	-5.386703	5.671E-07
ETAE_0863	esaD	type-III secretion protein	28	680.38207	611.25028	625.89621	10.4	0	9.54	-6.387494	7.65E-06
ETAE_0864	esaC	Type II secretory pathway, component PulD like protein	47	1973.2798	2003.8669	1860.4225	15.6	46.21	6.36	-6.358696	1.833E-06
ETAE_0865	esaB	two-component sensor/regulator	14	317.85526	361.07964	371.2212	26	26.4	22.26	-3.761404	3.832E-05
ETAE_0868	eseE	type III secretion system effector protein E	12	396.88954	441.13424	373.37946	7.8	4.4	15.9	-5.287189	4.019E-05
ETAE_0869	eseD	type III secretion system effector protein D	18	534.34046	527.86007	495.32131	148.22	74.81	15.9	-2.689367	0.0003948
ETAE_0870	eseC	type III secretion system effector protein C	30	445.85643	486.99886	498.5587	15.6	4.4	168.54	-2.904744	0.0016989
ETAE_0871	escA	type III secretion low calcium response chaperone	15	683.81834	688.80319	731.65109	13	46.21	168.54	-3.190974	0.0002289
ETAE_0872	eseB	EspA family secreted protein	22	752.5438	733	749.99632	325.04	204.64	25.44	-2.003911	0.0030267
ETAE_0873		conserved hypothetical protein	5	185.55875	199.30262	194.24365	23.4	0	25.44	-3.489142	4.132E-05
ETAE_0875	esaP	putative major facilitator family transporter	7	244.83446	266.84869	238.48804	7.8	13.2	3.18	-4.79236	1.172E-05
ETAE_0876	esaO	type III secretion system ATPase	5	80.752417	100.90216	94.963563	0	0	0	-6.542352	0.0001031
ETAE_0877	esaN	type III secretion system ATPase	24	530.90419	537.03299	519.0622	0	11	6.36	-6.287145	1.154E-07
ETAE_0878	esaV	type III secretion protein, HrcV family	43	1205.2728	1221.6667	1249.6342	18.2	24.2	22.26	-5.765092	8.328E-08
ETAE_0879	esaM	type III secretion apparatus protein	7	210.47173	256.00796	228.77586	7.8	0	9.54	-5.101364	7.575E-05
ETAE_0880	esaR	type three secretion apparatus protein R	18	375.41283	355.24232	413.30732	0	4.4	0	-7.276077	2.422E-05
ETAE_0881	esaS	type III secretion apparatus	6	222.49868	199.30262	241.72543	0	4.4	0	-6.492994	5.869E-05
ETAE_0882	esaT	type III secretion system EscT homologue	24	496.54146	456.97838	506.11262	0	4.4	3.18	-7.111084	5.641E-06
ETAE_0883	esaU	type III secretion system EscU homologue	24	891.71286	868.92605	858.98859	0	0	63.6	-5.299347	3.344E-06
ETAE_0884		putative transglycosylase signal peptide protein	29	925.21653	883.10239	1038.1244	31.2	99.02	120.84	-3.487439	8.603E-05
ETAE_0885	esrA	two-component sensor/regulator	69	2133.9256	2175.6507	2254.3055	23.4	2.2	47.7	-6.427382	5.497E-07
ETAE_0888		putative TTSS effector protein	92	2063.482	2153.1354	1923.0121	197.63	272.85	292.56	-3.003365	1.629E-05
ETAE_0956	ahpC	alkyl hydroperoxide reductase, small subunit	23	122.84676	125.91923	169.42363	2.6	6.6	9.54	-4.276046	0.0009299
ETAE_0959	tgt	queuine/archaeosine tRNA-ribosyltransferase	49	514.58189	481.99545	522.2996	137.82	114.42	95.4	-2.117789	2.341E-05
ETAE_0973		conserved hypothetical protein	8	53.262233	62.542662	63.668752	0	2.2	15.9	-3.112373	0.0008389
ETAE_0993		ATP-dependent protease	16	54.121301	46.698521	53.95657	10.4	0	6.36	-2.997226	0.0002934
ETAE_0997	comEA	competence protein ComEA	3	12.026956	19.17975	12.949577	3.8	0	3.18	-2.66132	0.0256509
ETAE_1003	glnK	nitrogen regulatory protein P-II	5	43.812482	44.196815	33.453073	5.2	8.8	3.18	-2.624712	0.0008621

ETAE_1021		hypothetical protein	7	47.248755	62.542662	57.193964	15.6	19.8	0	-2.146232	0.004279
ETAE_1025	adk	adenylate kinase	22	18.899502	10.006826	16.186971	2.6	0	3.18	-2.453543	0.0095307
ETAE_1086	purM	phosphoribosylformylglycinamidine cyclo-ligase	20	851.33665	842.24118	887.04601	106.61	107.82	130.38	-2.893025	1.18E-06
ETAE_1095	gcvR	glycine cleavage system transcriptional repressor	19	151.19602	136.75995	162.94884	44.21	8.8	34.98	-2.31861	0.0007491
ETAE_1098	purC	phosphoribosylaminoimidazole-succinocarboxamide synthase	17	485.37357	444.46985	488.84652	49.41	39.61	114.48	-2.783393	0.0001232
ETAE_1128		hypothetical protein	15	290.36507	292.69966	268.70372	46.81	30.81	117.66	-2.107994	0.0013998
ETAE_1131	ptsI	phosphoenolpyruvate-protein phosphotransferase	43	47.248755	58.373151	59.352227	15.6	19.8	0	-2.129061	0.0038179
ETAE_1167		hypothetical protein	16	4.2953413	9.1729238	5.395657	0	0	2.18	-3.11323	0.0452115
ETAE_1169		hypothetical protein	122	56.698506	45.864619	39.927862	2.6	2.2	6.36	-3.361037	0.0010007
ETAE_1201	galE	UDP-glucose 4-epimerase	56	1262.8304	1299.2196	1101.7932	75.41	72.61	66.78	-4.073463	4.581E-05
ETAE_1207	neuB	sialic acid synthase	81	24.91298	25.017065	25.899153	2.6	0	3.18	-3.166437	2.213E-05
ETAE_1208	neuA	acylneuraminate cytidylyltransferase	118	42.094345	52.535836	39.927862	5.2	2.2	9.54	-2.786303	0.0009056
ETAE_1212	gnd	6-phosphogluconate dehydrogenase	48	768.8661	738.83732	789.92418	75.41	8.8	181.26	-3.099195	0.0002058
ETAE_1407	hemK	N5-glutamine S-adenosyl-L-methionine-dependent methyltransferase	17	233.66657	223.48578	200.71844	96.21	15.4	0	-2.527635	0.0043904
ETAE_1445	msbB	lipid A biosynthesis (KDO)2-(lauroyl)-lipid IVA acyltransferase	28	298.09669	341.89989	338.84726	57.21	17.6	15.9	-3.389219	0.0001105
ETAE_1449	zwf	glucose-6-phosphate 1-dehydrogenase	38	758.55728	791.37315	786.68679	199.27	110.26	237.77	-2.087982	0.000108
ETAE_1450	devB	6-phosphogluconolactonase	14	340.19103	326.88965	331.29334	67.61	45.23	66.78	-2.455064	5.113E-06
ETAE_1461	minE	cell division topological specificity factor	11	21.476707	40.861206	19.424365	0	2.2	0	-4.026839	0.018129
ETAE_1462	minD	septum site-determining protein	24	420.94345	381.09329	343.16378	83.21	26.4	63.6	-2.704007	0.0003169
ETAE_1463	minC	septum site-determining protein	25	749.9666	747.17634	679.85278	202.83	85.82	149.81	-2.311821	0.0030053
ETAE_1468	dsbB	disulphide bond formation protein	12	188.13595	202.63823	207.19323	20.8	15.4	34.98	-3.018185	2.801E-05
ETAE_1472	fadR	fatty acid metabolism regulator	36	45.530618	44.196815	41.006993	10.4	0	12.72	-2.356144	0.0009716
ETAE_1486	pncA	nicotinamidase/pyrazinamidase	11	487.95078	478.65984	466.18476	41.61	72.61	143.1	-2.463492	0.0002167
ETAE_1518	cls	cardiolipin synthetase	50	130.57838	147.60068	125.17924	23.4	24.2	25.44	-2.417922	8.423E-05
ETAE_1545	rluB	ribosomal large subunit pseudouridine synthase B	22	23.194843	30.020478	30.215679	7.8	0	3.18	-2.628184	0.001718
ETAE_1553	cysB	transcriptional regulator	35	10.308819	15.010239	15.10784	3.2	0	3.18	-2.663687	0.0081815
ETAE_1554	cspC	cold shock protein	6	67.866393	73.38339	87.409643	10.4	0	9.54	-3.336068	0.0004868
ETAE_1557	manZ	PTS system, mannose-specific IID component	31	658.90536	669.62344	659.34928	130.63	183.85	176.66	-2.010413	8.092E-06
ETAE_1558	manY	PTS system, mannose-specific IIC component	25	724.19455	795.54266	663.66581	188.87	160.87	163.41	-2.082697	0.0001419
ETAE_1559	manX	PTS system, mannose-specific IIB component	34	877.96777	831.40046	834.16857	179.88	244.48	199.27	-2.022851	1.249E-05
ETAE_1614		regulatory prophage protein cI	20	115.97422	107.57338	111.15053	15.6	46.21	12.72	-2.122908	0.001394
ETAE_1615	cro	putative phage transcriptional regulatory protein	11	85.906827	94.230944	124.10011	18.2	11	25.44	-2.414214	0.0025085
ETAE_1632		hypothetical protein	3	60.993847	59.207053	46.40265	2.6	0	31.8	-2.181056	0.0169463
ETAE_1655	prc	carboxy-terminal protease	61	174.39086	168.44824	176.97755	7.8	11	9.54	-4.060228	4.347E-07
ETAE_1675		hypothetical protein	5	32.644594	28.352673	36.690467	5.2	0	12.72	-2.266933	0.0038064
ETAE_1695	rsxE	SoxR-reducing system protein	17	91.920305	84.224118	90.647037	33.8	4.4	6.36	-2.504024	0.0016318
ETAE_1696	rnfG	electron transport complex protein	16	34.362731	33.356086	14.028708	5.2	0	0	-3.369475	0.020289
ETAE_1697	rnfD	electron transport complex protein	23	46.389686	40.861206	46.40265	7.8	2.2	0	-3.393939	0.0001554
ETAE_1698	rnfC	electron transport complex protein	46	157.20949	151.77019	142.44534	44.21	33.01	15.9	-2.241134	0.0002112
ETAE_1700		Na(+)-translocating NADH-quinone reductase subunit E	20	29.208321	19.17975	21.582628	0	0	0	-4.604283	0.0015192
ETAE_1705	add	adenosine deaminase	23	353.07706	321.88623	311.86897	28.6	11	54.06	-3.356193	7.179E-05
ETAE_1712		hypothetical protein	9	55.839437	41.695108	61.51049	5.2	18.61	6.36	-2.398249	0.0146758
ETAE_1786		predicted permease	34	693.26809	696.3083	656.11189	202.83	72.61	128.46	-2.340516	0.00217
ETAE_1792	aroH	3-deoxy-7-phosphoheptulonate synthase	25	81.611485	80.88851	90.647037	0	0	0	-6.415866	1.139E-05
ETAE_1822	pfkB	6-phosphofructokinase	26	1254.2397	1239.1786	1238.8428	310.12	201.66	298.53	-2.199332	9.649E-06
ETAE_1839		hypothetical protein	4	125.42397	112.57679	108.99227	10.4	24.2	12.72	-2.798122	0.0001087
ETAE_1840	pabB	anthranilate/para-aminobenzoate synthases component I	31	584.16642	615.4198	575.17703	18.2	13.2	12.72	-5.23758	1.245E-06
ETAE_1851		hypothetical protein	14	21.476707	18.345848	7.5539198	0	0	0	-4.069716	0.0200376
ETAE_1883	potC	spermidine/putrescine ABC transporter membrane protein	22	159.7867	203.47213	187.76886	44.21	19.8	56.32	-2.195128	0.0027405
ETAE_1910		hypothetical protein	35	972.46528	1040.7099	966.90173	231.43	160.63	318	-2.064706	0.0001232
ETAE_1967		HpcH/HpaI aldolase family protein	9	121.98769	117.5802	90.647037	13	6.6	38.16	-2.455259	0.002714
ETAE_1981		hypothetical protein	3	16.322297	19.17975	14.028708	5.2	2.6	0	-2.666779	0.0073317
ETAE_1982	leuD	3-isopropylmalate dehydratase small subunit	19	469.05127	483.66325	444.60213	86.27	62.65	52.45	-2.776498	1.246E-05
ETAE_2044	uvrC	excinuclease ABC subunit C	51	923.49839	969.82821	1095.3184	289.32	185.54	252.25	-2.034753	0.0002255
ETAE_2071		transcriptional regulator, DeoR family	13	450.15177	456.14448	473.73868	60.05	62.63	54.25	-2.94233	7.32E-07
ETAE_2079		DedA-family membrane protein	12	232.8075	240.16382	254.67501	75.41	8.8	79.5	-2.131833	0.0013896
ETAE_2099	fabG	3-ketoacyl-(acyl-carrier-protein) reductase	28	12.886024	10.006826	21.582628	2.2	2.2	3.18	-2.55274	0.034601
ETAE_2114	fumA	hydro-lyase, Fe-S type, tartrate/fumarate subfamily, beta subunit	59	927.79373	885.6041	911.86603	101.41	26.4	238.5	-2.885079	0.0002415
ETAE_2176	cmk	cytidylate kinase	19	24.053912	27.518771	25.899153	10.4	0	6.36	-2.025901	0.0031556
ETAE_2177	aroA	3-phosphoshikimate 1-carboxyvinyltransferase	35	572.99854	569.55518	467.26389	2.6	2.2	3.18	-7.198561	0.0001039
ETAE_2178	serC	phosphoserine aminotransferase	36	11.167887	9.1729238	5.395657	2.2	0	0	-3.548239	0.047556
ETAE_2202	trxB	thioredoxin reductase (NADPH)	29	329.02315	317.71672	311.86897	26	8.8	57.24	-3.338843	4.337E-05
ETAE_2241	grxA	glutaredoxin 1	11	110.81981	91.729238	76.618329	26	19.8	12.72	-2.197424	0.0022761
ETAE_2260		undecaprenyl-diphosphatase	17	250.84793	281.85893	283.81156	18.2	0	69.96	-3.168304	0.0004969
ETAE_2281	hisF	imidazole glycerol phosphate synthase subunit	16	413.21184	437.79863	405.7534	75.22	96.82	120.84	-2.101332	3.442E-05
ETAE_2298		NLP/P60 protein	29	852.19572	833.90216	836.32683	91.01	123.22	111.3	-2.942429	3.066E-07
ETAE_2306		hypothetical protein	12	19.75857	23.349261	22.661759	5.8	6.6	0	-2.407081	0.0030077
ETAE_2324		putative transcriptional regulator	20	871.09522	778.03072	883.80861	137.82	11	152.64	-3.058193	0.0001852
ETAE_2326		transcriptional regulator, AraC family	13	271.46557	277.68942	308.63158	93.61	26.4	50.88	-2.307481	0.0005486
ETAE_2327	rhlE	ATP-dependent RNA helicase	36	1499.0741	1433.4778	1411.5039	281.98	491.87	224.32	-2.118352	0.0001989
ETAE_2334	rcsB	two-component system, NarL family, captular synthesis response regulato	14	140.02813	134.25825	105.75488	20.8	35.21	0	-2.698468	0.0018366
ETAE_2346	moaC	molybdenum cofactor biosynthesis protein C	10	615.95195	585.39932	512.58741	86.46	102.06	97.85	-2.568851	0.0001052
ETAE_2347	moaA	molybdenum cofactor biosynthesis protein A	22	382.28538	434.46303	382.01251	79.65	43.48	47.65	-2.789816	8.022E-05
ETAE_2359	menF	isochorismate synthase	29	652.89188	676.29465	693.88149	190.28	155.25	120.11	-2.112131	2.476E-05
ETAE_2373	nuoN	NADH:ubiquinone oxidoreductase subunit 2 (chain N)	38	109.10167	102.56997	85.25138	2.6	4.4	3.18	-4.50817	0.0001796
ETAE_2374	nuoM	NADH:ubiquinone oxidoreductase subunit 4 (chain M)	45	170.95459	180.12287	183.45234	7.8	0	3.18	-5.264908	2.348E-06
ETAE_2375	nuoL	NADH:ubiquinone oxidoreductase subunit 5 (chain L)/multisubunit Na+/H+	56	267.17023	260.17747	295.682	5.2	4.4	9.54	-5.221467	1.67E-05
ETAE_2376	nuoK	NADH:ubiquinone oxidoreductase subunit 11 or 4L (chain K)	7	36.939936	50.03413	46.40265	0	0	3.18	-4.463847	0.0004274
ETAE_2377	nuoJ	NADH:ubiquinone oxidoreductase subunit 6 (chain J)	12	90.202168	95.064846	83.093117	13	6.6	19.08	-2.702782	0.0001067
ETAE_2378	nuoI	formate hydrogenlyase subunit 6/NADH:ubiquinone oxidoreductase 23 kD	18	42.094345	50.868032	36.690467	0	0	0	-5.466549	0.0004718
ETAE_2380	nuoG	NADH dehydrogenase/NADH:ubiquinone oxidoreductase 75 kD subunit (c	68	349.64079	371.08646	397.12035	15.6	2.2	12.72	-5.063424	1.446E-05
ETAE_2381	nuoF	NADH:ubiquinone oxidoreductase, NADH-binding (51 kD) subunit	29	92.779373	87.559727	87.409643	5.2	0	0	-5.045187	3.812E-06
ETAE_2382	nuoE	NADH:ubiquinone oxidoreductase 24 kD subunit	11	30.926458	26.684869	39.927862	0	0	0	-5.066652	0.0011363
ETAE_2383	nuoD	NADH:ubiquinone oxidoreductase 49 kD subunit 7	49	288.64694	242.66553	270.86198	18.2	2.2	6.36	-4.757855	5.386E-05
ETAE_2384	nuoB	NADH:ubiquinone oxidoreductase 20 kD subunit and related Fe-S oxidore	27	185.55875	161.77702	215.82628	5.2	0	0	-6.109447	0.0002933
ETAE_2385	nuoA	NADH:ubiquinone oxidoreductase subunit 3 (chain A)	15	32.644594	46.698521	37.769599	2.6	0	0	-4.422818	0.0008103
ETAE_2391		aminotransferase class I and II	31	1456.1207	1477.6746	1533.4457	228.83	330.06	324.36	-2.334567	7.568E-06
ETAE_2398	pta	phosphotransacetylase	39	16.322297	18.345848	15.10784	5.2	0	4.36	-2.380367	0.0042173
ETAE_2410	cvpA	colicin V production protein	19	274.04278	238.49602	212.58888	46.81	6.6	44.52	-2.850836	0.0006934
ETAE_2428	evpP	type VI secretion system protein EvpP	29	377.99004	371.92036	441.36474	143.02	61.61	15.9	-2.417595	0.0017144
ETAE_2429	evpA	type VI secretion system protein EvpA	12	267.17023	216.81456	247.12109	0	0	0	-7.934882	7.623E-05
ETAE_2430	evpB	type VI secretion system protein EvpB	50	898.58541	848.0785	946.39823	270.44	26.4	22.26	-3.065273	0.0008037
ETAE_2431	evpC	type VI secretion system protein EvpC	16	73.020803	89.227531	137.04969	2.6	2.2	0	-5.276354	0.006968
ETAE_2432	evpD	type VI secretion system protein EvpD	33	885.69938	842.24118	822.29812	41.61	22	15.9	-4.951616	2.189E-06
ETAE_2433	evpE	type VI secretion system protein EvpE	8	83.329622	73.38339	96.042694	0	2.2	0	-5.620111	0.0002243
ETAE_2434	evpF	type VI secretion system protein EvpF	41	1395.1269	1346.752	1401.7917	13	35.21	9.54	-6.092925	2.326E-07
ETAE_2435	evpG	type VI secretion system protein EvpG	18	668.35511	681.29807	741.36327	7.8	26.4	34.98	-4.85853	9.378E-06
ETAE_2436	evpH	type VI secretion system protein EvpH	39	1187.2323	1117.4289	1128.7714	39.01	4.4	3.18	-6.114719	1.351E-06
ETAE_2437	evpI	type VI secretion system protein EvpI	55	1906.2725	1882.1172	1964.0191	26	37.41	41.34	-5.739159	1.784E-07
ETAE_2438	evpJ	type VI secretion system protein EvpJ	4	124.5649	125.08532	106.83401	0	0	0	-6.904822	3.832E-05
ETAE_2439	evpK	type VI secretion system protein EvpK	26	831.57808	908.11945	926.97387	23.4	4.4	15.9	-5.837096	7.914E-06
ETAE_2440	evpL	type VI secretion system protein EvpL	18	373.6947	385.2628	374.45859	5.2	11	0	-5.887241	1.802E-07

ETAE_2441	evpM	type VI secretion system protein EvpM	38	1110.7753	1144.9477	1225.8933	10.4	39.61	25.44	-5.473083	5.483E-06
ETAE_2442	evpN	type VI secretion system protein EvpN	20	970.74714	999.84869	1038.1244	20.8	50.61	34.98	-4.783035	1.412E-06
ETAE_2443	evpO	type VI secretion system protein EvpO	86	2226.705	2208.1729	2314.7368	41.61	50.61	47.7	-5.562167	3.007E-07
ETAE_2445	aroC	chorismate synthase	19	374.55377	376.08987	336.689	88.41	35.21	115.36	-2.185832	0.00263
ETAE_2448	sixA	phosphohistidine phosphatase	10	53.262233	47.532423	53.95657	7.8	0	12.72	-2.745691	0.0004502
ETAE_2488		hypothetical protein	9	25.772048	19.17975	32.373942	5.2	2.2	9.54	-2.010197	0.0099396
ETAE_2524		hypothetical protein	12	21.476707	25.017065	26.978285	7.8	4.4	3.18	-2.056796	0.0007999
ETAE_2547	uvrB	excinuclease ABC subunit B	43	1812.634	1826.2457	1890.6382	455.24	340.04	281.56	-2.357119	1.24E-05
ETAE_2575	tolR	colicin uptake protein	13	3.7181365	1.6678043	4.3165256	0	0	0	-2.01	0.0425803
ETAE_2582	sucC	succinyl-CoA synthetase subunit beta	27	422.66159	406.94425	374.45859	46.81	57.21	38.16	-3.055588	2.028E-05
ETAE_2583	sucB	2-oxoglutarate dehydrogenase, E2 subunit, dihydrolipoamide succinyltrans	28	173.53179	162.61092	185.6106	13	6.6	6.36	-4.179506	1.897E-05
ETAE_2584	sucA	component of the 2-oxoglutarate dehydrogenase complex,thiamin-binding	59	824.70554	778.03072	796.39897	0	8.8	9.54	-6.814613	5.663E-07
ETAE_2585	sdhB	succinate dehydrogenase iron-sulfur subunit	20	297.23762	288.53015	285.96982	78.81	63.62	64.94	-2.055921	3.082E-06
ETAE_2586	sdhA	succinate dehydrogenase catalytic subunit	33	977.61969	1006.5199	1015.4626	218.43	288.25	157.58	-2.169892	3.887E-05
ETAE_2587	sdhD	succinate dehydrogenase cytochrome b556 small membrane subunit	15	902.88075	927.2992	904.31211	179.42	74.81	168.54	-2.684709	2.281E-05
ETAE_2588	sdhC	succinate dehydrogenase cytochrome b556 large membrane subunit	11	193.29036	180.12287	173.74015	57.61	33.01	34.98	-2.123109	0.0004052
ETAE_2589	gltA	type II citrate synthase	41	1353.0325	1366.7656	1427.6908	176.82	244.24	337.08	-2.447048	2.617E-05
ETAE_2593	edwR	AHL-dependent transcriptional regulator	32	275.76091	287.69625	247.12109	67.61	35.21	38.16	-2.498413	0.0001484
ETAE_2617	nagB	glucosamine-6-phosphate deaminase	33	446.7155	467.81911	468.34303	140.42	68.21	114.48	-2.087369	9.26E-05
ETAE_2619	nagC	putative N-acetylglucosamine regulatory protein	28	168.37738	185.96018	173.74015	41.61	8.8	12.72	-3.005546	0.0001802
ETAE_2649	lipB	lipoate-protein ligase B	23	329.88222	331.05916	240.6463	101.41	28.61	87.66	-2.050259	0.0057991
ETAE_2700	purE	phosphoribosylaminoimidazole carboxylase catalytic subunit	8	164.94111	156.77361	149.99926	7.8	2.2	22.26	-3.750954	3.788E-05
ETAE_2701	purK	phosphoribosylaminoimidazole carboxylase	22	752.5438	804.71559	735.96761	187.23	170.65	181.26	-2.088647	0.0001005
ETAE_2724	lepA	GTP-binding protein	48	79.034281	70.881684	85.25138	26	6.6	6.36	-2.504889	0.0010659
ETAE_2731	srmB	ATP-dependent RNA helicase	31	399.46674	342.73379	362.58815	46.81	17.6	47.7	-3.266598	6.846E-05
ETAE_2738	smpA	SmpA/OmlA domain protein	14	79.893349	82.556314	66.906146	10.4	6.6	19.08	-2.571833	0.00045
ETAE_2739		hypothetical protein	7	18.899502	16.678043	39.927862	7.8	0	0	-2.861761	0.045251
ETAE_2786	guaA	GMP synthase, large subunit	31	108.2426	105.07167	135.97056	15.6	2.2	0	-4.082087	0.0005442
ETAE_2787	guaB	inositol-5-monophosphate dehydrogenase	35	621.96543	642.10466	614.02576	0	0	0	-9.292395	1.903E-07
ETAE_2812	hscB	co-chaperone Hsc20	11	20.617638	15.010239	20.503497	3.8	0	6.36	-2.465907	0.0098739
ETAE_2855	gshA	glutamate--cysteine ligase	47	134.01465	123.41752	133.81229	2.6	8.8	25.44	-3.306801	0.0001034
ETAE_2876	surE	stationary phase survival protein	14	315.27805	311.04551	305.39418	57.42	50.61	85.86	-2.264655	0.0005739
ETAE_2877	truD	tRNA pseudouridine synthase D	18	500.8368	474.49033	433.81082	111.82	63.81	124.02	-2.222159	0.0001596
ETAE_2879	ispD	2-C-methyl-D-erythritol 4-phosphate cytidylyltransferase	13	18.040434	32.522184	49.640044	0	0	0	-5.104374	0.0216312
ETAE_2947		Z-ring-associated protein	13	348.78172	346.9033	339.92639	110.82	63.81	50.88	-2.199219	0.0012334
ETAE_2964	metK	S-adenosylmethionine synthetase	30	14.604161	12.508532	8.6330512	4.8	0	0	-2.896665	0.0410327
ETAE_3036		hypothetical protein	12	28.349253	17.511945	14.028708	7.8	0	3.18	-2.169464	0.0286353
ETAE_3148	panF	sodium/panthothenate symporter	37	285.21067	335.22867	328.05594	65.01	59.41	79.5	-2.201123	0.00012
ETAE_3248	trpD	anthranilate synthase component II	17	702.71784	636.26735	623.73795	31.2	15.4	85.86	-3.859121	4.742E-05
ETAE_3278	envZ	osmolarity sensor protein	44	786.90653	751.34585	841.72249	109.21	79.21	159	-2.765607	4.248E-05
ETAE_3312	glpD	glycerol-3-phosphate dehydrogenase	41	42.094345	65.044369	31.29481	7.8	2.2	0	-3.443541	0.0138098
ETAE_3327		cell division protein	26	2007.6425	2027.2162	1773.0129	518.88	255.25	575.59	-1.999998	0.0004977
ETAE_3328	ftsE	cell division protein	17	1525.7052	1475.1729	1310.0655	405.66	239.84	386.55	-2.062491	0.0004073
ETAE_3367	gor	glutathione-disulfide reductase	42	809.24231	883.93629	793.16158	260.04	116.62	146.28	-2.242793	0.0002275
ETAE_3400	proC	pyrroline-5-carboxylate reductase	16	210.47173	203.47213	199.63931	5.2	2.2	9.54	-4.950558	8.151E-07
ETAE_3438	menA	1,4-dihydroxy-2-naphthoate octaprenyltransferase	33	1108.1981	1129.1035	1148.1958	313.91	231.28	226.47	-2.129011	9.101E-06
ETAE_3446	fpr	ferredoxin-NADP reductase	23	394.31234	361.07964	353.9551	41.61	22	66.78	-3.059885	5.398E-05
ETAE_3450	pfk	6-phosphofructokinase	35	240.53912	276.02162	279.49503	65.01	30.81	69.96	-2.243152	0.0002762
ETAE_3461	gpm	phosphoglycerate mutase	45	173.53179	150.93629	152.15753	62.41	0	22.26	-2.451754	0.0026717
ETAE_3462		membrane-bound metallopeptidase	35	1879.6414	1886.2867	2006.1053	309.44	72.61	314.82	-3.04467	4.677E-05
ETAE_3476		transcriptional regulator, LysR family	29	1140.8427	1159.9579	1083.4479	72.81	2.2	216.24	-3.525	0.0001043
ETAE_3481	argB	acetylglutamate kinase	19	1043.7679	1050.7167	1016.5418	117.47	359.38	244.47	-2.104082	0.0003523
ETAE_3492	yihK	GTP-binding protein	64	111.67887	116.7463	98.200957	0	2.2	3.18	-5.297737	4.449E-05
ETAE_3493	glnA	glutamine synthetase	44	944.9751	953.98407	1026.254	252.23	55.01	155.82	-2.651433	0.000194
ETAE_3531	atpA	F-type H+-transporting ATPase alpha chain	50	5.1544096	8.3390216	5.395657	0	0	1.18	-4.000694	0.0237262
ETAE_3540	pstA	ABC-type phosphate transport system, permease component	26	24.053912	19.17975	21.582628	5.2	0	0	-3.047936	0.0008805
ETAE_3554	lpxH	UDP-2,3-diacylglucosamine pyrophosphatase	24	18.899502	17.511945	22.661759	0	2.2	0	-3.577387	0.0003716

Table S11 Regions for genes of interests after in vivo and in vitro screening

ID	loc-s	loc-e	gene	Annotation-nr	DMEM/Input	J774A.1/Input	Turbot/Input	category
ETAE_0073	65362	66456	wabH	putative glycosy	-2.131967136	0.753208244	1.042644337	region1
ETAE_0074	66460	67587	waaG	lipopolysacchari	-1.12998707	1.177650735	-3.191256379	region1
ETAE_0075	67584	68660	waaQ	heptosyl III transf	-2.856865972	0.586506554	-2.036103053	region1
ETAE_0076	68793	69764	walW	lipopolysaccahri	-3.033742991	-0.904675783	-2.703135853	region1
ETAE_0077	69850	71061		putative glycosy	-0.012558773	-0.235049314	0.780377638	region1
ETAE_0078	71268	72374	walR	putative glycosy	-2.503221036	0.126252918	1.592898884	region1
ETAE_0079	72378	73535	wabK	putative glycosy	-3.104561798	0.255657819	0	region1
ETAE_0080	73537	74670	waaL	lipid A core - O-c	0.11381022	-0.867720963	0.1398864	region1
ETAE_0081	74660	75625	waaC	ADP-heptose:LPS	1.097024454	4.07980996	-1.315193724	region1
ETAE_0082	75613	76674	waaF	ADP-heptose:LPS	0.952243775	0.383626693	-1.191401195	region1
ETAE_0083	76698	77627	rfaD	ADP-L-glycero-D	-1.659230386	0.639753601	-1.355002573	region1
ETAE_0860	942694	942915	esaG	putative type III s	0.335681578	-2.735750711	-4.451342723	region2
ETAE_0861	942934	943626	esrC	putative transcrip	0.684854525	-3.500291293	-5.386702891	region2
ETAE_0862	943711	943935		hypothetical pro	0.40428455	0.289725369	0.764671248	region2
ETAE_0863	943946	945136	esaD	type-III secretion	0.030868954	0.183084454	-6.387494218	region2
ETAE_0864	945144	946628	esaC	Type II secretory	0.081003617	-0.488940103	-6.358695937	region2
ETAE_0865	946625	947104	esaB	two-component	-0.074744379	-0.89731476	-3.761403766	region2
ETAE_0866	947143	948162	eseG	two-component	-0.132075936	0.233248623	-1.015808013	region2
ETAE_0867	948050	948541	escB	type III secretion	0.210345642	0.08486143	-1.413532895	region2
ETAE_0868	948697	949080	eseE	type III secretion	0.102403366	-0.139261225	-5.287189162	region2
ETAE_0869	949091	949672	eseD	type III secretion	0.121914919	0.030338547	-2.689366966	region2
ETAE_0870	949688	951208	eseC	type III secretion	0.057012458	-0.015564898	-2.90474386	region2
ETAE_0871	951121	951588	escA	type III secretion	0.000339695	0.099214783	-3.190974411	region2
ETAE_0872	951599	952195	eseB	EspA family secre	0.303516655	0.083900032	-2.003910926	region2
ETAE_0873	952220	952567		conserved hypo	-0.04188396	-0.448116749	-3.48914182	region2
ETAE_0874	952871	953785	esaQ	translocation pro	0.125934069	-0.383922713	-5.315107022	region2
ETAE_0875	953763	954236	esaP	putative major fa	-0.073484791	0.072366716	-4.792360448	region2
ETAE_0876	954233	954601	esaO	type III secretion	0.007363707	-1.358719487	-6.542351654	region2
ETAE_0877	954595	955911	esaN	type III secretion	-0.061162966	1.099063679	-6.287144834	region2
ETAE_0878	955898	957955	esaV	type III secretion	-0.100326418	-0.140884208	-5.765091606	region2
ETAE_0879	957939	958319	esaM	type III secretion	-0.016531647	0.653106873	-5.101363541	region2
ETAE_0880	958499	959146	esaR	type three secre	-0.160763926	1.154581364	-7.27607721	region2
ETAE_0881	959165	959434	esaS	type III secretion	-0.039179404	-2.101048748	-6.492993654	region2
ETAE_0882	959434	960216	esaT	type III secretion	0.087116512	-2.967488623	-7.111083855	region2
ETAE_0883	960213	961271	esaU	type III secretion	0.050794596	-3.749764336	-5.299346927	region2
ETAE_0884	961264	961914		putative transgly	0.172018165	-3.553164088	-3.487438937	region2
ETAE_0885	961860	964661	esrA	two-component	0.344473177	-3.261240893	-6.427381621	region2
ETAE_0886	964658	965302	esrB	two-component	0.099314503	-3.141890979	-1.667898125	region2
ETAE_2373	2498661	2500118	nuoN	NADH:ubiquinon	0.029350574	-1.694218146	-4.508169964	region3
ETAE_2374	2500125	2501648	nuoM	NADH:ubiquinon	-0.061208448	-2.495901617	-5.264908444	region3
ETAE_2375	2501726	2503570	nuoL	NADH:ubiquinon	-0.050097379	-1.71155172	-5.221466542	region3
ETAE_2376	2503567	2503869	nuoK	NADH:ubiquinon	-0.350862071	-1.924347325	-4.463846693	region3
ETAE_2377	2503866	2504438	nuoJ	NADH:ubiquinon	-0.430819243	-3.582410392	-2.702781594	region3
ETAE_2378	2504449	2504991	nuoI	formate hydroge	0.093756537	-2.221482716	-5.4665493	region3
ETAE_2379	2505009	2505986	nuoH	NADH:ubiquinon	0.171767748	-0.594618037	-3.324725804	region3
ETAE_2380	2505983	2508718	nuoG	NADH dehydrog	0.044950791	-1.717393614	-5.063424172	region3
ETAE_2381	2508779	2510125	nuoF	NADH:ubiquinon	0.114994175	-3.648998663	-5.04518692	region3
ETAE_2382	2510122	2510622	nuoE	NADH:ubiquinon	0.399321671	-1.204341271	-5.066651638	region3
ETAE_2383	2510625	2512421	nuoD	NADH:ubiquinon	0.110122605	-2.274364101	-4.757854957	region3
ETAE_2384	2512521	2513195	nuoB	NADH:ubiquinon	-0.117939029	-1.810318535	-6.109447314	region3
ETAE_2385	2513259	2513618	nuoA	NADH:ubiquinon	0.445872139	-2.500223919	-4.422818233	region3
ETAE_2428	2554573	2555136	evpP	type VI secretion	-0.011017199	-0.192785759	-2.417594876	region4
ETAE_2429	2555386	2555901	evpA	type VI secretion	0.194115069	-0.699248533	-7.934881853	region4
ETAE_2430	2555898	2557385	evpB	type VI secretion	-0.052361621	-0.402694053	-3.065273183	region4
ETAE_2431	2557455	2557946	evpC	type VI secretion	-0.044305356	-0.429432845	-5.276353601	region4
ETAE_2432	2558043	2559248	evpD	type VI secretion	0.039331342	-0.079935946	-4.951615624	region4
ETAE_2433	2559257	2559733	evpE	type VI secretion	0.001068584	-0.160079486	-5.620110996	region4
ETAE_2434	2559737	2561578	evpF	type VI secretion	-0.092801513	-0.021723099	-6.092925209	region4
ETAE_2435	2561575	2562600	evpG	type VI secretion	-0.055207938	-0.417009205	-4.85852982	region4
ETAE_2436	2562719	2565331	evpH	type VI secretion	0.0317927	-0.165080774	-6.114718663	region4
ETAE_2437	2565331	2567316	evpI	type VI secretion	0.051936205	-0.262586565	-5.739158632	region4
ETAE_2438	2567411	2567713	evpJ	type VI secretion	0.123923695	0.138112081	-6.904822177	region4
ETAE_2439	2567727	2568794	evpK	type VI secretion	0.027725446	-0.232445393	-5.83709582	region4
ETAE_2440	2568715	2569422	evpL	type VI secretion	0.299428151	0.058126482	-5.887241041	region4
ETAE_2441	2569522	2570910	evpM	type VI secretion	0.211728325	-0.087730055	-5.473082509	region4
ETAE_2442	2570907	2571557	evpN	type VI secretion	-0.531149416	-0.106168872	-4.783034998	region4
ETAE_2443	2571545	2575336	evpO	type VI secretion	0.030628451	-0.184312318	-5.56216652	region4

Table 12 Intracellular growth deficient mutants

Strain with mutation in WT	Annotation	Gene name	Intracellular growth	Autoaggregation
/			+	+
ETAE_0854	Putative type III secretion apparatus	esaL ETAE_0854	-	-
ETAE_0856	Uncharacterized protein	ETAE_0856	-	-
ETAE_0857	Lipoprotein	esaJ ETAE_0857	-	-
ETAE_0860	Putative type III secretion system needle protein	esaG ETAE_0860	-	-
ETAE_0861	Putative transcriptional regulator EsrC	esrC ETAE_0861	-	-
ETAE_0863	Type-III secretion protein	esaD ETAE_0863	-	-
ETAE_0864	Type II secretory pathway, component PulD like protein	esaC ETAE_0864	-	-
ETAE_0865	Uncharacterized protein	esaB ETAE_0865	-	-
ETAE_0872	EspA family secreted protein	eseB ETAE_0872	-	-
ETAE_0875	Putative major facilitator family transporter	esaP ETAE_0875	-	-
ETAE_0877	Type III secretion system ATPase	esaN ETAE_0877	-	-
ETAE_0878	Type III secretion protein, HrcV family	esaV ETAE_0878	-	-
ETAE_0879	Type III secretion apparatus protein	esaM ETAE_0879	-	-
ETAE_0880	Type three secretion apparatus protein R	esaR ETAE_0880	-	-
ETAE_0881	Type III secretion apparatus	esaS ETAE_0881	-	-
ETAE_0882	Type III secretion apparatus protein	esaT ETAE_0882	-	-
ETAE_0883	Type III secretion apparatus protein	esaU ETAE_0883	-	-
ETAE_0884	Putative transglycosylase signal peptide protein	ETAE_0884	-	-
ETAE_0885	Two-component sensor/regulator EsrA	esrA ETAE_0885	-	-
ETAE_0886	Two-component response regulator EsrB, LuxR family	esrB ETAE_0886	-	-
ETAE_0861-62	/	/	-	-
ETAE_0863-64	/	/	-	-
ETAE_0873-74	/	/	-	-
ETAE_0879-80	/	/	-	-
ETAE_2071	Transcriptional regulator, DeoR family	ETAE_2071	-	-
ETAE_0323	Putative invasin	ETAE_0323	-	-
ETAE_1437	Probable transcriptional regulatory protein ETAE_1437	ETAE_1437	-	-
ETAE_1039	Copper transporter	ybaR ETAE_1039	-	-
ETAE_1720	Putative porin	ETAE_1720	-	-
ETAE_2185	Uncharacterized protein	ETAE_2185	-	-
ETAE_3320	Glycerol-3-phosphate transporter permease	ugpA ETAE_3320	-	-
ETAE_1709	DNA replication terminus site-binding protein	tus ETAE_1709	-	-
ETAE_3474	HTH-type transcriptional repressor FabR	fabR ETAE_3474	-	-
ETAE_3493	Glutamine synthetase	glnA ETAE_3493	-	-

Table S14 Bacterial strains and plasmids used in this study

Strain or plasmid	Genotype
Escherichia coli	
SM10 λpir	*thi thr leu tonA lacy supE recA::RP4-2-Tc::Mu, pirR6K,* Kan^r
DH5a λpir	*λpir lysogen D(ara-leu) araD D(lacX74) phoA20 thi-1 rpoB argE (am) recA1*
BL21(DE3)	Host for protein expression
Plasmid	
pMKGR	Mariner Himar1 transposon encoding a gentamycin resistance gene. Suicide plasmid, *pir* dependent, R6K, Gm^r
pDM4	Suicide plasmid, *pir* dependent, R6K, SacBR, Cm^r
pDMK	pDM4 derivative with Kan resistance gene inserted in SalI site, Kan^r, Cm^r
pUTt	Complementation vector, Amp^r
pET28b-HisSumo	Protein expression vector, Km^r
pET28b-HisSumo-*evrA*	Protein expression vector, Km^r
pET28b-HisSumo-$evrA^{R221A}$	Protein expression vector, Km^r
pET28b-HisSumo-$evrA^{R7A}$	Protein expression vector, Km^r
pET28b-HisSumo-$evrA^{R178A}$	Protein expression vector, Km^r
pUTt-evrA	Complementation vector, ETAE_2071, Amp^r
pUTt-P_{eseB}-EGFP	Complementation vector, *eseB* promoter driven EGFP exprssion, Amp^r
pUTt-P_{eseB}-*luc*	Complementation vector, *eseB* promoter driven luciferase exprssion, Amp^r
pUTt-P_{esrB}-*luxAB*	Complementation vector, *esrB* promoter driven luxAB exprssion, Amp^r
pUTt-P_{esrC}-*luxAB*	Complementation vector, *esrC* promoter driven luxAB exprssion, Amp^r
Edwardsiella piscicida	
EIB202	Wild type strain, CCTCC M 208068, Col^r, Cm^r, Kan^s
wt_ΔP	EIB202, pEIB202 cured, Col^r, Cm^s, Kan^s
EIB202::Tn	EIB202, transposon insertion mutant, labelling mCherry, locus between ETAE_3351 and ETAE_3352
esrB::Tn	EIB202, transposon insertion mutant
eseB::Tn	EIB202, transposon insertion mutant
2071::Tn	EIB202, transposon insertion mutant
pdhR::Tn	EIB202, transposon insertion mutant
2342::Tn	EIB202, transposon insertion mutant
esaB::Tn	EIB202, transposon insertion mutant
esaM::Tn	EIB202, transposon insertion mutant
ΔwaaQ	EIB202, in-frame deletion of ETAE_0075
ΔwalW	EIB202, in-frame deletion of ETAE_0076
ΔwabK	EIB202, in-frame deletion of ETAE_0079
ΔesrA	EIB202, in-frame deletion of *esrA*
ΔesrB	EIB202, in-frame deletion of *esrB*
ΔesrC	EIB202, in-frame deletion of ETAE_0861
ΔeseB	EIB202, in-frame deletion of ETAE_0872
ΔesaM	EIB202, in-frame deletion of ETAE_0879
ΔnuoM	EIB202, in-frame deletion of ETAE_2374
ΔnuoJ	EIB202, in-frame deletion of ETAE_2377
ΔnuoI	EIB202, in-frame deletion of ETAE_2378
ΔevpP	EIB202, in-frame deletion of ETAE_2428
ΔevpC	EIB202, in-frame deletion of ETAE_2431
ΔevpI	EIB202, in-frame deletion of ETAE_2437
ΔmanX	EIB202, in-frame deletion of ETAE_1559
ΔevrA	EIB202, in-frame deletion of ETAE_2071
ΔevrA+pUTt	EIB202, in-frame deletion of ETAE_2071 complemented with pUTt vector
ΔevrA+pUTt-2071	EIB202, in-frame deletion of ETAE_2071 complementation
ΔevrAΔesrB	EIB202, doube in-frame deletion of ETAE_2071 and *esrB*
ΔevrAΔesrB+pUTt-P_{esrB}-esrB	EIB202, doube in-frame deletion of ETAE_2071 and *esrB* complemented with *esrB* driven by it own promoter
ΔevrAΔesrB+pUTt-P_{lac}-esrB	EIB202, doube in-frame deletion of ETAE_2071 and *esrB* complemented with *esrB* driven by *lac* promoter
ΔevrA+P_{eseB}-*luc*	EIB202, in-frame deletion of ETAE_2071 complemented with luciferase driven by *eseB* promoter
WT+P_{eseB}-*luc*	EIB202, wild type complemented with luciferase driven by *eseB* promoter

Table S15 Primers used in this study

primer name	primer sequence
transposon mutant library construction and validation	
evpP-F	TCATCGCACATACAGAATAAACGCC
evpP-R	CCGTAACATTTCTTACAACACTGCG
pG1	AGGTGATGCTACATACGGAAAG
pmh1	AGCGCATGAACTCCTTGATG
PpMar1	AAAAGTCCGCTGGCAAAG
PpMar2	CCCTTCAAGAGCGATACAAC
Sp1	GCTCCGTAGTAAGACATTCATCGCG
Sp2	GCTTACGTTCTGCCCAAGTTTGAG
ABS	GGCCACGCGTCGACTAGTAC
AB2	GGCCACGCGTCGACTAGTACNNNNNNNNNNCCTGG
Seq2	CAATTCGTTCAAGCCGAGATCG
mutants construction	
pDMK-2071-P1	ccccccgagctcaggttacccggatctatGGCCAGATAGCTCAGCGCATCG
pDMK-2071-P2	CGCAGGATCACATAGTGTCCTGTGCGGGCAG
pDMK-2071-P3	GGACACTATGTGATCCTGCGCAGAGAAAAATC
pDMK-2071-P4	gagtacgcgtcactagtggggcccttctagCGGGATGCGTCTGGATAACT
pDMK-2071-in-F	AGCTACCTCAAGCGGGTGCA
pDMK-2071-in-R	GAACTTGGAGGCGTCGGTCA
pDMK-2071-out-F	GCTCGGCAACCAGCAGCGTAT
pDMK-2071-out-R	GTGCTAATCCCACCGTCCCT
pDM4-esrA-P1	ccccccgagctcaggttacccggatctatTGGTGCTCCGCTTAAATGG
pDM4-esrA-P2	AGTTTTAATCCATAGGGGATTCCTTTATG
pDM4-esrA-P3	ATCCCCTATGGATTAAAACTCCAGAACCCC
pDM4-esrA-P4	gagtacgcgtcactagtggggcccttctagCGGCGTTGACGTGATCCGTC
pDM4-esrA-in-F	GCCGAAACGGTCTATGAGC
pDM4-esrA-in-R	CCTCGTCAAAATTACTCTCC
pDM4-esrA-out-F	TGGAGAATATTCCGCTGGC
pDM4-esrA-out-R	GGGCTGGCCGTTTATGAGG
pDM4-eseB-P1	gtggaattcccgggagagctCACCCGAGAAAAACCAACG
pDM4-eseB-P2	GGCCTCCTTACATAGTGCTCTCCTCTGAG
pDM4-eseB-P3	GAGCACTATGTAAGGAGGCCACGATGACCG
pDM4-eseB-P4	aagcttatcgataccgtcgaGAACTGACGCAGTATTTCCC
pDM4-eseB-in-F	CGATAGCATCATGTCCGAC
pDM4-eseB-in-R	CTGGGTGACAAAGTCGGAGC
pDM4-eseB-out-F	CGGCTGGACGATGGCTGG
pDM4-eseB-out-R	GGTGATCGTGCTGCGACTGC
pDM4-esaM-P1	gtggaattcccgggagagctAGCTCTTTGTCGCCACCTG
pDM4-esaM-P2	TAGCCAGCTACATGAATATCCTCCGCGATC
pDM4-esaM-P3	GATATTCATGTAGCTGGCTACACAAACTC
pDM4-esaM-P4	aagcttatcgataccgtcgaCTGCACGACGGTAATGATGG
pDM4-esaM-in-F	GCAAACCGAACTTTGGCTAC
pDM4-esaM-in-R	CATGGGGATTCTCCATCACG
pDM4-esaM-out-F	CGACACCATCATCATCCCC
pDM4-esaM-out-R	AGAGCTGGCTCTCTTTTTGC
pDM4-waaQ-P1	gtggaattcccgggagagctATAGCCGCTGTAGTCACTAC
pDM4-waaQ-P2	AATTGGGTCACATTCTTTTGCCTTTGACTG
pDM4-waaQ-P3	CAAAAGAATGTGACCCAATTCAGATTGGC
pDM4-waaQ-P4	aagcttatcgataccgtcgaTGGCATTGTAGATGACGTGG
pDM4-waaQ-in-F	GGATATGTTGTCGGCTAATC
pDM4-waaQ-in-R	CGGAGGTGAGCAAAATAGGG
pDM4-waaQ-out-F	CAGGTGATTAAACAGCGGAG
pDM4-waaQ-out-R	GACATAGATCAGGCAGGAGG
pDM4-walW-P1	gtggaattcccgggagagctGCTATATCCCATGGTGACGC
pDM4-walW-P2	AACGAAATTACATACTGATACGTCTTCTTC
pDM4-walW-P3	TATCAGTATGTAATTTCGTTTGGGCGCATG
pDM4-walW-P4	aagcttatcgataccgtcgaCTAGAGGCTGGAACCTATGG

pDM4-walW-in-F	CCGCTATTTGCCTCGATTCC
pDM4-walW-in-R	GCGTCCACAAAATAGGCG
pDM4-walW-out-F	GAGAGCATTAATGACCTCGC
pDM4-walW-out-R	CCGCATCATTGCTATATCG
pDM4-wabK-P1	gtggaattcccgggagagctGCATCGTTTTATTAGCTGGC
pDM4-wabK-P2	TCATTATCTACATGTTATACTTGCTCCGAT
pDM4-wabK-P3	GTATAACATGTAGATAATGAATATCGCCCAC
pDM4-wabK-P4	aagcttatcgataccgtcgaGGGAGCAACCAGCGTTTTATC
pDM4-wabK-in-F	GTTGAGCGTCTTATTTTAGAC
pDM4-wabK-in-R	GCAATCAGGGGAAGTAATCC
pDM4-wabK-out-F	CGATAGATTCTATCCAATCC
pDM4-wabK-out-R	TCCACATAATAGTTTTGCCC
pDM4-nuoM-P1	gtggaattcccgggagagctCCGAATGATCTTCATCGTGT
pDM4-nuoM-P2	TGGCGATTTACATGGCGTTTGGTTTCCCTT
pDM4-nuoM-P3	AAACGCCATGTAAATCGCCATGACAATAAC
pDM4-nuoM-P4	aagcttatcgataccgtcgaCTCTATCCCCAGGAACAGCG
pDM4-nuoM-in-F	GCTGAAAGCGCCGCGCTGG
pDM4-nuoM-in-R	CGATCAGGAAGTACATCGGC
pDM4-nuoM-out-F	GCAGAACATCTTCAAGATG
pDM4-nuoM-out-R	CGGCGAAGGAGAGATCGC
pDM4-nuoJ-P1	gtggaattcccgggagagctGCTGGCGTATTTGCCTGCC
pDM4-nuoJ-P2	AACGGGATCACATGCTCGGCTCCTTAGGG
pDM4-nuoJ-P3	GCCGAGCATGTGATCCCGTTACAACATGGG
pDM4-nuoJ-P4	aagcttatcgataccgtcgaCGGGAAAAGGCCAGGATCAG
pDM4-nuoJ-in-F	CCGTGTTGGCGACGATCCG
pDM4-nuoJ-in-R	CAGCATCGAGACCAGCTCC
pDM4-nuoJ-out-F	CACCCTGTTCTTCGGCGGC
pDM4-nuoJ-out-R	CGGTAAAGTTACCGACCGC
pDM4-nuoI-P1	gtggaattcccgggagagctCTGTTCTTCCTGATGATGGC
pDM4-nuoI-P2	CGGCTCCTTATGTCATGGTTACACTCACC
pDM4-nuoI-P3	AACCATGACATAAGGAGCCGAGCATGGAAT
pDM4-nuoI-P4	aagcttatcgataccgtcgaCAATGTGGAAGGCCACGAC
pDM4-nuoI-in-F	GGTTGGTTTCGGCACCCAAG
pDM4-nuoI-in-R	CCATACGGTAAAAGTTGTAG
pDM4-nuoI-out-F	GATCAAGATGTTCTTCAAGG
pDM4-nuoI-out-R	CCTTATTGCTCAGTACCTC
pDM4-evpC-P1	gtggaattcccgggagagctGCACACCTTTACCACCGATG
pDM4-evpC-P2	CGTCTTACTTCATAGCGGACCTCTCTTGTG
pDM4-evpC-P3	GTCCGCTATGAAGTAAGACGGTCAAACAGG
pDM4-evpC-P4	aagcttatcgataccgtcgaCCAGCACATTGGACGCCGTC
pDM4-evpC-in-F	CGATAAGCACAAAAAATGG
pDM4-evpC-in-R	CATGCGTAAATTTGTAGATG
pDM4-evpC-out-F	CAGGCCTATGCCAAATATGG
pDM4-evpC-out-R	ATTGGTCAGCGCGATATAGG
pDM4-evpI-P1	gtggaattcccgggagagctGTTCTTCCAGGTGTTTGAC
pDM4-evpI-P2	AAAATCAGTTCAAGGATGCCTTACAGGTG
pDM4-evpI-P3	GGCATCCTTGAACTGATTTTCGCTATCCGC
pDM4-evpI-P4	aagcttatcgataccgtcgaGTCATACAGCGGGTCGAAGC
pDM4-evpI-in-F	GGCATTTTCTACTGGTTCG
pDM4-evpI-in-R	GAGACAGATAAAGTGGTTC
pDM4-evpI-out-F	CAACCTGTCGGAGTTTCAG
pDM4-evpI-out-R	CAGCTGCAGATCTTTGCTGC
pDM4-manX-P1	gtggaattcccgggagagctCATGGGTTATTCTGCCCTCG
pDM4-manX-P2	CGGCATATCAAATACTCACTCGCTACCTCC
pDM4-manX-P3	AGTGAGTATTTGATATGCCGTAAGGCATTG
pDM4-manX-P4	aagcttatcgataccgtcgaGGTACGTACGATGATGGTC
pDM4-manX-in-F	GTAACGTTGGCTTTATCGAC
pDM4-manX-in-R	GGTTTCCTTGGTCCAGCG

pDM4-manX-out-F	ATCAGCGCTAAACTGAGC
pDM4-manX-out-R	GTGACGACCTCCGGAATGG
pUTt-2071-F	ctcatccgccaaaacagccaGCAGCGGCTTCCACAGGTGG
pUTt-2071-R	ttaaaaattaaggaggaattTCAGCGGATGCCGTTTTCAGAG
pUTt-P$_{eseB}$-luc-1	ctcatccgccaaaacagccaGTTAGTCCTCGGCTGGTGCTGG
pUTt-P$_{eseB}$-luc-2	cgtcttccatAGTGAAACCTCCTATTGACTAC
pUTt-P$_{eseB}$-luc-3	aggtttcactATGGAAGACGCCAAAAACATAA
pUTt-P$_{eseB}$-luc-4	ttaaaaattaaggaggaattTTACACGGCGATCTTTCCGCC
pUTt-P$_{eseB}$-EGFP-1	ctcatccgccaaaacagccaGTTAGTCCTCGGCTGGTGCTGG
pUTt-P$_{eseB}$-EGFP-2	tgctagccatAGTGAAACCTCCTATTGACTAC
pUTt-P$_{eseB}$-EGFP-3	aggtttcactATGGCTAGCAAAGGAGAAG
pUTt-P$_{eseB}$-EGFP-4	ttaaaaattaaggaggaattTTATTTGTACAGTTCATCCATG
pET28b-Sumo-2071-F	tcacagagaacagattggtggatccATGAACGCCAGACAACAACG
pET28a-Sumo-2071-R	agtggtggtggtggtggtgctcgaTCAGCGGATGCCGTTTTCAG
pUTt-luxAB-F	TGGCTGTTTTGGCGGATGAG
pUTt-luxAB-R	CAAATAAGGAAATGTTATGAAAT
pUTt-P$_{esrB}$-luxAB-F	ctcatccgccaaaacagccaGTTATCGGCATATAAAAATATT
pUTt-P$_{esrB}$-luxAB-R	atttcataacatttccttatttgATTTAAAGGGTACTCCGAATC
pUTt-P$_{esrC}$-luxAB-F	ctcatccgccaaaacagccaGCCAACGCCTGATCGACTGC
pUTt-P$_{esrC}$-luxAB-F	atttcataacatttccttatttgAGGTGCTCCTGACTGAGGTAC
qRT-PCR	
qPCR-esrA-F	TAGCGCCGTAGAGAAAACCC
qPCR-esrA-R	TCGCGGCAGATGGAGAATAC
qPCR-esrB-F	CGACCAGCTTGAGAATTTGCC
qPCR-esrB-R	GTAGCCTCGTCCGATATGGC
qPCR-esrC-F	CCATGCCGAACTTGTCGTTG
qPCR-esrC-R	GAGTGTCAACGGACCTCCAC
qPCR-eseB-F	CCCGCTTTCTTGAACTTGGC
qPCR-eseB-R	ACGCTATTCACCGATCTGGC
qPCR-eseE-F	ATAACGGCCTGTCCATCGTC
qPCR-eseE-R	TTTCTCATGGGACAGCGCAT
qPCR-evpP-F	GAATGGGGACGACTCACCTC
qPCR-evpP-R	AAATCCACCGAACCAGGCAT
qPCR-evpC-F	CGATAAGCACAAAAAATGG
qPCR-evpC-R	CTCCATCGTGCATTCATTGC
qPCR-pdhR-F	ATCTGTTGGAAACCCGCCAT
qPCR-pdhR-R	TCGCGCAGACGAACAAAATC
qPCR-2342-F	CCATCCCAGACAGGACGAAC
qPCR-2342-R	AGGTGTATGGCTGGATGTGC
qPCR-2071-F	AAAACGCAGCTACCTCAAGC
qPCR-2071-R	AAGATGGTCTCCCCGTCGTT
qPCR-esaM-F	CTGAAATCCACAGCGCATCG
qPCR-esaM-R	GGGATCGCGACCGTATCTTT
RT-*gyrB*-F	CCGATGATGGTACGGGTCTG
RT-*gyrB*-R	GCTTTTCAGACAGGGCGTTC
EMSA	
EMSA-P$_{esrB}$-F	tgcctgcaggtcgacgatCATGATGATCCATACTCCAAAG
EMSA-P$_{esrB}$-R	AAACTTCATATAGCTCGCTCGG
EMSA-P$_{manX}$-F	tgcctgcaggtcgacgatCGGCTACATTTGTTCACGTC
EMSA-P$_{manX}$-R	ACGCCGTAAAATAAACACGG
Cy5-F	tgcctgcaggtcgacgat
FAM-F	tgcctgcaggtcgacgat

Transparent Methods

Bacterial strains and culture conditions

A list of the strains used in this study is in Table S14. *E. piscicida* EIB202 cured of the endogenous plasmid pEIB202, (*E. piscicida* EIB202 ΔP), was used as the parental strain for generation of the transposon insertion mutant library. *E. coli* SM10*λpir* was used as the donor for conjugations. *E. piscicida* strains were grown in Luria-Bertani broth (LB) or on LB agar (LBA) (Oxoid, England) and in Dulbecco's modified Eagle's medium (DMEM) (Invitrogen, USA) at 28^{o}C. DMEM was used to induce T3/T6SS production as well as to yield auto-aggregation phenotypes mimicking in macrophages and *in vivo* conditions (Zheng and Leung 2007). Where required, antibiotics were supplemented at the following concentrations: polymyxin B (Col, 20 μg/mL), ampicillin (Amp, 100 μg/mL), kanamycin (Km, 25 μg/mL), streptomycin (Str, 100 μg/mL) and gentamicin (Gm, 15 μg/mL).

Generation of the MKGR transposon

The transposon derivatives were constructed within pMar2xT7, a vector containing the *mariner* transposase outside the *Himar1* transposon (Jacobs et al., 2003). First, an *mcherry* gene with a constitutive promoter, P_{tetA}, was inserted into the *Dra*III site in pMar2xT7 (yielding PMmch). Promoterless *km* and *egfp* with their respective ribosome binding sequences (RBS) were amplified from the appropriate templates (Dennis and Zylstra 1998; Gu et al., 2016) and fused together with overlap PCR (Table S15) and then the triplet terminator TGACTAGCTAA and a 48-bp T7 terminator were introduced at the 5' and at 3' ends, respectively. After sequence verification, the complete amplicon was cloned into the *NheI* site of pMmch, yielding pMKGR.

Preparation of the transposon mutant library

Transposon insertion mutants were generated by conjugative transfer of pMKGR into *E. piscicida* EIB202 (Δp) from *E. coli* SM10*λpir* on LBA plates containing Gm and Col (Yang et al., 2017). The mutants were then manually picked into 96-well plates, containing 200 μL LB per well. After incubation at 28^{o}C for 16-20 h, 20% glycerol was added to the wells and the plates were stored at -80^{o}C. Transposon insertion sites for each mutant were determined by thermal asymmetric interlaced PCR (TAIL-PCR) (Liu and Chen 2007) as follows: the first round of PCR was performed with a transposon-specific primer SP1 and a degenerate primer AB2 (Table S15). The PCR products were then diluted 12-fold and used as the template for a second round of PCR, using a nested transposon-specific primer SP2 and a primer ABS that hybridizes to the defined portion of AB2. The third nested transposon-specific primer Seq2

was used for sequencing and the sequencing results were batch mapped by local BLAST (https://blast.ncbi.nlm.nih.gov).

Five subset libraries were assembled from the original set of 20,346 unique insertion mutants to facilitate targeted studies with smaller libraries (Tables S1-S7). The 1st (2,759 mutants) and 2nd (2,235 mutants) subset libraries each contained distinct insertion mutants for each disrupted gene, with insertion sites located within the central 40-60% of each coding sequence. Mutants in genes that only contained a single insertion were preferentially selected for inclusion in the first subset library. The 3rd subset library (3,705 mutants) contained transcriptional fusions and priority was given to mutants that had insertions close to beginnings of ORFs in the creation of this library. The 4th library (2,305 mutants) consisted of insertions within intergenic regions. The 5th library was a composite composed of equally mixture of mutants from the 1st, 2nd and 4th subset libraries and contained 7,299 distinct insertion mutants (Table S1).

Construction of deletion mutants and complemented strains

In-frame deletion mutants were generated using *sacB*-based allelic exchange (Yin et al., 2018). Overlap PCR was used to generate appropriate DNA fragments for creating in-frame deletions in each target gene. The fragments were inserted into the suicide vector pDM4 with Gibson assembly (Gu et al., 2016) and the resulting plasmids were introduced into *E. coli* SM10 λ*pir* for conjugation into *E. piscicida* EIB202. Transconjugants were selected on LBA containing Km and Col. Double-crossover events were subsequently selected on LBA containing 12% sucrose. To complement the *evrA* deletion in Δ*evrA*, an intact *evrA* containing the putative promoter region was amplified and introduced into plasmid pUTt (Yin et al., 2018); the sequence of the insert was subsequently verified.

Growth conditions for TIS studies

To prepare input inocula for the TIS studies, the 5th composite library (Table S7) was grown in LB medium with shaking at 28°C for 12 h, collected by centrifugation at 8,000 × *g* for 2 min and washed twice with filter sterilized PBS. Then, the input library was subjected to three selective growth conditions as follows. For growth in DMEM, the input was diluted 1:100 into DMEM and incubated at 28°C for 24 h after which genomic DNA extraction was performed. For growth in macrophages, the input was inoculated into J774A.1 cell cultures at an MOI of 10 at 37ºC for 2 h, followed by killing of extracellular bacteria with Gm. The J774A.1 cells were incubated for an additional 4 h and lysed with 1% Triton X-100 as described (Okuda et al., 2009). Bacterial cells from the lysate were pelleted and resuspended into 30 mL LB with

shaking at 28°C until OD_{600} reached 1.0 (~ 3 h), eliminating DNA contamination from dead *E. piscicida* cells before genomic DNA extraction. For growth in turbot, the input was used to intraperitoneally (i.p.) inoculate six-month old naïve turbot fish (~100 g), with 3 x 10^6 CFU/fish. At 14-days post infection (d.p.i.), each output library was generated from pooled livers of 5 cohoused fish. The pooled livers were homogenized and plated on the LBA plates supplemented with Col and Gm. After overnight incubation at 28°C, bacterial colonies were scraped, resuspended into fresh LB and ~1:10 back-diluted into 30 mL LB with shaking at 28°C until OD_{600} 1.0 before genomic DNA was extracted (Fu et al., 2013).

Transposon insertion sequencing (TIS)

TIS libraries were analyzed by the STAT-Tn-seq bioinformatic pipeline (Fu et al., 2013). Briefly, genomic DNA was extracted and fragmented by sonication. Then, DNA fragments were end-repaired, A-tailed and P5/P7 adaptor sequences were added by two rounds of PCR. Experimental triplicate libraries of inputs and outputs were sequenced on an Illumina Miseq platform; ~ 2 million reads were generated for each library. The sequencing results were processed with adapter trimming, mapping to the genome, and tallying as described (Fu et al., 2013). The read counts for each locus were normalized among the three libraries according to sequencing depth. The fold change of each locus was generated by dividing the output over the input read counts.

HeLa, J774A.1, and turbot macrophage infection assays

HeLa or macrophage cells (J774A.1 and turbot primary macrophages) were seeded at a density of 1.0 × 10^5 and 3.0 × 10^5 cells/well, respectively, in 24-well plates and incubated overnight at 37°C with 5% CO_2. *E. piscicida* cultures were inoculated into fresh DMEM and statically grown for 12 h at 28°C. J774A.1 or HeLa cells were infected with *E. piscicida* at an MOI of 10 or 100, respectively, followed by centrifugation at 600 × *g* for 10 min to facilitate bacterial attachment to cells. After 2 h infection, cells were washed twice with PBS. DMEM was added into cell cultures with 50 μg/mL Gm to kill extracellular bacteria and cells were incubated at 37°C with 5% CO_2 for another 4-6 h. Then the cultures were treated for 10 min with 1% Triton X-100 to disrupt the cells. Intracellular bacteria were enumerated by serial dilution plating on LBA. For lactate dehydrogenase (LDH) detection, supernatants were transferred to a new centrifuge tube and spun at 5,000 × *g* for 5 min at 4°C and LDH was measured with a CytoTox 96 assay kit (Promega, USA). For fluorescence microscopy, cells were washed twice with PBS and fixed with 4% paraformaldehyde for 10 min, washed with PBS, permeabilized with 0.1% Triton X-100 for 5 min, and washed with PBS again. Nuclei

were stained with DAPI (Beyotime Biotechnology, China) for 30 s, washed 3x with PBS, and coverslips were sealed with nail polish. Images were acquired by a Nikon A1R confocal microscope and analyzed with NIS-Elements Viewer (Nikon, Japan).

Total RNA extraction and qRT-PCR

Overnight cultures of WT and Δ*evrA* were cultured statically in DMEM or DMEM supplemented with various sugars at 28°C for 12 h, respectively. RNA samples were extracted with a commercial RNA isolation kit (Tiangen, China) and mRNA was reverse-transcribed into cDNA using the FastKing RT kit (Tiangen, China). qRT-PCR was performed with an Applied Biosystems 7500 cycler (Applied Biosystems, USA) with triplicate reactions for each sample. The comparative C_T ($2^{-\Delta\Delta C_T}$) method (Gu et al., 2016) was used to quantify the relative levels of each transcript with the housekeeping *gyrB* gene as an internal control and the specific primer pair (Yin et al., 2018).

RNA-seq

For preparation of mRNA for RNA-seq, the Ribo-Zero-rRNA kit (Epicentre, USA) was initially used to remove rRNA from the RNA samples. The final concentration of RNA samples was determined with a Qubit 2.0 Fluorometer (Thermo Fisher, USA). The VAHTS Stranded mRNA-seq Library Prep Kit for Illumina (Vazyme, China) was used to construct strand-specific RNA-seq libraries, and sequencing was conducted on an Illumina HiSeq 2500 platform, yielding 101-bp paired end-reads. Adapter sequences and low-quality bases (PHRED quality scores ≤5) were trimmed with the Trimmomatic package (Bolger et al., 2014) using the default parameters and reads smaller than 35 bp were discarded. The RNA-seq data processing procedures and statistical analysis were performed (Tjaden 2015). The SRA accession number for the RNA-seq data is SRP156435.

SDS-PAGE and Western blotting analysis

Whole cell proteins (WCPs) and extracellular proteins (ECPs) were extracted and concentrated (Yin et al., 2018; Zheng and Leung 2007). Overnight cultures of *E. piscicida* were subcultured into 50 mL fresh DMEM and statically incubated for 24 h at 28^{o}C; bacteria were then harvested by centrifugation at 5,000 × *g* for 10 min at 4^{o}C for WCPs. For ECPs, culture supernatants were filtered with 0.22 μm filters (Millipore, USA), and concentrated using 10 kDa cutoff centrifugal filter devices (Millipore, USA). Proteins were separated by 12% SDS-PAGE, followed by Coomassie Blue staining or Western blotting. For Western blots, separated proteins were wet transferred onto PVDF membranes (Millipore, USA) and incubated with a 1:1000 dilution of mouse anti-EseB (GL Biochem, China). HRP-conjugated anti-mouse IgG

(Santa Cruz Biotechnology, CA) was used at a 1:2,000 dilution as a secondary antibody. Proteins were visualized with TMB substrate (Amresco, USA). Mouse anti-DnaK (Santa Cruz Biotechnology, USA) was used as a cytoplasmic protein control.

Luminescence and fluorescence assays

For assays involving luminescence and fluorescence, pUTt derivative plasmids bearing P_{esrB}-*luxAB*, P_{esrC}-*luxAB* and P_{eseB}-*luc* (luciferase) reporters were introduced into WT and Δ*evrA E. piscicida*. For luminescence assays, strains were inoculated into 50 mL DMEM and statically incubated at 28°C. Pellets of 150 μL culture of each strain were mixed with 40 μL capraldehyde dissolved in ethanol as substrate, and OD_{600} was determined using a Microplate Reader (Bio-Tek, USA) and luminescence values were monitored using a Microplate Luminometer Orion II (Titertek-Berthold, Germany) every 2 hours.

For *in vivo* fluorescence detection, overnight cultures of WT+P_{eseB}-*luc* and Δ*evrA*+P_{eseB}-*luc* were i.p. injected into turbot. At 5 d.p.i., the fish were anesthetized with tricaine methanesulfonate (MS-222) (Sigma-Aldrich, USA) and i.p. injected 100 μL of a 1 mg/mL beetle luciferin solution (Promega, USA). At 10 min post-injection, fluorescence was detected with a Kodak In-Vivo Multispectral System FX (Carestream Health, USA). After fluorescence measurements were taken, the fish were killed with overdose of MS-222 and livers from each fish were obtained for bacterial CFU plating (Yin et al., 2018).

Protein purification

Recombinant EvrA (WT and mutant variants) with N-terminal HisSumo tags were purified from BL21 (DE3) *E. coli*. Expression of the EvrA-HisSumo fusion was induced by growth in LB medium supplemented with 0.2 mM isopropyl β-D-1-thiogalacto-pyranoside at 22°C at 200 rpm. At 18 h post-induction, the cells were harvested by centrifugation, resuspended in lysis buffer (20 mM Tris, 500 mM NaCl, pH 9.0) and lysed with a French press (Glen Mills, USA). Following centrifugation at 12,000 rpm for 30 min, the supernatant was loaded onto a pre-packed Ni-NTA column (GE Healthcare, Sweden) for purification. The loaded column was washed with a lysis buffer gradient supplemented with 40-100 mM imidazole on an ÄKTA protein purification system (GE, Healthcare, Sweden). Proteins were eluted with lysis buffer supplemented with 500 mM imidazole. The SUMO protease ULP1 (Thermo Fisher, USA) was added into the purified protein at the ratio 1:500 to digest HisSumo tag at 4°C in statics. After digestion of the HisSumo tag with ULP1 for 10 h, reaction mixtures were reloaded on to a Ni-NTA column to isolate EvrA protein in the flowthrough. Purified proteins were stored in 10% glycerol at 4°C and their purity was confirmed by SDS-PAGE. Protein concentrations were

298 determined by the bicinchoninic acid protein assay (Thermo Fisher, USA).

299 ***Electrophoretic mobility shift assay (EMSA) and DNase I footprinting assay***

300 For EMSAs, purified EvrA protein was incubated with Cy5-labeled DNA probes (P_{esrB},
301 P_{esrC}, and P_{manX}) (Genewiz, China) in 20 μL of binding buffer (10 mM Tris, 50 mM KCl, 5 mM
302 $MgCl_2$, 0.1 mM DTT, pH 7.4). In all EMSA analysis, excess (10-fold) of the nonspecific
303 competitor poly(dI-dC) was used to determine the specificity of the binding. After incubation at
304 25°C for 30 min, the samples were loaded on a 6% polyacrylamide gel and electrophoresed in
305 0.5 × TBE (Tris/Boric acid/EDTA) buffer at 4°C at 100 V for 120 min. Gels were imaged using a
306 Typhoon FLA 9500 (GE Healthcare, Sweden) with the Cy5 channel set at a 531 nm excitation
307 wavelength (Gu et al., 2016).

308 Dye primer-based DNase I footprinting assays were performed (Gu et al., 2016). Briefly,
309 the promoter region of *esrB* was PCR-amplified to include a 6-FAM moiety at the 5' end (S14
310 Table). For each assay, 200 ng of probe was incubated without or with the presence of 200 ng
311 EvrA in a total volume of 40 μl. After the mixture was incubated for 30 min at 25°C, a 10 μL
312 solution containing approximately 0.015 units of DNase I (Promega, USA) and 100 nmol of
313 freshly prepared $CaCl_2$ was added. The mixture was then incubated for 1 min at 25°C. The
314 reaction was stopped by adding 140 μL of DNase I stop solution (200 mM unbuffered sodium
315 acetate, 30 mM EDTA and 0.15% SDS). The samples were first extracted using
316 phenol/chloroform and then precipitated using ethanol, and the pellets were dissolved in 10 μL
317 of MilliQ water. Approximately 2 μL of digested DNA was added to 7.9 μL of HiDi formamide
318 (Applied Biosystems. USA) and 0.1 μL of GeneScan-500 LIZ size standards (Applied
319 Biosystems, USA). The samples were analyzed using a 3730 DNA Analyzer with a G5 dye set
320 that was run on an altered default genotyping module that increased the injection time to 30 s
321 and the injection voltage to 3 kV. The results were analyzed using GeneMapper 4.0 (Applied
322 Biosystems, USA).

323 ***Chromatin immunoprecipitation quantitative PCR (ChIP-qPCR)***

324 ChIP-qPCR was performed (Liu et al., 2017). Briefly, strains expressing functional
325 FLAG-tagged EvrA or FLAG only vectors (WT+EvrA-Flag and WT+Flag) (Fig. S7C) were
326 cultured in DMEM at 28°C for 12 h without shaking. Bacteria were treated with 1%
327 formaldehyde at room temperature for 10 min and the cross-linking reaction was stopped with
328 125 mM glycine. The bacteria were then washed twice with cold sterile PBS and resuspended
329 in 5 mL of SDS lysis buffer (Liu et al., 2017). Next, the bacteria were sonicated, and the DNA
330 was fragmented to 100-500 bp at 200 W (Diaenode, USA). Insoluble cellular debris was

removed via centrifugation, and the supernatant was used as the input sample in IP experiments. Both the input and the IP samples were washed with 50 μL protein G beads for 1 h, and incubated overnight with 30 μL anti-Flag M2 magnetic beads (Sigma-Aldrich, USA). The beads were washed twice with 1 mL of each of the following buffers: low salt wash buffer, high salt wash buffer, LiCl wash buffer, and standard TE buffer (Liu e al., 2017). The beads were resuspended in 200 μL of elution buffer, incubated at 65°C for 2 h, and then centrifuged at 5,000 × *g* for 1 min. The supernatants containing the immunoprecipitated DNA were collected, and 8 μL of 5 M NaCl was added to all of the tubes (IPs and Inputs). The tubes were then incubated at 65°C overnight to reverse the DNA-protein crosslinks. After treatment with RNase A (10 μg/mL) and Proteinase K (1 mg/mL), the enriched DNA was purified using phenol-chloroform and amplified using qPCR.

For each DNA target, ΔC_T of the Input fraction and IP fraction was calculated in both the WT+EvrA-Flag and WT+Flag samples. Each value was then divided by the corresponding ΔC_T that was obtained for the non- specific *gyrB* intragenic region in the strains. Then, the enrichment ratio was calculated from the $\Delta\Delta C_T$ value in WT+EvrA-Flag strain divided by that of WT+Flag strain. The formula of EvrA binding is as following: $(\Delta\Delta C_T)$ = IP{[C_T (WT+EvrA-Flag) - C_T (WT+Flag)] - C_T*gyrB*} - Input{[C_T (WT+EvrA-Flag) - C_T (WT+Flag)] -C_T *gyrB*}.

Electrospray ionization mass spectrometry (ESI-MS)

ESI-MS based determination of EvrA interaction with man-6P (Zhou et al., 2018). Purified EvrA (20 μM) was buffer-exchanged into 100 mM ammonium acetate (pH 7.5) using a centrifugal buffer exchange column (Micro Bio-Spin 6, Bio-Rad, USA), and one aliquot was denatured by adding formic acid to a final concentration of 0.1%. Both native (non-formic acid-treated) and denatured protein samples were analyzed by direct infusion. Specifically, 15 μL of each protein sample was loaded into a nano-flow borosilicate emitter (NanoES spray capillaries, Thermo Scientific, USA) and sprayed into an Orbitrap Fusion mass spectrometer through a Nanospray FLEX Ion Source (Thermo Scientific, USA). The mass spectrometer settings were: spray voltage 1.3 kV for native samples and 2.2 kV for denatured samples; S-lens RF level of 150, SID 100 for complete desolvation of the native protein sample; capillary temperature at 150^{o}C for native protein samples or 300^{o}C for denatured samples; scan range 1500–5500 m/z for native samples and 1000–5000 for denatured samples; intact protein mode with trapping gas pressure set as 0.2. Mass spectra were analyzed using Thermo Scientific Protein Deconvolution software (Thermo Scientific, USA). The parameters for spectra analysis were specified according to the mass spectrometer settings. The minimum adjacent range of

charges was 4–8 for native proteins or 5–10 for the denatured proteins, and mass tolerance was 30 p.p.m. The deconvoluted mass of the most abundant ion was selected as the mass of the target protein. The mass of the bound ligand was calculated as the difference between the native protein and the denatured protein.

Turbot virulence and competitive index assays

Turbot experiments were performed according to protocols approved by the Animal Care Committee of the East China University of Science and Technology (2006272) and the Experimental Animal Care and Use Guidelines from the Ministry of Science and Technology of China (MOST-2011-02). Healthy turbot weighing 30.0 ± 3.0 g (~ 2 months' old and ~1:1 female to male) were obtained from a commercial farm (Yantai, China) and acclimatized to laboratory conditions for at least 7 days. Competitive assays were performed between WT or the indicated gene-deletion mutant strains and WT(Δp), the WT strain cured of its endogenous Cm and Str resistance plasmid pEIB202 (Wang et al., 2009). WT(Δp) does not exhibit impaired growth in LB, DMEM, J774A.1 or turbot. Inocula were prepared using fresh cultures of bacteria that were diluted and mixed at a 1:1 ratio. The i.p. injection dose was ~10^5 CFU/fish in a 100 μL inoculum. At 8 d.p.i., the livers from fish in each group (5 animals/group) were sampled, homogenized and plated on LBA plates with or without the presence of 34 μg/mL chloramphenicol (Cm) to distinguish WT(Δp) (Cm^s) or other strains (Cm^r) (Yang et al., 2017) and enumerate the ratio of the competing strains. The ratios of the bacterial counts were used to determine competitive indices.

For fish survival assays, overnight cultures were harvested by centrifugation at 8,000 × *g* for 2 min at 4°C and washed three times with PBS. A total of 2.0 × 10^4 CFU bacteria suspended in PBS containing 5 mg/mL mannose or glucose was i.p. injected into each fish; PBS or PBS supplemented with 5 mg/mL mannose and glucose was used as negative control. A total of 30 fish were injected with each strain and fish mortality was monitored daily. The infection experiments were performed at least three independent times.

Turbot macrophage separation

The separated head kidney of turbot fishes was homogenized with woven nylon mesh, and macrophages obtained from the organ were collected using the continuous gradient Percoll separation method (Vray and Plasman 1994). Nine volumes of Percoll with 1 volume of sterile 1.5 M NaCl were mixed to make stock isotonic Percoll (SIP). The initial density of 1.065 g/mL was obtained by mixing 4 mL of the head kidney cell suspension in pH 7.6 heparin/L-15 with 4.2 ml of SIP. To make a self-generated continuous gradient, the prepared sample

solution was centrifuged for 20 min, 20,000 × *g*, at 5°C. Macrophages were obtained from the third band with a density distribution of 1.069-1.075 g/mL. The collected cell suspended solution was washed three times by centrifugation for 10 min at 300 × *g* and at 4°C with 10 mL of incomplete L-15. The washed cell suspension was counted with a 0.4% solution of Trypan Blue in HBSS to determine cell viability.

Isothermal titration calorimetry (ITC)

All ITC titrations were performed at 25°C using a MicroCal iTC200 instrument (Malvern Panalytical Ltd). A binding buffer consisting of 20 mM Tris and 500 NaCl (pH 9.0) was used for all measurements. Assays were performed with 20 total injections with 100 μM EvrA in the sample cell and 2 mM sugar in the injection syringe. Buffer-only runs were performed to quantify the heat of dilution for background subtraction from binding runs. Thermal data were fitted to the One Set of Sites binding model with the N value fixed at 1 to yield the equilibrium dissociation constant (K_d) according to the modeling alignment to RpiA (Ishikawa et al., 2002). Each binding run was carried out at least 2 independent times.

Quantification of mannose and man-6P/man-1P in bacterial cells and fish tissues

Metabolites quantification was performed (Cheng et al., 2019; Guo et al., 2014). After 5 d.p.i. with *E. piscicida* WT or PBS as a control, turbot livers and intestines were harvested and weighted. To extract mannose and its derivatives, 1 mL methanol was added to the liver, vortexed for 10 s, ultrasonicated for 20 min, and centrifuged for 20 min with 12,000 rpm at 4°C. 700 μL of the resulting supernatant was taken for UPLC-TQS MS/MS (Waters, USA). UPLC-TQS MS/MS settings were set as follows: column temperature 35°C, sample chamber temperature 10°C, carrier speed 0.3 ml/min, electronic press of spray 2.5 kV. The sample of bacterial cells cultivated in DMEM condition was treated with the same procedures.

Bioinformatics analysis of EvrA

Structural homology modeling of EvrA was performed with Phyre 2.0 (Kelley et al., 2015). The structural model with the highest confidence was from an alignment to the structure of RpiA (PDB: 1LK7) (Ishikawa et al., 2002). The Phyre-predicted structure of WT EvrA was used for ligand (man-6P) docking with AutoDock (http://autodock.scripps.edu) with the default docking parameters and the top ligand-binding site with lowest ΔG was selected. Multiple sequence alignments were performed using ClusterX 1.8, and the phylogenetic tree was drawn using MEGA 6.0 (Tamura et al., 2013). COG counts were based on the previous COG annotation of EIB202 genome (Wang et al., 2009). EvrA was searched against Uniprot database (https://www.uniprot.org) to predict its conserved domains. STRING analysis was

performed with the default parameters (Szklarczyk et al., 2019).

Statistical analysis

GraphPad Prism (version 6.0) was used to perform the statistical analyses. Data are presented as the mean ± SD of triplicate samples per experimental condition unless otherwise noted. Statistical analyses were performed using unpaired two-tailed Student's *t* test for the metabolite level analysis, One-way ANOVA analyses followed by Bonferroni's multiple-comparison post-test comparing the data of CI values, or Kaplan-Meier survival analysis with a log-rank test. Differences were considered significant at $*P < 0.05$, $**P < 0.01$, and $***P < 0.001$.

Supplemental References

Bolger, A.M., Lohse, M., and Usadel, B. (2014). Trimmomatic: A flexible trimmer for Illumina sequence data. Bioinformatics 30, 2114-20.

Cheng, Z.X., Guo, C., Chen, Z.G., Yang, T.C., Zhang, J.Y., Wang, J., Zhu, J.X., Li, D., Zhang, T.T., Li, H., Peng, B., and Peng, X.X. (2019). Glycine, serine and threonine metabolism confounds efficacy of complement-mediated killing. Nat. Commun. 10, 3325.

Dennis, J.J., and Zylstra, G.J. (1998). Plasposons: modular self-cloning minitransposon derivatives for rapid genetic analysis of Gram-negative bacterial genomes. Appl. Environ. Microbiol. 64, 2710-5.

Fu, Y., Waldor, M.K., and Mekalanos, J.J. (2013). Tn-Seq analysis of *Vibrio cholerae* intestinal colonization reveals a role for T6SS-mediated antibacterial activity in the host. Cell Host Microbe 14, 652-63.

Gu, D., Guo, M., Yang, M.J., Zhang, Y.X., Zhou, X.H., and Wang, Q.Y. (2016). A σ^E-Mediated temperature gauge controls a switch from LuxR-mediated virulence gene expression to thermal stress adaptation in *Vibrio alginolyticus*. PLoS Pathog. 12, e1005645.

Guo, C., Huang, X.Y., Yang, M.J., Wang, S., Ren, S.T., Li, H., and Peng, X.X. (2014). GC/MS-based metabolomics approach to identify biomarkers differentiating survivals from death in crucian carps infected by *Edwardsiella tarda*. Fish Shellfish Immunol. 39, 215-222.

Ishikawa, K., Matsui, I., Payan, F., Cambillau, C., Ishida, H., Kawarabayasi, Y., Kikuchi, H., and Roussel, A. (2002). A hyperthermostable D-ribose-5-phosphate isomerase from *Pyrococcus horikoshii* characterization and three-dimensional structure. Structure 10, 877-886.

Jacobs, M.A., Alwood, A., Thaipisuttikul, I., Spencer, D., Haugen, E., Ernst, S., Will, O., Kaul, R., Raymond, C., Levy, R., Chun-Rong, L., Guenthner, D., Bovee, D., Olson, M.V., and Manoil C. (2003). Comprehensive transposon mutant library of *Pseudomonas aeruginosa*. Proc. Natl. Acad. Sci. U. S. A. 100, 14339-44.

Kelley, L.A., Mezulis, S., Yates, C.M., Wass, M.N., and Sternberg, M.J.E. (2015). The Phyre2 web portal for protein modeling, prediction and analysis. Nat. Protocols 10, 845-858.

Liu, Y., Zhao, L.Y., Yang, M.J., Yin, K.Y., Zhou, X.H., Leung, K.Y., Liu, Q., Zhang, Y.X., and Wang, Q.Y. (2017). Transcriptomic dissection of the horizontally acquired response regulator EsrB reveals its global regulatory roles in the physiological adaptation and activation of T3SS and the cognate effector repertoire in *Edwardsiella piscicida* during infection toward turbot. Virulence 8, 1355-77.

Liu, Y.G., and Chen, Y. (2007). High-efficiency thermal asymmetric interlaced PCR for amplification of unknown flanking sequences. BioTechniques 43, 649-56.

Okuda, J., Kiriyama, M., Suzaki, E., Kataoka, K., Nishibuchi, M., and Nakai, T. (2009). Characterization of proteins secreted from a type III secretion system of *Edwardsiella tarda* and their roles in macrophage infection. Dis. Aquat. Organ. 84, 115-21.

Szklarczyk, D., Gable, A.L., Lyon, D., Junge, A., Wyder, S., Huerta-Cepas, J., Simonovic, M., Doncheva, N.T., Morris, J.H., Bork, P., Jensen, L.J., and von Mering, C. (2019). STRING v11: protein-protein association networks with increased coverage, supporting functional discovery in genome-wide experimental datasets. Nucleic Acids Res. 47, D607-613.

Tamura, K., Stecher, G., Peterson, D., Filipski, A., and Kumar, S. (2013). MEGA6: molecular evolutionary genetics analysis Version 6.0. Mol. Biol. Evol. 30, 2725-2729.

Tjaden, B. (2015). De novo assembly of bacterial transcriptomes from RNA-seq data. Genome Biol. 16, 1.

Vray, B., and Plasman, N. (1994). Separation of murine peritoneal macrophages using Percoll density gradients. J. Immunol. Methods 174, 53-9.

Wang, Q.Y., Yang, M.J., Xiao, J.F., Wu, H.Z., Wang, X., Lv, Y.Z., Xu, L.L., Zheng, H.J., Wang, S.Y., Zhao, G.P., Liu, Q., and Zhang, Y.X. (2009). Genome sequence of the versatile fish pathogen *Edwardsiella tarda* provides insights into its adaptation to broad host ranges and intracellular niches. PLoS ONE 4, e7646.

Yang, G.H., Billings, G., Hubbard, T.P., Park, J.S., Leung, K.Y., Liu Q., Davis, B.M., Zhang, Y.X., Wang, Q.Y., and Waldor, M.K. (2017). Time-resolved transposon insertion sequencing reveals genome-wide fitness dynamics during infection. mBio. 8, e1517-81.

Yin, K.Y., Guan, Y.P., Ma, R.Q., Wei, L.F., Liu, B., Liu, X.H., Zhou, X.S., Ma, Y., Zhang, Y.X., Waldor, M.K., and Wang, Q.Y. (2018). Critical role for a promoter discriminator in RpoS control of virulence in *Edwardsiella piscicida*. PLoS Pathogen. 14, e1007272.

Zheng, J., and Leung, K.Y. (2007). Dissection of a type VI secretion system in *Edwardsiella tarda*. Mol. Microbiol. 66, 1192-206.

Zhou, P., She, Y., Dong, N., Li, P., He, H., Borio, A., Wu, Q., Lu, S., Ding, X., Cao, Y., Xu, Y., Gao, W., Dong, M., Ding, J., Wang, D.C., Zamyatina, A., and Shao, F. (2018). Alpha-kinase 1 is a cytosolic innate immune receptor for bacterial ADP-heptose. Nature 561, 122-126.